University of Stavanger

KATHERINE BELTRÁN JIMÉNEZ FACULTY OF SCIENCE AND TECHNOLOGY

Characterization of annulus well cement quality to estimate the leakage potential in cement well barriers

PhD Thesis UiS No. 676 - December 14th

Characterization of annulus well cement quality to estimate the leakage potential in cement well barriers

by

Katherine Beltrán Jiménez

Thesis submitted in fulfillment of
the requirements for degree of
PHILOSOPHIAE DOCTOR
(PhD)

Faculty of Science and Technology
Department of Petroleum Science and Engineering

2022

University of Stavanger
N-4036 Stavanger
NORWAY
www.uis.no

ISBN: 978-82-8439-135-9
ISSN: 1890-1387
PhD thesis UiS No. 676

Dedicated to my family: Agustín,
Gloria and Andrea

Acknowledgement

I would like to use this part of my thesis to write some words of gratitude and show my deepest appreciation to all of you that have been by my side during my PhD journey. This has been a long-term project with a very exciting journey involving people in Brazil, Colombia, USA and Norway. Thank you all for your help and support to make the dream of concluding a PhD a reality.

First, I would like to thank my supervisors: Marcelo Igor de Souza, Steinar Kragset and Jan Aasen. I am grateful for your trust and continuous support. I appreciate a lot your patience during the bureaucratic process of the cotutelle agreement, which took us almost two years to complete and was processed in the middle of a pandemic. You three have been extremely generous with your time to discuss monthly with me and review my advances. Without your support, patience and guidance it would not have been possible to complete this cotutelle degree.

I am also thankful for my coworkers from the well operations and risk management group at NORCE. Since 2018, you have given me the opportunity to learn and grow by your side; first as visiting researcher and then as coworker. It is a great pleasure and an honor to work as part of such a talented group of researchers; you keep me inspired and busy. My deepest appreciation goes to Hans Joakim Skadsem and Dave Gardner, you both have lead projects where I have had the opportunity to get involved in the planning and execution. You have given me the opportunity and freedom to investigate further some questions, to collect results and try to do some new experiments that I am including as part of this thesis. Thank you for the opportunity, I have learned quite a lot from our discussions and my collaboration with you has been without doubts of paramount importance for my PhD journey. I would also like to thank the ullrigg team, especially Ronny Håland, Arne Haaverstein, Krister Dahl, Samuel Poudroux, Stig Lomeland and Gunnar Mæland who helped me with the fabrication of pieces, core plug cutting and instrumentation for testing; they are also the ones who made possible the execution of the well completion in the last chapter of this document.

In addition, I would like to thank the LTS (Subsea Technology Laboratory) team: professors, technicians and researchers. My PhD journey started in your corridors as well as my interest in P&A operations. My time working as part of your team

inspired in me the desire of cultivating an academic career, and I will always be grateful for it. I have learned from all of you many important things as a professional and as a human, you are the best example of high quality research developed in Latin America. I could not mention the UFRJ team without acknowledge Lucianita, who supports the Ocean Engineering Department. She has, in so many ways, impacted my PhD journey, supporting me during my exchange and my period abroad. Pessoal da UFRJ, Obrigada para todos voces, voces estão sempre no meu coraçao!

As maybe this is the only part of my thesis that my friends will read, I would like to share some words of appreciation with all of you my friends: Iara Balo, Mariana Montenegro, Roman Demchenco, Eliane Ferreira, Luis Ruiz, Leiner Lache, Rafael and Carol, Harold Cifuentes, Wilman Terreros and Jerson Becerra. Many times your questions of "how it is going with your PhD?" and "when you will finish it?" were really difficult for me to answer. But I appreciate that you always found kind words when my answers had frustration or when I was sharing my struggles. I am grateful for your support; you were very important in keeping my personal life balanced during this journey. I would like to thank my family, my parents Agustin and Gloria, my sister Andrea and my boyfriend Evan and his family. I could not be more lucky to have such wonderful humans by my side, always cheering me up and continuously supporting me in all my projects. I still do not know how I manage to get involved in so many things at the same time. I am looking forward to celebrate the conclusion of this project and share and celebrate the gift of life together with you!

To finalize, I would like to acknowledge the partners of the P&A Innovation Program – a program for accelerating P&A technology development for facilitating the access to samples and permission to publish. Aker BP is thanked and acknowledged in particular for providing the Transition joint and Fish 1 sections for study. Equinor ASA is acknowledged for the permission to publish the work of U7 well construction, especial thanks to Ioan Alexandru Merciu and Pål Hemmingsen. Schlumberger is acknowledge for the collaboration in logging activities and interpretation, especially by the support received by Amit Govil and Guillermo Obando. Finally, the Coordenação de Aperfeiçoamento de Pessoal de Nível Superior - Brasil (CAPES) is acknowledge - Part of this work was conducted during a one year scholarship supported by the Program CAPES/PDSE 47, Process 88881.187006/2018-01.

Resumo da Tese apresentada à COPPE/UFRJ como parte dos requisitos necessários para a obtenção do grau de Doutor em Ciências (D.Sc.)

CHARACTERIZATION OF WELLBORE MICRO ANNULI TO ESTIMATE THE LEAKAGE POTENTIAL IN CEMENT WELL BARRIERS

Katherine Beltrán Jiménez

Setembro/2022

Orientadores: Marcelo Igor Lourenço de Souza
Jan Aage Aasen
Steinar Kragset

Programa: Engenharia Oceânica

Cimento é hoje em dia o material mais usado no interior dos poços como elemento barreira para garantir isolamento de camadas e evitar a migração de fluidos entre o reservatório e a superfície. Às vezes a integridade do poço pode ser comprometida pela presença de caminhos de vazamento de fluidos. Alguns deles podem ser o resultado de defeitos durante a construção do poço como uma consequência de processos mecânicos, químicos ou físicos durante a vida do poço que induzem a alteração e degradação das barreiras. Barreiras anulares são o objeto de estudo de esta tese. Seções de teste em grande escala foram construidas para investigar a qualidade da barreira e sua correlação com as taxas de vazamento monofasicas de gás e água. Um estudo de durabilidade do cimento de poço de petróleo com mais de 30 anos também é apresentado analisando a variação das propriedades mecânicas, petrofísicas e composicionais em relação ao comportamento geral da permeabilidade das seções Por fim, é apresentada a pesquisa realizada para a construção de uma instalação para o teste de tecnologias de perfilagem de barreiras anulares de poços. Os resultados mostram que os caminhos de migração se correlacionam bem com a interpretação de perfilagem e se ajustam bem às variações das propriedades hidráulicas medidas nas células.

Abstract of Thesis presented to COPPE/UFRJ as a partial fulfillment of the requirements for the degree of Doctor of Science (D.Sc.)

CHARACTERIZATION OF ANNULUS WELL CEMENT QUALITY TO ESTIMATE THE LEAKAGE POTENTIAL IN CEMENT WELL BARRIERS

Katherine Beltrán Jiménez

September/2022

Advisors: Marcelo Igor Lourenço de Souza
Jan Aage Aasen
Steinar Kragset

Department: Ocean Engineering

Cement is nowadays the most used material that is placed inside of wells as a barrier element to ensure zonal isolation and avoid migration of fluids between the reservoir and surface. Sometimes the well integrity can be compromised due to the presence of imperfections called leakage paths. Some of those paths can be the result of defects during the well construction or can be the consequence of mechanical, chemical and physical processes during the well life that induce alteration and degradation in the barriers. Annular cement barriers are the object of study of this thesis. Full-size test sections have been constructed to investigate barrier quality and their correlation with single phase gas and water leakage rates. A durability study of oil well cement 30+ years old is also presented analyzing the variation of mechanical, petrophysical and compositional properties in connection with the overall cell permeability behavior. Finally, the research conducted to construct a facility for the testing of logging technologies of annular well barriers is presented. Results show that migration paths correlate well with the logging interpretation and fit well with the variations of hydraulic properties measured on the cells.

Contents

List of Figures

List of Tables

Introduction

Decommissioning of oil facilities is a process that can occur for several reasons, amongst them the end of the production life, end of the concession contract, resource depletion, and the low price of oil. Activities included in the decommissioning phase typically involve the following : plug and abandonment of the well; removal of the top side (well head); removal of the platform and submarine structures (pipeline, umbilical, riser, submarine equipment, etc.); remediation and in some cases monitoring [6]. It is estimated that between 2021 and 2030 decommissioning activities will cost almost 100 billion USD worldwide, with the largest cost and markets in Europe, Asia and North America [7]. Technology developments and innovative solutions with the potential to minimize decommissioning costs and at the same time reduce the complexity of operations are mostly concentrated in the activities of well plug and abandonment (P&A), which normally represent 50% of the total cost of the decommissioning [7, 8].

Activities of P&A are not new for the oil and gas industry. They are particularly common in exploratory wells where reserves do not present an economic potential for exploration or where no hydrocarbons are discovered. Hence, the risk of migration of fluids to the surface after P&A is low or nonexistent. As P&A activities are becoming more and more common at the end of the productive life of oil and gas fields, some authors imply that the oil industry is dealing with a P&A wave occurring especially in mature fields and offshore areas [9]. These wells present more complexity and the probability of an unexpected migration of fluids (hydrocarbons, gases or water) might be higher. Note that in all depleted fields the reservoir always contains hydrocarbons. Per today's technology only 30% of the reserves in place can be produced to surface using primary oil recovery techniques. If secondary and tertiary enhanced oil recovery techniques are used the recovery factor increase to a maximum of 50-80% [10].

To produce hydrocarbons, millions of wells have been drilled worldwide and more are being drilled every year. Despite the global tendency to push towards a low carbon economy, drilling activity reports indicate that between 2015 and 2020, an average of 70,000 new wells were drilled every year, with 2,500 of those being drilled offshore [11, 12]. A comparison between the number of drilled and P&A

wells is presented below for three different locations. Reviewing the first case in the United States, the Department of Energy estimates that a total of 10 million of wells exist in the country. In the state of Texas alone a total of 1,649,305 wells have been drilled but only 405,122 are P&A with modern techniques (representing 24% of the total). The remaining wells correspond to 811,889 legacy and orphan wells, 290,110 wells in operation and 326,904 at risk [13]. Reviewing a second case, in the North Sea it is observed that a total of 20,507 wells have been drilled and of those 6,254 wells correspond to the Norwegian Continental Shelf (NCS) [14]. In 2020, the Norwegian regulator (PTIL) reported that 1,397 wells were under production, 376 were under injection and 290 were temporarily abandoned. However, their historical data shows that in 10 years (between 2010 and 2019), only 101 boreholes were slot recovered and 118 wells were permanent P&A [15]. Looking at the forecast for P&A activities in NCS, the Norsk Olje & gas estimates that between 2021-2026 a total of 136 wells will need to be P&A and 175 wellbores will be slot recovered [16]. A third case shows that by 2020, Brazil has drilled 30,000 wells, 7000 of them offshore. Classifying them in terms of their status around 42.53% are in production, 49.47% are in temporary abandonment and only 8% are P&A with modern techniques [15]. Reviewing the data between 2016 and 2020, only 174 wells were P&A (68 onshore and 106 offshore) [15] and it is estimated that at least 350 wells need to be P&A in the Campos, Santos and Espiritu Santos Basins in the next years [17]. The revision of the three previous cases gives insight about the abundance of wells to be abandoned, but also highlights that the P&A phase is just the next phase after the process of drilling, completing and producing wells. In the regulatory environment of these three countries all the drilled wells will move to a P&A phase without exception.

The final P&A designs should comply at least with the following minimum objectives: isolate and protect all the fresh water zones; isolate and ensure all the possible production areas and prevent any type of flow from the well or between rock layers. As a general rule, for each formation with potential to flow, at least two barrier envelops need to be present to prevent flow and ensure a safe condition that protects the environment in a perpetual way [18]. The sequence of activities to complete the P&A starts with the identification of formations with potential to flow and the integrity evaluation of all barrier elements. Such evaluation includes the qualification of casings, annular cement and impermeable formations in the overburden. The well barrier elements need to be proven in integrity and capacity to act as permanent barriers in length intervals defined by local regulations. Many countries follow the recommendations given by NORSOK D-010 and the UK guidelines which suggest a minimal length barrier of 50 m and 30 m respectively [19, 20]. If failures are observed on some of the barrier elements or the minimal requirements are not

fulfilled, remediation operations are executed. Once the well presents a "healthy" condition the planning of the abandonment starts. Here, a P&A design is submitted for the regulator's approval, containing the position of the barrier envelops and documenting the qualification of barrier elements. After approval, the final step consists in placing a set of plugs into the well to complete the cross sectional barriers and ensure the sealing capability. However, the perception that well abandonment is a reverse engineering problem that requires only basic tools and that one already has sufficient knowledge is far from the reality.

As observed, the well barrier envelops are formed by several elements (internal plugs, annular cement, casing and formation), which together try to re-establish the natural seal (cap rock) removed during the drilling phase. Cement is an essential material used to construct barriers nowadays, not only for internal plugs but also for annular barriers. The internal plugs are installed during the abandonment phase and have less risk of being defective. Even so, there exists a possibility that during placement, operative conditions can compromise the zonal isolation due to incomplete fluid displacement resulting in voids, channels and slurry contamination [21–23]. The case of the annular cement barriers installed between the casings during the drilling phase is different. These cement barriers are pumped into annular spaces during well construction to ensure well integrity, provide zonal isolation along the annulus, maintain mechanical support and prevent communication between the surroundings and the well fluids. So this material has been in service in some cases for decades, and the possibility of having failures is higher. Sometimes the cement integrity is compromised due to the presence of channels called leakage paths. Some of these channels can be the result of defects during the well construction or can be the consequence of mechanical, chemical and physical processes during the well life that induce alteration and degradation in the barriers. For this reason, the evaluation and quality assessment of annular cement elements become of paramount importance. The consequence of an incorrect evaluation can be critical and may compromise the planning and execution of the P&A project as a whole.

In this thesis, annular cement barriers are the object of study. The research presented aims to improve the understanding of the correlation between the annular cement barrier quality and their potential to leak. The study was consisted of three main parts. First, studying how the annular cement barriers fail, what regulations are in force for their qualification and which techniques are used for their evaluation in the field. This part is presented in Chapters 1 and 2. The second part presents the planning and execution of full-scale experiments where annular well barriers with typical defects were investigated using six cell specimens. The results presented include leak testing with gas and water, ultrasonic logging and infrared thermography. Additionally, the characterization of bulk cement properties is presented as

part of this thesis so that the macro properties of the cells and micro properties of the bulk cement can be discussed. The results of this second part can be found in Chapter 3 and 4. Finally, Chapter 5 presents the construction of a well facility, currently available for the testing of logging tools used in the field as solutions for the qualification of annular cement barriers.

This document is organized by compiling the studies and research developed during the PhD. An important part of the results presented in this document was published in journal and conference papers listed in this document. Each chapter can be read stand alone and each includes a general introduction to the topic, aa discussion of the results and conclusions. The units of the original publications have been maintained in this thesis, so a mix of international units and field units are included and some inconsistencies between the chapters can be found. This thesis is submitted to fulfill the requirements of the PhD cotutelle degree, established in the agreement between the University of Stavanger and the Federal University of Rio de Janeiro- COPPE and a thesis with identical content and in two formats is being delivered for each institution.

Objectives of this study

0.1 Main Objective

Study the correlation between integrity assessment and sealing capacity of annular cement well barriers in the context of permanent plug and abandonment of oil and gas wells.

0.2 Detailed Objectives

- To review the international regulations and best practices for the evaluation of annular cement barriers.
- To carry out a comparative analysis of P&A requirements for qualification of annular cement well barriers, with a particular focus on Brazil and Norway.
- To present state-of-art of cement evaluation technologies used in the oil industry and their technical limits.
- To perform leakage experiments in full-scale test cells reproducing typical downhole defects.
- To evaluate the correlation between cement properties, microannuli development and leakage rates.
- To perform physical characterization of annular cement well barriers and evaluate their in-situ ageing.

0.3 Thesis Structure

The current document tries to compile the research efforts completed in the last years to better understand the problem of well integrity due to the migration of fluids in annular cement barriers. Some of the results presented in this document are part of ongoing research projects such as the Fluid Migration Project granted

by the Research Council of Norway and activities developed under the joint industrial program led by NORCE entitled the P&A innovation program. The thesis is structured as follows:

Chapter 1 compares the current regulation and guidelines for P&A for the North Sea and Brazil. The chapter concludes by discussing the road maps for new P&A technologies in the last five years and the period ahead.

Chapter 2 highlights the importance of annular well barriers. It briefly introduces the process of cement degradation using a diagram that interconnects degradation reactions with consequences leading to a barrier failure. Relevant technologies used by the oil industry to evaluate annular barriers and technical gaps are also presented and discussed.

Chapter 3 presents studies of leakage potential for four different cases of cement defects. The cases evaluate different downhole scenarios. First, Case 1 simulates a perfect debonding around the casing. Second, Case 2 studies a water channel present in the cement. Third, Case 3 presents a heterogeneous defect with irregular microannuli where the migration path is more complex. Finally, Case 4 presents results from real field sandwich sections recovered from an oil well cemented in 1985. Results of leakage are compared and analyzed with typical equations used to evaluate permeability. In the final part of this section, the results are discussed.

Chapter 4 introduces a study of cement durability using samples cut from the field sandwich sections that were leak tested in the previous chapter (Case 4). The Valhall cells offered a unique opportunity to characterize cement samples cured in downhole conditions for more than 30 years. The results of cement samples recovered from oil wells are rare. The results presented include petrophysical, mechanical and chemical properties to complete the characterization of cement core plugs. Also, it is presented a study of the distribution of cement properties within a cross-sectional slice of cement and casings. All the results collected are discussed in light of the durability diagram presented in Chapter 2, to establish the current alteration/ degradation in the samples.

Chapter 5 presents the construction of a well completion to support the qualification of cement logging tools. The facility was constructed as a joint effort between different organizations to attend to the need for a large-scale facility to evaluate the performance of logging tools to detect cement defects with known properties. First, material selection and criteria used are presented, followed by a discussion of the well for installation of well completion and a pretest to evaluate survival. Finally, the design of the well completion and cementing operation are included.

Finally, Chapter 6 presents the final discussions and recommendations of the research results presented in this thesis.

List of Publications

0.4 Publications as the main author

1. **Construction of a reference well to support the qualification of cement evaluation logging tools and data processing.**
   Paper to be presented at the SPE/IADC International Drilling Conference and Exhibition -2022
   Katherine Beltrán-Jiménez, Ioan Alexandru Merciu, Dave Gardner, Amit Govil, Sandip Bose, Stig Lomeland, Pål Viggo Hemmingsen, Olga Kuragina, Rune Godoy, Konstantin Mitelshtet, Eirik Berg
   `https://doi.org/10.2118/208699-MS`
   Contribution: Research, planned and execution of experiments, interpretation of results, lead the manuscript writing.

2. **Restoration of annular zonal isolation using localized casing expansion (LCE) technology: Treatment of near-horizontal test sections containing a free-water channel**
   Journal of Petroleum Science and Engineering
   Katherine Beltrán-Jiménez, Hans Joakim Skadsem, Jonas Kristoffer Sunde, Dave Gardner, Tim Wolterbeek, Erik Cornelissen, Wout Keultjes
   `https://doi.org/10.1016/j.petrol.2021.109792`
   Contribution: experimental methodology, investigation, discussion of results, contributions in writing the manuscript.

3. **Cement properties characterization from a section retrieved from an oil production well after 33 years of downhole exposure.**
   Journal of Petroleum Science and Engineering, Volume 208, Part A, January 2022, 109334
   Katherine Beltrán-Jiménez, Dave Gardner, Steinar Kragset, Kidane F Gebremariam, Oscar AM Reales, Mona W Minde, Marcelo IL de Souza, Jan A Aasen, Hans J Skadsem, Laurent Delabroy.

https://doi.org/10.1016/j.petrol.2021.109334
Contribution: Desing and implementation of methodology, planning and execution of analyses,lead the manuscript writing

4. **Assessment of Corrosion in the Interface Casing-Cement and its Effect on the Leakage Potential.**
Paper presented at the SPE/IADC International Drilling Conference and Exhibition -2021
Katherine Beltrán-Jiménez, Ishtiaque Anwar, Kidane F Gebremariam, Steinar Kragset, Dave Gardner, Hans Joakim Skadsem, John C Stormont.
https://doi.org/10.2118/204080-MS
Contribution: Experimental planning, Experimental execution, paper writing

5. **Leakage Through Micro-Annulus Geometries Incorporating Pressure-Driven Elastic Deformation.**
Paper presented at the Offshore Technology Conference Brasil, Rio de Janeiro, Brazil, October 2019.
Katherine Beltrán-Jiménez, Hans Joakim Skadsem; Dave Gardner; Steinar Kragset; Marcelo Igor Lourenco de Souza.
https://doi.org/10.4043/29718-MS
Contribution: experimental execution, discussion, lead the manuscript writing.

6. **Comparative Analysis of Permanent P&A Requirements and Consequences in Terms of Leakage - A Case Study.**
Paper presented at the Offshore Technology Conference Brasil, Rio de Janeiro, Brazil, October 2019.
Katherine Beltrán-Jiménez, Hans Petter Lohne; Eric Patrick Ford; Hans Joakim Skadsem; Marcelo Igor Lourenco de Souza; Øystein Arild.
https://doi.org/10.4043/29814-MS
Contribution: Research, bibliographic review of regulations, case test planning, lead the manuscript writing.

0.5 Aditional Publications as coauthor

1. **Effects of confinement pressure on the mechanical behavior of an oil well cement paste.**

Journal of Petroleum Science and Engineering, Volume 208, Part E, January 2022, 109769

Victor Nogueira Lima, Flavio de Andrade Silva, Hans Joakim Skadsem, **Katherine Beltrán-Jiménez**, Jonas Kristoffer Sunde.

https://doi.org/10.1016/j.petrol.2021.109769

Contribution: bibliographic review, discussions and review of manuscript draft.

2. **Study of ultrasonic logs and seepage potential on sandwich sections retrieved from a North Sea production well.**

   SPE Drilling & Completion 1–15.

   Hans Joakim Skadsem; Dave Gardner; **Katherine Beltrán-Jiménez**; Amit Govil; Guillermo Obando Palacio; Laurent Delabroy.

   https://doi.org/10.2118/206727-PA

   Contribution: Experimental execution, contributed to the interpretation of the results, discussions and review of manuscript draft.

3. **A Comparison of the Measured Properties of Annular Cement with Ultrasonic Cement Evaluation Logs**

   Paper presented at the SPE/IADC International Drilling Conference and Exhibition -2021

   Dave Gardner; Hans Joakim Skadsem; **Katherine Beltrán-Jiménez**; Amit Govil; Guillermo Obando Palacio; Laurent Delabroy.

   https://doi.org/10.2118/204015-MS

   Contribution: Experimental execution, contributed to the interpretation of the results, discussions and preparation of manuscript draft.

4. **Fluid Migration Characterization of Cemented Sections Retrieved from a North Sea Production Well**

   Paper presented at the SPE/IADC International Drilling Conference and Exhibition -2020

   Hans Joakim Skadsem; Dave Gardner; **Katherine Beltrán-Jiménez**; Steinar Kragset; Laurent Delabroy; Frank Ruckert.

   https://doi.org/10.2118/199662-MS

   Contribution: contributed to experimental execution and interpretation of the results, discussions and preparation of manuscript draft.

0.6 Awards, oral presentations and press release

1. Winner of the PhD student of the year award given by SPE Stavanger Section, May 2022

2. Article intitle "O poço do futuro, perfurando para o tamponamento e Abandono". TN petroleo Magazine edition 137-202. Pages 36-37.
   `https://tnpetroleo.com.br/revistas/issu/2021-setembro-outubro/`

3. Offshore Well Integrity - OWI LATAM 2021. Invited as speaker in the Panel discussion "Driving Forward P&A In Latin American Waters".
   `https://offsnet.com/content/latin-america/driving-forward-p-a-in-latin-american-waters`

4. Offshore Well Integrity - OWI LATAM 2020 - Virtual. Speaker.

5. Webinar in decommisioning and P&A session, Event organized unver `https://www.youtube.com/watch?v=d_tneUVyJ-w&t=9s`

6. Offshore Well Integrity - OWI LATAM 2019. Speaker.

Chapter 1

Plug and Abandonment an overview

1.1 Well abandonment Regulations and guidelines

When the decision for well abandonment has been taken, a process to study, document and select the optimal P&A design for the well in question starts. The complexity or simplicity of the design is mostly ruled by the well integrity status. However, other factors play a role, such as:

- Well Design: depths, rock intervals and casing points. Cement conditions behind the casings, open well sections and well deviations.
- Stratigraphic sequence of each well showing presence and quantity of formations with potential to flow with flow potential and information about the types of fluids and reservoir pressures for the whole period of abandonment.
- Logging and data about the cementing jobs.
- Identification of sealing formations and their mechanical properties, so that they prove to be suitable to constitute element of barriers
- Specific conditions of the well such as the presence of scales, casing collapse, presence of hydrates, H2S or other peculiar situations.
- Local regulations

Once the assessment of well status is completed, the planning for the installation of a set of internal plugs into the well follows. The goal of these internal plugs is to create impermeable barriers with good adherence to the well diameter, which are be

able to contain the fluids inside the wellbore, preventing any type of migration from the well to the sea or atmosphere or between formations [6, 18]. Here, it is relevant to define three important terms normally used when talking about well barriers: barrier envelope, well barrier element and primary/secondary barrier.

The international well control forum (IWCF) defines the well barrier envelope as a combination of one or more element barriers that together constitute a method of containment of fluids that prevents uncontrolled fluid movement into another formation, or from escaping to the surface. A Well Barrier Element (WBE) is defined as a part of a well designed to prevent fluids from flowing unintentionally. The primary well barrier element is the first level of protection that prevents fluid flow, while the secondary barrier is the second element. Note that the primary barrier indicates the first element that could stop a possible influx coming from the formation with a potential to flow while the second barrier can act as a contingency in case of a failure of the first one. The well barrier elements are defined in all well stages but regulators have introduced the explained concepts to account for the fulfilment of requirements. The terminology of well barrier envelope, WBE and distinctions between primary and secondary barriers are frequently used in official documents submitted by oil field operators. It was found that international regulations present slight differences in wording to introduce those concepts but in principle, their conception and application are similar[19, 20, 24].

In the context of P&A, common WBE are casing strings, annular cement, internal plugs and impermeable formations. Internal plugs can be installed inside the casings or in contact with the formation, covering all the well diameter, as presented in Fig. 1.1

Figure 1.1: Two cases of well barrier envelopes, indicating the well barrier elements (WBE) present

For each formation with a potential to flow, two barriers are normally installed: a primary well barrier and a secondary barrier. Both well barriers comprise the barrier envelope, whose goal is to try to re-establish the natural seal (cap rock) removed during the drilling phase [6]. The sealing must be effective in all directions: vertical, radial and azimuthal. Fig. 1.2 shows two hypothetical designs of P&A for

a well. The primary and secondary barriers are indicated. The figure also shows, the surface barrier, also known as an environmental barrier, which is the last option to retain a possible influx into the well. This environmental barrier, however, is not mandatory in all countries. To understand better the difference between regulations, the next section will discuss the well barrier definition in depth.

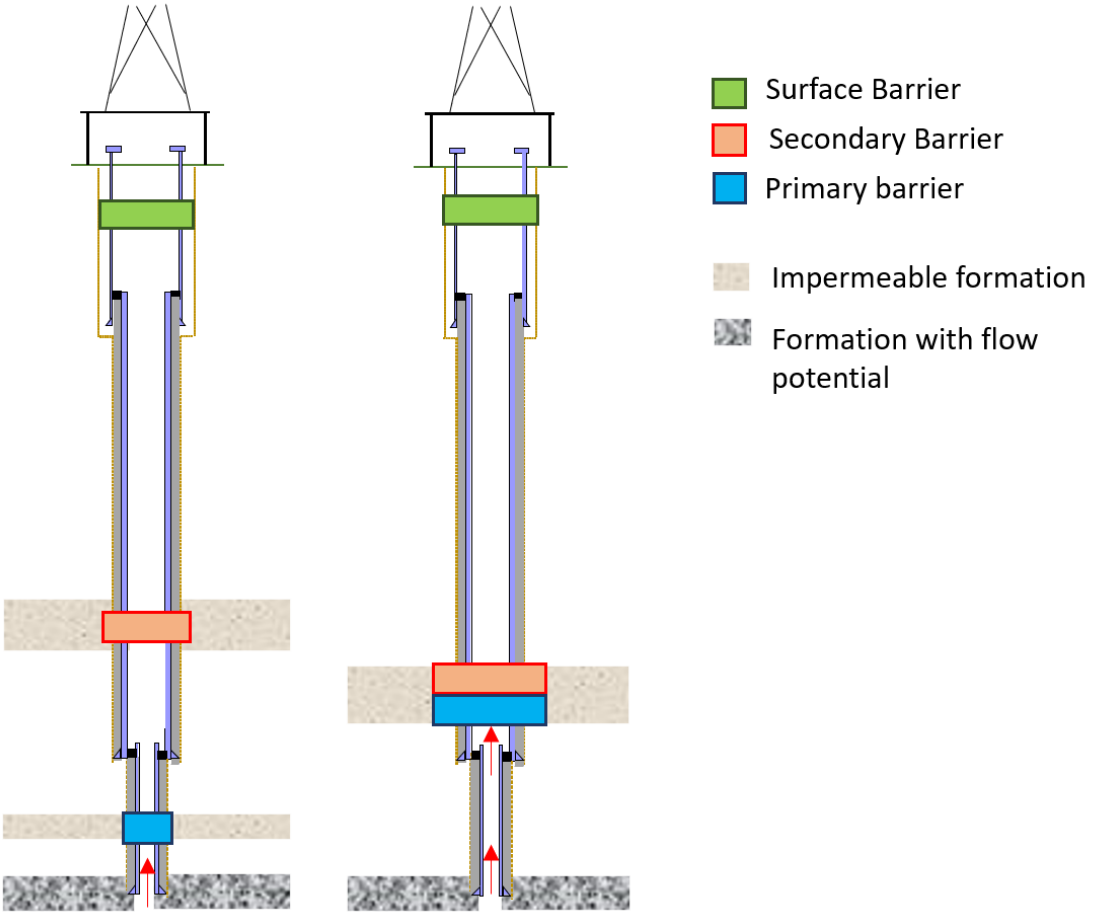

Figure 1.2: Diagram showing two simple P&A designs, indicating the first, second and surface barriers.

1.1.1 P&A in the International Agenda

Just a few studies have been performed concerning legislation, guidelines and procedures for P&A. Among them, an overview considering 10 countries and their legal regulations of Plug and Abandonment was presented by Van der Kuip et al [25]. Also, the International Association of Oil & Gas Producers published an overview of P&A regulations considering 32 countries on five continents [26]. Both studies pointed out that there do no exist specific P&A rules or guidelines with international obligation applied by sovereign states as part of a treaty or international agreement.

Instead, the standards have a more national coverage and it is up to each country to create its own rules for P&A. The result is that national requirements for P&A are minimal or absent in most countries of the world. As a consequence, it is often the oil operator who determines the optimal approach. The problem with the lack of specific regulation is that the operators can choose wheater to apply their company standard, which can be stricter than the local regulation, or to simply perform the abandonment using the cheapest way.

In the countries that have specific regulations for P&A, there is a general agreement that wells need to be abandoned in a way where the preservation of the environment is the highest priority, and that the well integrity needs to be maintained over the long term. On the other hand, one of the main points of disagreement is the minimum length barrier accepted [27]. The minimum length barrier applies for both the length of an internal cement plug and the cement placed in the annular space between the casings, which is usually called primary cement. It is also observed that there is rarely clear reasoning behind the "rules" on minimum length; rather they seem to be a result of national consensus or similar.

Reviewing in detail the guidelines in different countries, it was found that some consider one long barrier of 100 m to be acceptable, while other countries consider two barriers (primary and secondary) of 30 meters each as the minimum. Table 1.1 shows the requirements found and their differences for some of the countries reviewed.

Table 1.1: Minimum cement length barrier required based on regulations/guidelines for different countries

Country	Number of barriers	Barrier length (m)	Reference
UK	2	30	UK Guidelines [20]
Norway	2	50	NORSOK[28]
Netherlands	1	100	Dutch Mining Act [29]
USA [1]	2	30	30 CFR 250 [30]
Canada	1	30	Drilling and production guidelines [31]
Abu Dhabi	1	50	ADNOC [32]
Australia	1	not specified	NOPSEMA [33]
Malaysia	1	30	Petronas [34]
Brazil	2	30	IBP[24]

Recently, the American Petroleum Institute-API, published the API BULLETIN E3: Wellbore Plugging and Abandonment Practices [35] which compiled recommendations for the industry. However, regulators and oil operators in the North Sea and the Norwegian Continental shelf (NCS) have been documenting discussions, lessons learned and incidents for a long time, those resulting in the guidelines and recommended standardized practices for P&A in The Norsk Sokkels Konkuranseposisjon

[1]Note that the guidelines are for the Outer Continental Shelf Lands Act (OCSLA). However, each state may have its own variations.

- NORSOK[28] and Oil and Gas UK (O&GUK)[20]. Both documents represent the most important references to consult on wells P&A, and they are normally updated from time to time based on discussions and following up new technological developments. The latest versions of the reference guidelines from the North Sea (NORSOK and Oil and Gas UK) are presented in detail, together with the current Brazilian regulation [24], so that a comparison between them can be made.

1.1.2 North Sea Overview

Norway

The regulating body in Norway is the Petroleum Safety Authority Norway (PSA), established by the Norwegian Petroleum Directorate (NPD) in 2004. The PSA is responsible for determining parameters for the oil industry and ensuring that activities in this sector are conducted in a prudent manner. The current regulations for P&A operations are included in two documents. The first one is the Activities Regulation, Chapter XV, Sections 85 (Well barriers) and 88 (Securing wells) [36]. The second one is the Facilities Regulation, Chapter VII Section 48 (Well barriers)[37].

The NORSOK standards are a group of guidelines developed by the Norwegian petroleum industry to help understand the regulations for oil development in Norway. They depict ways to do operations, that ensure compliance with regulations. The NORSOK D-010 document is focused on well integrity in drilling and well operations throughout the well life (from drilling to abandonment). The first version was published in 2004 and five revisions have since been published. The new version normally includes changes in the legislation and adaptations in relation to the evolution of new technologies. NORSOK D-010 states the minimum requirements to maintain the well integrity during well operations. Well integrity is defined as the "application of technical, operational and organizational solutions to reduce risk of uncontrolled release of formation fluids throughout the life cycle of a well".

Table 1.2 presents the minimum requirements for P&A in Norway. This type of table was previously presented in other publications [26, 38] and the same categories are used for reference. The information included in the table corresponds with the latest update in guidelines, which in this case corresponds to the 5th revision of the NORSOK D-010[19]. Among the important inclusions in the 5th revision, it is worth noting the acceptance of Perforate Wash and Cement (PWC) as an alternative method to establish a permanent barrier. A more flexible approach regarding the inclusion of cables and control lines as part of the barriers when it is possible to completely isolate the elements; and the inclusion of creep shale as an additional well barrier element which can form the well integrity envelope.

Table 1.2: Barrier requirements for permanent P&A in Norway

Item		Minimum requirement
Barrier	Material	Cement or other verified Materials
	Verification	Open hole: depth verification by tagging. Cased Hole: depth verification by tagging and pressure test of 1000 psi above the expected leak off pressure below the casing point or the leak formation. For surface plug 500 psi. Comments: If the cement plug is placed on a foundation (as a bridge/mechanical plug), the pressure test is not required, only the depth verification by tagging. Casing cement length shall be verified by one of the following: 1. Bonding logs: FIT for purpose, azimuthal/segmented data; 2. 100% displacement efficiency. Actual displacement pressure/Volumes vs. simulation losses.
Plug Requirements	Reservoir	Two well barriers are required. Primary barrier: length should be 100 m with, 50 m above any source of inflow /leakage point. Secondary barrier as back up to primary, minimum 100 m MD. If is placed in transition from open hole to casing should extend at least 50 m MD below casing shoe.
	Intermediate zones	Barrier must be installed between zones with different pressures to prevent flow with a minimum length of 100 m. This barrier also can act as a primary barrier for the lower reservoir.
	Surface	50 m MD if the plug is set on a mechanical plug otherwise 100 m MD. The casings should be cut and retrieved, and the plug will be placed to isolate flow to the surface.
Annular barrier requirements		Cement in the liner/ casing / tubing annulus can be accepted as a permanent well barrier when: 1. 30 m MD verified by bonding logs 2. 50 m MD verified by displacement calculations 3. 60 m MD verified by bonding logs when the same annular cement will be part of the primary and secondary well barrier.
Control lines		In general, control line and cables shall not form part of the permanent well barrier. However, they may form part if complete isolation is achieved
Seabed		In shallow waters (600 m) total removal of wellheads and cutting of casing below the seabed should be performed. In deep waters, it may be acceptable to leave or cover the wellhead.
Monitoring		No specific guidance. But tests may be required to document the long-term integrity

United Kingdom

Offshore activities in the United Kingdom Continental shelf (UKCS) are regulated by the Department for Business, Energy and Industrial Strategy (BEIS) through The Petroleum Act 1998[39], amended by the Energy act in 2008 [40] and 2016 [41]. Section 75 of the Energy Act grants the right to the state to acquire information and take action regarding well abandonment operations under oil licenses. This, combined with the regulations for Offshore Installation and Wells [42] provide the basis for P&A requirements in the UK.

The O&GUK is a community representing the UK offshore oil and gas industry, which works closely with operators and the government to address issues that impact

their business. P&A has been a topic of their interest since 1995 when their first guidelines for well decommissioning was published. Since then, the document has been updated six times (in July 2001, July 2005, March 2009, July 2012, July 2015 and June 2018). The version reviewed in this document corresponds to the sixth edition [20], which applies to all exploration, appraisal and development wells that are being P&A. Additionally, the O&GUK have published guidelines on qualification of materials [43] and on well abandonment cost estimation [44]. These last two documents were not reviewed in detail in this thesis but are recommended to consult.

Particularities are observed in the O&GUK guidelines [20], such as the inclusion of an exceptional recognition of the singularity of each well, proposing that their P&A should be considered on an individual basis. It also presents an extensive review describing the verification of annular well barriers in specific scenarios such as through-tubing, cased hole on a mechanical barrier and the combination of both. Table 1.3 presents an overview including similar items to the table presented for Norway.

Table 1.3: Barrier requirements for permanent P&A in the United Kingdom based on O&GUK guidelines and recommendations

Item		Minimum requirement
Barrier	Material	Cement is the primary material, but this does not preclude the use of other materials.
	Verification	Verification requirements are dependent on the individual well and job design. In general, for barriers placed into the wellbore or tubing, tag and pressure tests are required.
Plug Requirements	Reservoir	All zones with flow potential require a minimum of one permanent barrier. Hydrocarbon-bearing or over-pressured and water-bearing zones require two permanent barriers. Barriers are required to be of 100ft of good cement, set above the zone of flow potential and across suitable caprock.
	Intermediate zones	All zones with flow potential require a minimum of one permanent barrier. Hydrocarbon-bearing or over-pressured and water-bearing zones require two permanent barriers. Barriers are required to be of 30 m of good cement, set above the zone of flow potential and across suitable caprock.
	Surface	permanent barrier, for shallow zone with flow potential, of 30 m of good cement.
Annular barrier requirements		Good cement bond, minimum 30 m if previously logged or 300 m above the base of the barrier if estimated from differential pressures
Control Lines and cables		These should not form part of permanent barriers since they may be a potential leak path.
Seabed		Reviewed on well by well basis. Subsea/wellhead equipment to be removed and debris retrieved where practical to a minimum radius of 70 m and seabed clearance certificate issued.
Monitoring		Well examination is not required once wells are "Phase 3" abandoned (i.e. wellhead and conductor removed (definitions of Phase 1 and 2 abandonment provided in Guidelines for the Abandonment of Wells).

1.1.3 Brazilian Overview

According to official numbers from ANP, by February 2019, the total number of drilled wells in Brazil was 29,752, out of which 23,070 correspond to onshore wells and 6,700 to offshore wells. Activities of P&A have increased since the change in regulations in November 2016. For instance, in 2020 alone, 20 wells were permanently plugged and abandoned with an average operational time of 36 days, all of them offshore abandonment[15].

The regulatory agency is the National Agency of Petroleum, Natural Gas and Biofuels (ANP), established in 1998. ANP oversees operations and is responsible for the regulation of the entire oil industry supply chain. In well abandonment operations, the SGIP (Sistema de Gerenciamiento da Intergridade de Poços) is the technical regulation that should be followed for onshore and offshore wells. The last version of this document is presented in the Resolution ANP N 46/2016 of November 2016, which is replacing the regulation ANP N 25/2002. The main changes between the two versions are the inclusion of the well barrier concept and taking a more preventative and less prescriptive approach. Which also considers monitoring after abandoned and a period of two years to adapt irregular wells to the new regulatory standard.

The updated version N46/2016 references the consultation of international regulation, so that NORSOK D-010 standard [28] and Guidelines for the Suspension and Abandonment of Wells by Oil and Gas UK [20] were reference documents for its upgrade.

As a response to this change of regulation, which established a shorter deadline to fulfill the requirements by operators and a non-prescriptive approach, the Brazilian Institute of Oil, Gas and Biofuels (IBP) invited oil operators to create a group to discuss the minimum requirements for P&A between operators in Brazil.

IBP is a private institution that, among its activities, promotes the dissemination of knowledge related to the oil industry in Brazil. The guidelines for well abandonment [24] were released in May 2017 as the result of more than one year of discussions by a technical commission composed of professionals from oil operation companies and governmental institutions. The document intends to help the current and new operators in Brazil to understand the requirements of ANP N 46/2016 for different scenarios. Included were not only the typical offshore scenarios in Brazil of deep and ultradepth waters but also operations in shallow waters and on land.

An overview of the requirements for Brazil is presented in Table 1.4.

Table 1.4: Barrier requirements for permanent P&A in Brazil

Item		Minimum requirement
Barrier	Material	Cement or other material with similar properties. Mechanical barriers.
	Verification	Open hole: depth verification by tagging applying a weight of of 10 -15 Klb with drill pipe . Cased Hole: depth verification by tagging and pressure test applying 500 psi over the LOT pressure in the casing shoe or pressure expected in the leak point. If a surface plug is placed, the verification is not required. Comments: The verification by weight can be avoided if a risk analysis is performed showing no risk. The pressure test is not required in case of inconclusive results, and when three conditions are present: 1. Plug in a cased hole. 2. Presence of foundation that was verified by pressure (mechanical plug, shoe track, or cement plug) 3. The section below the plug is not a zone that was perforated or a leak source.
Plug requirements	Reservoir	Two well barriers are required. The second barrier should be as close as possible the primary barrier.
	Intermediate zones	Barrier must be installed between zones with different pressures to prevent flow. IBP suggest a minimum length of 30 m MD.
	Surface	Is not a requirement. In cases of aquifers with a public interest, a surface plug shall be installed. In cases where the wellhead was removed, and the casing was cut, a plug of 60 m should be placed.
Annular barrier requirements		The IBP suggest that the cement in the annulus can be accepted when: 1. 30 m of good cement are proved using logs (no specific details are mentioned about the criteria of good quality of cement) 2. If the well has absence of abnormalities during the primary cement job execution and the well life cycle (60 m of good cement are required).
Control lines		Control line and cables shall not form part of the permanent well barrier
Seabed		Total removal and casing cutting are not required. In offshore wells when the wellhead is less than 80 m water deep, total wellhead removal and casing cutting is a requirement.
Monitoring		No specific guidance.

1.1.4 Comparison Between Regulations

In this section, a comparison between the interpretation of the regulations (guidelines/standards) in the North Sea and Brazil is presented. The following findings can be highlighted: first, the difference in the plug lengths.The Brazilian requirement of a shorter plug of 30 m is in alignment with the length proposed by Oil P&A Gas UK, however the Norwegian regulations propose a plug 20 m longer as a barrier.

Secondly, the lack of surface plug and removal of wellhead for offshore wells in Brazil differs from both UK and Norwegian guidelines where the environmental plug is always recommended. In Brazil, the installation of a surface plus is a requirement only for onshore wells. The requirement of the surface plug represents an increase in

cost due to the time-consuming activities of cutting and retrievaling casings before plug placement.

Thirdly, there are differences in the verification of annular cement between the 3 regulations. Norwegian regulations require logging to prove 30 m of good cement bonding while the Brazilian guidelines are less clear about the method to prove annulus cement quality. In Brazil, good annular cement quality can be proven using different methods such as well historical records, logging and operational parameters. The length requirements are similar but the acceptance criteria concerning requirements to define a good cement condition are not explicit. This looks to be more in agreement with the guidelines in the UK where in lieu of logging, 300 m of barrier could be approved by differential pressure.

Regarding verification of internal plugs, all three guidelines consider the verification by tagging and pressure, however, the Brazilian guidelines include a verification by weight that can be dispensed in exceptional cases if a risk analysis is done, proving no risk. As to the positioning of well barriers, in Brazil, the plugs shall be aligned with the cap rock just over the leak source or as close as possible to it, while in Norway the positioning is more dependent on the well design. If the plug is placed in a transition between open and cased hole, 50 m of the plug should be in the cased hole.

Comparing the three regulations is not a straightforward task due to the differences in the well designs and geological characteristics of their basis. It is also complicated to decide which of the requirements minimize the risk of a well barrier failure. For this reason, there is a need for methodologies that can quantify the quality of a given P&A solution, where variables such as the risk of leakage in the long term are evaluated. A paper previously published by the author of this thesis presented a case study comparing different P&A designs for the same well based on the regulations in Norway and Brazil [17].

1.2 Roadmaps for P&A technologies

Adherence to prescriptive regulations and standards may reduce the probability of leakage, but it does not help the industry to generate improvements in cost reduction. Nowadays, P&A represents a notably high cost for oil operators, thus there is a need for innovative solutions that can cut costs or improve the efficiency of processes. According to IHS, the average rental cost of a semisubmersible is 140,000 USD/day, for a drillship, it is 250,000 USD/day and a Jackup costs 62,000 USD/day [45]. On the Norwegian continental shelf, a permanent P&A can take two to four weeks and in Brazil, it takes approximately four weeks. If an innovative solution reduces the platform time by 20%, this will represent a relevant impact on the cost

reduction of P&A operations.

Even though the oil industry is normally slow to introduce radical changes in its operations, in Norway the *Norsk olje & gass* has been working to establish a roadmap for P&A technologies [1]. The goal is to guide focus areas with the potential to generate technological developments and identify areas with high demand for innovation. One of the first roadmaps was released in 2017, see Fig. 1.3. By then, the overall goal was to move operations towards rigless P&A, aiming to cut the cost of platform rental.

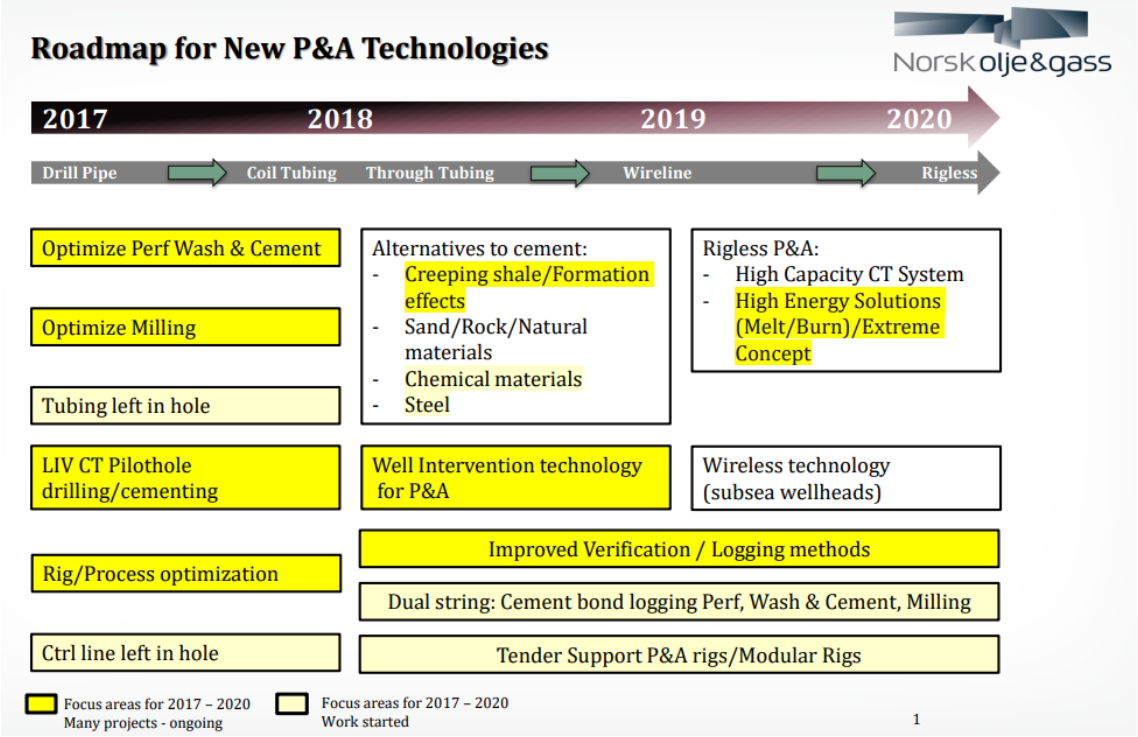

Figure 1.3: Roadmap for new P&A Technologies period 2017-2021, Issued by Norsk Olje & gas in 2017 [1]

Since 2017, some efforts have materialized in the increase of technological maturity of some of the activities listed in the P&A roadmap. A way to measure the advance of the technology is using their Technology Readiness Level (TRL). Levels of TRL are ranked from 1 to 9, where TRL 4 considers a proof of concept tested in the laboratory, TRL 7 includes a demonstration in the operational environment and TRL 9 presents a system completed, qualified and proven in its operational environment.

If an evaluation of the advance in TRL of technologies included in the 2017 roadmap is studied, it is observed that since then, technologies such as Perforate Wash and Cement (PWC) have been proved as an alternative for section milling. PWC is now in a higth TRL, according to several studies and field cases published [46–50]. Even the Norwegian regulator published a report documenting its final

qualification [51]. Tubing and control line left in hole continues in a TRL 3 since 2016 when the proof of concept was published [52]. In alternative materials to cement, important advances took place in the last years on Geopolymers and thermal solutions such as Bismuth [53–56] and Thermite [54, 57–60], but both are still in a low TRL of 3-4, with the first field trial tested only recently [61]. Regarding creeping shale as complementary barriers, studies of formations and creeping effects have been widely studied in the laboratory [62–65] and in field cases [66–68], so that they can be considered in a TRL between 5-6.

More recently, the *Norsk olje & gas* published a new roadmap for P&A technologies from 2021 to 2025 +, as an updated version of the previous version of 2017 [69]. The updated roadmap is presented in Fig. 1.4, which certainly continues with the overall goal of moving to a rigless P&A operation but also highlights 5 areas for development: well diagnostics, access to establish barriers, establishing barriers, verification and casing and conductor removal.

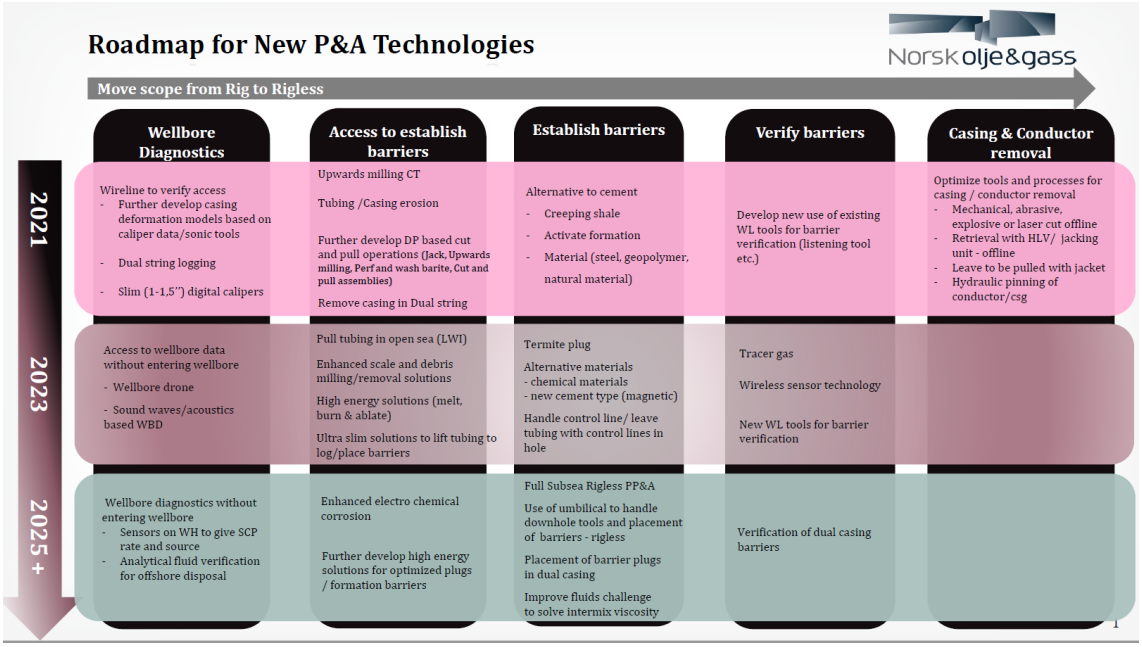

Figure 1.4: Roadmap for new P&A Technologies period 2021-2025+, Issued by Norsk olje & gas in 2021

Besides the reduction in cost of rigless operations, advances in the diagnosis and verification of annular well barriers seem to be a relevant challenge for technologies in the upcoming years. In a survey completed in 2016, the committee of the Plugging and Abandonment Collaborative Environment (PACE) defined the priorities for research and development on P&A. The committee is mostly composed of operators and service companies in the United States but also some companies operating in Europe. The survey revealed that 21% consider cost-effective plugging and sealing as the most important topic, while 20% consider Rigless P&A, 19% barrier

verification and string multilogging, 12% novel barrier materials, 10% monitoring of abandoned wells for leakage, 8% removing equipment, 5% remediation of poor P&A and 3% removal of casing and completion[70]. Clearly, the direction of the needs in technological development for P&A in the Norwegian continental shelf included in the roadmap seems to be in agreement with the consensus in PACE.

1.3 Final Remarks

Internationally, the concept of a well a barrier is well understood. In general terms, regulations (guidelines/standards) present similarities in the barrier principle and the elements required to constitute the well barrier systems. However, some differences were identified between countries, especially in the internal plug length, verification methods, depth of plug setting and the total number of plugs.

When comparing the two roadmaps for the development of P&A technologies, it is observed that in the last 5 years some technologies have been pushed to higher TRL. Even when the challenges continue focusing on the same areas for the period ahead, the more descriptive approach of sub-activities on the latest roadmap suggests that a better understanding of the sub-steps necessary to achieve technological development exists. The non-appearance of topics such as PWC (Perforate Wash and Cement) can suggest that the technology is ready to be absorbed as an industrial solution. In some countries as Norway is already used, while in other countries have not been use yet.

Further, on one hand there is an intention to develop non-invasive wellbore diagnostic tools and on the other hand the P&A roadmap calls for advanced downhole cutting and casing milling techniques. At first glance these two growth directions may see contradictory. While wellbore diagnostics relies in the possibility of evaluate cement and install the barriers without removing the casing, technologies for milling/cutting promote the removal of cement and casing, so that fresh cement can be placed as barrier. The author's view is that this indicates that a unique approach is insufficient to solve the various and diverse case scenarios found when the P&A phase comes. While in some cases the tubing left in the hole can be the best solution for the P&A design, in others the recovery of the tubing can be more suitable.

Chapter 2

Importance of annular cement well barriers

As presented in the previous chapter, an important component of the well barrier envelope is the annular cement, which is composed of the cement installed behind the casing strings during the construction phase . Primary cement jobs are planned to fill annular spaces between casing and formation but also between two casings with the objective of isolating and providing more strength to the wellbore.

Annular cement is present in most of the well stages from drilling to P&A, it is normally exposed to changes in temperature and pressure, penetration of fluid and its quality directly affects the well integrity. Fig. 2.1 shows the well construction stages highlighting occurrence of some typical well operations.

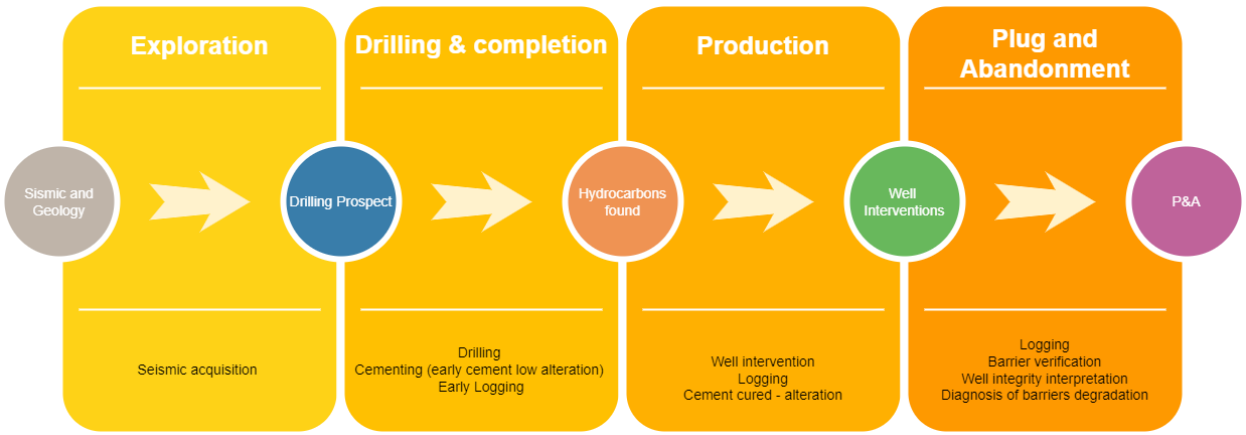

Figure 2.1: Well phases and verification of cement integrity at different times along the well life cycle

During the well life, from exploration to plug and abandonment, engineers look for indications or signs that can alert them to well integrity issues in the annular cement. Typically, the first evaluation is done some hours after the casing is run and the cement slurry is pumped downhole. At this early stage, the slurry has

developed some strength and is unaltered. It is a normal practice to collect cement samples to follow up the strength development using an Ultrasonic Cement Analyzer (UCA) [71]. Usually the drilling of the next section starts only when the cement is hard enough and the cement integrity is not compromised. Even though this is an industrially accepted practice, a few studies comparing UCA and downhole logs over time showed that temperature, contamination, mixing on field and wellbore conditions can lead to a lower real strength than the one observed by UCA [72, 73]. Later on, during the well production period, additional evaluations are collected to assess the integrity of well completion. If something anomalous is observed in the well, a well intervention is needed and it is not rare to evaluate the wellbore using logs prior to the intervention. Finally, prior to abandonment, it is common to collect data on the status of annular barriers to fulfill the quality verification requirement put in force by the regulatory agencies regulating P&A.

2.1 Cement Durability

An important factor when thinking about the long-term service of well cement is durability. One can suppose that several factors can lead to a cement well barrier failure. However, most of the studies in cement integrity are limited to the study of the creation of preferential fluid migration paths and focus on the initiation and propagation of fractures due to pressure changes and pressure/temperature cycling [74–80]. Nevertheless, barrier failure is not dependent only on pressure and temperature. Several other factors have been identified as root causes contributing to a cement barrier failure, for example the penetration of fluids [81] and the reaction with components such as ions than can lead to corrosion. Ferreira et al. [82] presented a complete study of cement durability in the long-term perspective for cement barriers used for radioactive storage. In their paper a conceptual map of cement degradation was prepared. The flow map was modified using the reactions that may occur in a oil and gas wellbore environment and is presented in Fig. 2.2

Numbers from 1 to 35 are included in Fig. 2.2. The numbers identified reactions occurring in the cement structure that as a consequence may lead to a barrier failure. The list below presents a short description and a few academic references that can be further consulted for each reaction. The references included may suggest, observe or prove that the reaction leads to the condition shown.

1. Loss of water due to drying at high temperatures [83–85]
2. Loss of water due to the reduction in the pore space
3. Chemical decomposition of cement phases at temperatures above 100 Celsius

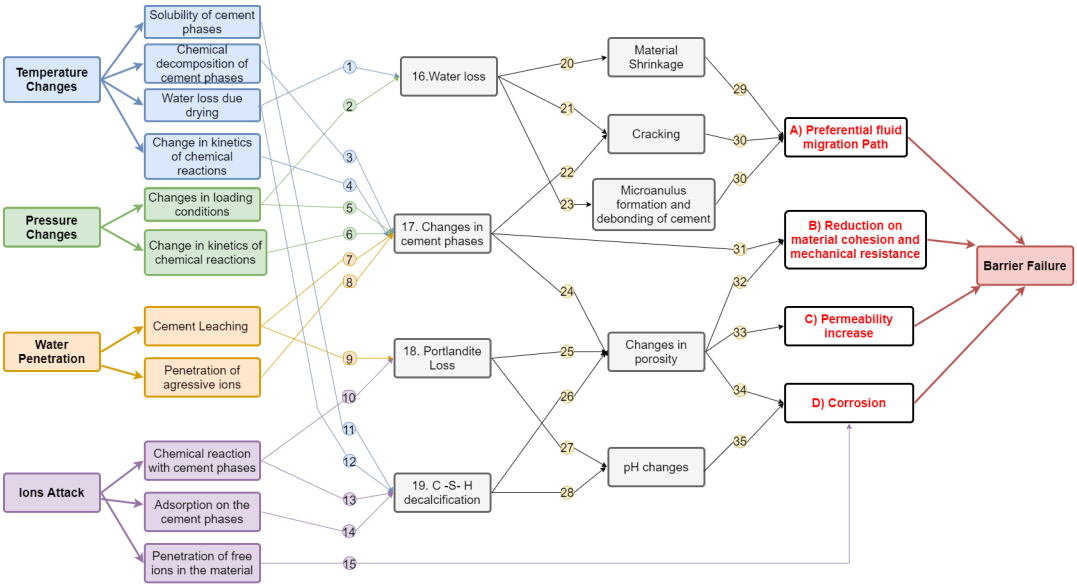

Figure 2.2: Conceptual map of cement long-term durability leading to well barrier failures.

4. Lower hydration degree in the long term, which favours deleterious reaction, as delayed ettringite Formation (DEF)

5. Microstructural changes by Calcium Silicate Hydrate phases (C–S–H) can cause volumetric changes on the cement as contraction and deformation.[86]

6. Lower hydration degree in the long term that favours carbonation reactions

7. Leaching and calcium loss. Formation of phases as brucite and M-S-H.

8. Penetration of ions and reactions with cement hydration compounds.

9. Loss of calcium from Portlandite. Reduces pH of the pore water.

10. Reactions that consume Portlandite. Sulfate[87, 88] chloride and magnesium attack.

11. Solubility changes of crystalline phases. Loss of calcium.

12. Shrinkage due to water loss at C–S–H layers. Changes in the Ca/Si ratio.

13. Reduction of calcium in pore water. Changes in the Ca/Si ratio of C–S–H.

14. Calcium substitution in C–S–H. Decalcification.

15. Chloride and carbonate penetration increases the corrosion of metallic structures.

16. Loss of water, lead to shrinkage and cracking

17. Changes in the cement phases. Loss of resistance and cohesion, cracking, porosity and permeability changes

18. Loss of Portlandite. Reduces pH and changes porosity and pore forms.

19. C–S–H decalcification. Produce changes in pH and porosity and pore forms.

20. Shrinkage due to loss of water

21. Loss of water leads to cracking

22. Changes in cement phases leading to volumetric changes and cracking.

23. Loss of water contracts the cement, allowing the creation of debonding between casing and cement

24. Changes in cement phases leading to volumetric changes and cracking.

25. Loss of calcium from Portlandite and changes in the porosity due to the formation of expansive products.

26. C–S–H decalcification leading to changes in the porosity due to the formation of expansive products.

27. Change of pH of pore water by loss of calcium and hydroxide ions.

28. Change of pH of pore water by loss of calcium and hydroxide ions.

29. Shrinkage of cement causes detachment of the material and leads to the formation of a preferential pathway between cement and geological setting or steel casing.

30. Cracking and microannuli lead to the formation of preferential pathway

31. Changes in cement phases lead to loss of resistance and cohesion by the formation of non-cementitious phases (as M-S-H).

32. Widening of pore size distribution and porosity lead to loss of resistance and cohesion.

33. Increases in porosity; normally lead to increases in permeability

34. Widening of pore size distribution and porosity lead to higher penetration of aggressive ions, increasing corrosion of metallic structures

35. Reduction of pH in pore water reduces the passivation layer provided by cement, which increases the corrosion of metallic structures.

Tracking the reactions listed previously in downhole conditions is quite challenging, especially those that required sampling and post laboratory analyses. Alternatively, the evaluation of cement well barriers in the industry nowadays is focused on the detection of 4 conditions. First, the presence of preferential fluid migration paths in the form of microannuli, channeling or others. Second, indication of loss of sealing as for example permeability increase in cement that allow migration of fluids to the wellhead with evidence of sustained casing pressure or recurrent fluid migration. Third, indications of reduction of mechanical resistance such as casing buckling or a big deformation that suggests possible changes in annular cement integrity. Fourth, evidence of corrosion and pitting on casing components allowing communication. If any of the previous conditions are found during well barrier verification at any stage, the barrier is not suitable to act as well barrier element. The four conditions listed correspond to the red components presented in Fig. 2.2 which can be interpreted as consequences of degradation.

2.2 Evaluation of Annular Well Barrier Quality

Evaluations of annular cement barriers throughout the life of the well can be seen as snapshots of the barrier integrity status and cement quality. As the barrier is varying with age, its working conditions "pictures" are taken to evaluate its status. A simile between the snapshot for a barrier quality and an object in movement being photographed can be imagined. The snapshots of the movements can say something about the position of the object but not the full history of their movement. If several verifications (photos during a dancing performance, for example) are collected, more information about the barrier quality (full set of movements) is collected so that there is a higher chance of a correct well integrity diagnosis.

In general, it is expected that at the time of well completion the cement is relatively young and low traces of alterations are found. Later on, when the well is in production more risk of barrier deterioration is present and the cement might start to show some signs of alteration due to contact with fluids, loading or other causes. Finally, if signs of loss of integrity such as as Sustained casing pressure (SCP) are present, one would expect evidence of degradation. However, as explained by the simile, the snapshots during verification need to be studied carefully to do a correct diagnosis.

While internal plugs can be verified directly within the well, annular well barriers need to be verified using different methods. For example, one can use sonic, ultrasonic and X-ray diagnostics but it is also possible to do hydraulic tests. An overview of methods for the evaluation of annular well barriers is presented in Fig. 2.3 and a short description of each of them is presented in the following paragraphs.

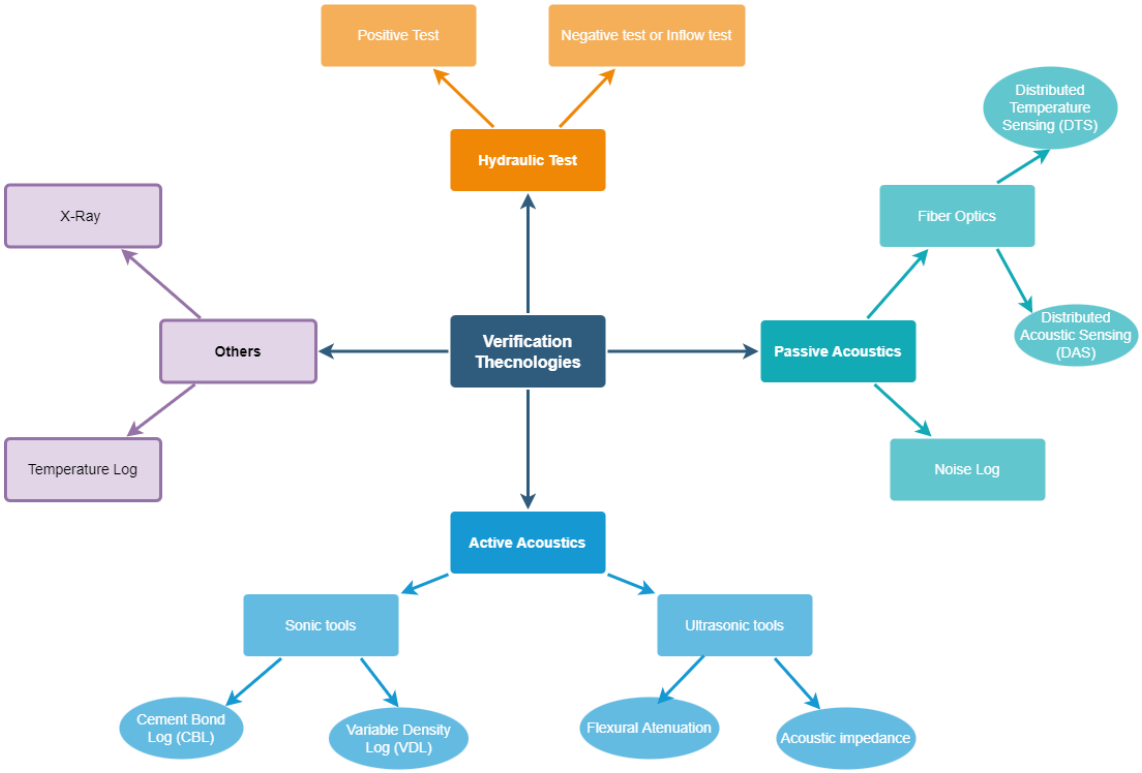

Figure 2.3: Techniques for verification of annular well barriers integrity.

2.3 Hydraulic pressure test

This type of verification is normally used early on during the well life cycle: well completion and production. Two tests that are typically used are known as the positive pressure test and the negative pressure test (also known as inflow test). Both of them allow the verification of isolation provided by the completion (cement and casing) and confirm or not the communication along the annular cement barrier[89, 90].

A positive pressure test is generally completed during well construction at the end of every cementing job (normally, for surface and intermediate casings). The test is performed once the cement has been set and, in some cases, after drilling the casing shoe and a few meters of formation below the casing point. At this stage, pressure is applied and held to verify the casing and cement integrity. Then, the test pressure is slowly increased inside the casing and monitored. A pressure drop could indicate a poor cement job and a remedial job (squeeze) may then be required. If the pressure holds, the hydraulic seal at the casing shoe and in the annular cement is proved. Sometimes the pressure is increased to a limit value to proof seal at a specific working pressure, for example, 5000 psi. In such a case, the test is called the Formation Integrity Test (FIT). On the other hand, if the pressure is increased until the formation is fractured then the test is called the leak-off test (LOT). In

this second case, the goal is to know at which pressure the integrity is compromised. FIT and LOT can be used for testing both formations and cement.

A negative pressure test or inflow test consists of the introduction of a lower pressure inside the casing. Thus, the inflow/pressure variation is monitored. If integrity issues are present the fluids will try to migrate into the casing and will be detected. While the positive tests are more ordinary, the negative test is only used in specific situations, for example, cement plug evaluation, top of liner evaluation and squeeze evaluation. Examples of full-scale test wells can be found published [91, 92]

When both positive and negative tests are completed, it is ensured that the seal is established in both directions. Examples of tools for hydraulic pressure testing for annular P&A barriers are under development by Interwell Norge [93, 94] and Exedra [95].

2.4 Logging Techniques

Cased hole logs have become an important tool for supporting well integrity analyses and helping to classify well barrier elements prior to P&A. Logging technologies intend to evaluate the well barrier's quality by interpreting their geometry and diagnosing the possibility of an integrity issue. In this section, logging technologies relevant to the study of annular cement well barriers are listed and briefly presented. In general terms, technologies used nowadays for the evaluation of cement elements are based on acoustic principles. While commercial wireline electromagnetic tools have shown potential to detect integrity problems associated with corrosion on casings, they cannot say anything about cement well barriers themselves. Hence, they are not presented in this document.

As previously mentioned, acoustic tools are the most common to evaluate annular well barrier integrity and their principles are based on acoustic contact. Acoustic tools can be classified into passive or active. Passive tools are normally simpler and use receivers in the form of microphones, hydrophones or accelerometers to collect the data at a specific point, so that they passively "hear" and record. In contrast, active tools emit a sound and then listen to the response with one or two transmitters and arrays of receivers with different azimuth orientations to collect data at different radial depths. While passive tools can be deployed by cable or wireline, the active acoustics have been developed exclusively as wireline tools and measure the acoustic contrast between the radial layers. The principle relies on the fact that the acoustic wave penetrates the barrier elements (mud, casing, cement and formation) and is reflected. The response observed in the P and S wave velocities are analysed. The wave reflection responses help to identify local variations and irregularities in the

contact between the elements surrounding the borehole.

2.4.1 Passive Acoustic - Noise Logs

Noise logging was first used in the 1950s [96], but it was only in the 1970s that more detailed laboratory studies and field investigations were carried out [97–100]. Nowadays, it is a technology used to detect fluids in motion, creating characteristic acoustic signals called the spectrum. Audible signals are in the range of 20 to 20,000 Hz while the useful low frequency signals for interpretation are often in the range between 100-5000 Hz. Normally, the frequency of the signal is related to the source of noise and flow regime and the amplitude with the flow rate. A flow in turbulence generates sound with high amplitude, making it is easy to detect.

In applications where a turbulent regime is present, noise logs have been successful at detecting flows occurring in operations such as sand production [101], to evaluate perforations to improve oil recovery [102] and to evaluate the magnitude of production flow rates [103, 104]. In the case of evaluation of annular well barriers, applications to identify big perforations, important leaks and channels are known and publications can be found [105, 106]. However, noise logs can be of limited use in detecting well integrity issues due to the weak acoustic signals that some small leaks can produce. Integrity issues with lower acoustic spectrum can be confused with wellbore background and mechanical noise. Examples of noise log tools for evaluation of annular P&A barriers are available in the market, such as the *Chorus* tool developed by TGT [107] and the *VIVID®* tool developed by Archer [108], but they are still trying to position the technologies as a solution.

2.4.2 Passive acoustic - Fiber Optics Technologies

Fiber optics is a technology with the potential for well integrity data acquisition in real-time. Two types of technologies are available on the market for engineering applications. One is the distributed acoustic sensing (DAS), which collects strain changes caused by the propagation of acoustic signals in the borehole; the second one is the distributed temperature sensing (DTS) which captures the changes in temperature along the fiber cable. Normal installation is done outside the tubing, with clamps to keep the fiber in tension and in the desired position.

Several studies for geothermal wells have found the use of DAS and DTS in combination to be a powerful tool for the evaluation of integrity [109–111]. Applications of fiber optic tools during pumping of cement and curing show that it is possible to track the exothermic reaction of cement. The heating profile helps evaluate problems during cement placement; an investigation of integrity can start when data shows anomalous behaviours indicating an integrity issue [109, 112]. Good matches were

observed when comparing data of fiber optics with CBL logs [109] and with wireline gamma and density log [113]. However, in geothermal wells, due to extreme conditions such as high temperature, the presence of unexpected or anomalous heating is easier to capture compared to gas wells.

The use of fiber optics in oil and gas wells is becoming more popular and it has been recently tested by Equinor on the Johan Sverdrup field. A paper published by them shows the application of fiber optics on wellbore monitoring using a combined set of DAS and DTS. Their experiment present the acoustic response when a wellbore is unloading and when a gas lift is slugging. The paper highlights the potential and benefit of the use of this technology[114]. The use of this technology along with acquisition and processing of data in real time is a big step for the oil and gas industry. However, the challenge of using them for P&A is an unsolved problem. A possible limitation of fibers is their capability to "hear" the disturbance generated by small leaks, like those occurring in a P&A well. Studies of fiber optics on field for P&A were not found. An article from Los Alamos Laboratory shared results of experiments using DAS in a uni-fracture specimen where 6 liquid flow rates were used to record the noise spectrum and the conclusion shows that the use of fiber optic technology can be promising for the detection of leakages between 0.4 and 5.5 ml/min [115].

2.4.3 Active Acoustics - Sonic tools

The acoustic logging method was introduced as a technology for cement evaluation in the 1950s[116]. Nowadays, it is a well-consolidated technique that can be run a few hours or several days after the cement placement. It evaluates the quality of the bond (acoustic coupling) between the casing and the cement by measuring the attenuation of a sound signal emitted at low frequency (10 - 30 kHz). The acoustic wave propagates through the casing, cement and formation but also emits reflected waves that return to the sensors (receivers). These reflected waves are recorded to evaluate the first wave arrival and arrivals at later times. This log is known as Cement Bond Log (CBL) and Variable Density Log (VDL) in the oil industry. CBL uses the attenuation of the first wave arrival measured by the first receiver (normally at 3 ft) while VDL maps in the radial depth for all wave peaks and valleys that are detected and reflected at the second receiver (normally at 5 ft). The combination of both allows the evaluation of bonding and the overall state of coupling between casing, cement and formation.

For proper interpretation of CBL and VDL, the log data must be validated (Quality Assurance/Quality Control) and an initial calibration is required in order to know the log response when the tool is used in a free pipe zone. The result

of CBL and VDL are normally translated into a Bond Index (BI), which without correlation with well data, well geometry and well history can be leading to wrong interpretations [73]. Some examples of issues interpreting cement bond logs for real wells are found in the public domain [117, 118].

The advantage of sonic tools is that they are not mud-type dependent and can also provide some information about the bonding in the second interface (bonding between cement and formation). As to the disadvantages, these tools are very sensitive to the material contact, have poor performance in light cement, their spatial resolution is very poor and only provide an average of cement strength around the wellbore without azimuthal orientation, thus becoming unreliable to determine isolation. Conventional acoustic logs can be used then only to identify free pipe, partially bonded cement or fully bonded pipe-cement. Even though the disadvantages are important and do not tell the full story of cement integrity, CBL is widely used for verification of well barriers. All wireline service providers (Schlumberger [119], Halliburton [120], Baker Hughes[121]) have different models of sonic tools available to the market.

2.4.4 Active Acoustics - Ultrasonic Tools

Ultrasonic tools were introduced in the 1980s to improve the evaluation done by sonic tools [122]. The Ultrasonic tool normally uses sets of rotating head transmitters and receivers to evaluate the transient time of an emitted signal to travel through the materials in the wellbore. Their operative frequency is in the ultrasonic spectrum and are normally between 200 and 700 kHz [123]. The acoustic wave forms of the reflected signals help to determined the casing and cement quality behind the casing. Factors such as the wave attenuation rate and the acoustic impedance are studied to map the elements behind the casing.

Two techniques are used by ultrasonic tools: the pulse echo and the pitch catch. Pulse echo measures reflections from different interfaces. Cement bond quality is defined using estimations of the acoustic impedance contrast between cement, fluid and casing obtained from the various reflection amplitudes. Assuming that cement is not in contact with fluid unless there is microannulus, which is either behind the casing or between cement and formation. The ultrasonic wave is affected by factors such as the cement weight and the mud properties. For example, low density cement and heavy mud tend to reduce the impedance contrast, so in such scenarios Pulse echo is not reliable [124].

In contrast, the pitch-catch method measures the shear attenuation of the material. The waves propagating in the casing, cement and annular are recorded while an additional pulse generated by an inclined transmitter propagates along the casing

and is reflected by the contact in the interfaces of elements behind the casing. The attenuation is interpreted to infer the cement bond quality [125, 126]. The combination of pulse echo and pitch catch measurements provide the P-wave impedance and shear attenuation of the materials behind the casing and the reflection of the interfaces. The tools use a set of rotating head transmitters providing the measurement with azimuthal resolution. [127]

Several tools of this type are available on the market by all wire line service providers. For example, Schlumberger has avaliable the isolation scanner tool [128], Halliburton the CAST-XR™ [129] and Baker Hughes the ULTeX™ [130]) all of them integrated with a pulse echo scanner.

2.4.5 X-ray Logging Technology

X-ray have been used for evaluation of cement integrity in laboratories as a technique for the visualisation of cement defects after mechanical loading or flooding [131–134], but it is also useful for visualising the creation of fractures due to casing pressures while these fractures are developing [135]. Due to its potential, efforts to deploy this technology as a downhole logging tool have been pursued. Visuray is the first company working to adapt this technique for the challenging downhole environments[136]. One of the powerful advantages of X-ray is that it is not affected by the fluid content in the well and can penetrate highly heterogeneous materials. Two models of X-ray tools are already available in the market, the *VR90* ® and its improved version *VR90s* ®[137]. Both tools are capable to detect and produce images of objects in the bottom hole in applications like equipment fishing and inspection of the integrity of valves and mandrels [138–142].

To evaluate the cement behind the casing, the mentioned tools are limited. In response to this challenge, Visuray is developing the tool *VR360 Diagnostic Cement Evaluation Service* that will be available by mid-2022, according to their official communication channels [137]. The availability of this tool might be revolutionary for the verification of annular well barriers for the oil industry.

2.4.6 Temperature Logs

The temperature logging technique is used to find out the depth of the top of cement. As the curing of cement is an exothermic reaction, a temperature survey several hours after the cement placement can pick up the increase of temperature in the annular space. The accuracy of this method also depends on wellbore geometry, formation temperature, length of the cement column and slurry design [90]. Temperature logs can also be used while a well is in production to assess fluid channelling behind the casing and identify the need for a remedial cement job [143]. The

use of temperature logs as a tool to identify cement well quality previous to a well abandonment operation is apparently nonexistent since no sources were found for applications in this stage. Alternatively, as fiber optics DTS registers temperature, the temperature log will most likely be replaced by DTS.

2.5 Knowledge Gaps

Nowadays, trained professionals oversee, analyze, and interpret a set of logs to conclude about the cement quality behind the casing. The process is based on the understanding of the physical logging tool principles and the empirical knowledge to interpret the measurements. It is recommended to run technologies using different principles in order to have a full picture of the well integrity and reduce the uncertainty of interpretation. Frequently, sonic and ultrasonic tools are run together to do an assessment and avoid the use of a unique tool. However, to have a complete overview the log interpretation should consider additional information such as well history, cementing jobs and well interventions.

A typical classification of cement barrier quality is "high/good", "moderate", and "poor" when all this information is observed together. The entire process of analyzing logs and classified intervals, however, can be ambiguous and subject to processing bias. It is not uncommon that two trained professionals that oversee the same data set can draw different conclusions. For example, in a specific interval, one professional can conclude a "high/good bonding" while another one can define the same region as "moderate to high/good bonding."

Annular cement needs to be classified as "high/good" or "moderate to high/good" to qualify as a primary and/or secondary well barrier, meaning that the interval can prevent flow from the reservoir to the surface and undesired cross-flow between formations. The challenge is that the correlation between the cement bond quality and the hydraulic sealing is not straightforward. As the categories used for cement quality classification do not follow any standard and their translation to the potential for hydraulic isolation is weighted in different ways, it is difficult to have a rule of thumb. The general agreement is that a segment with a poor log response is expected to have a greater flow than a segment with a good log response. Some examples found in the literature are presented and summarized in table 2.1.

To conclude, it is not clear what are the effects in terms of consequences (leakage) when the barrier classification changes. So, the question of how large the increase is the volume of gas/water that can cross the barrier when the barrier classification change from good to poor is still unresolved.

Table 2.1: Labeling use for cement quality classification and hydraulic isolation

Source	**Categories used for quality classification**	**Potential for hydraulic Isolation**	**Criteria used**
Lucas et al [144]	Good	Hydraulic isolated	CBL<5
	Intermediate	Not hydraulically isolated	6<CBL<14
	Poor	Not hydraulically isolated	CBL>15
Equinor [145]	Good	High	Not presented in source
	Good to Moderate	Medium	
	Moderate	Medium	
	Moderate to Poor	Low	
	Poor	Low	
Viggen et al [145]	Good	Yes	Not presented in source
	Moderate to poor	No or Uncertain	

Chapter 3

Experimental leakage test on cement sections

Cement is used in the oil industry as the main material for zonal isolation. During the construction, cement is set in annular spaces as a barrier to isolate formations. However, a considerable number of producing and abandoned wells present well integrity problems [146]. Shrinkage, micro structure cracking and debonding of cement-steel interfaces are responsible for the loss of integrity in cement well barriers. Within the industry it is understood that the presence of fluid migration paths such as cracks or micro-annuli can increase the effective permeability of cement barriers, allowing the migration of fluids to the wellhead and resulting in sustained casing pressure [147, 148]. Such flow paths can develop during the well life cycle due to different factors, as presented in the previous chapter in the cement durability discussion. Nevertheless, to have migration of fluids through an annular well barrier element it is necessary to have three basic elements: a leakage pathway, a leakage source (gas, hydrocarbons or water), and a driving force (pressure build-up, bottom pressure). In the field, it is impossible to ascertain the in-situ state of cement barriers. Secondary indicators are used to asses well barrier integrity, those indicators can be for example sustained casing pressure in the well head, corrosion, reduction of mechanical resistance and migration of unknown fluids to the well. The study present in this chapter attempts to replicate downhole conditions simulating annular pressure increase in the laboratory to verify leakage potential of specific leakage paths, where cement conditions can be closely monitored and controlled.

3.1 Previous experiments of cement integrity in full scale

Experiments in full scale have been previously performed to understand how cement sheaths can fail. The first investigation to understand the influence of mechanical loads on the loss of integrity was developed in 1992 by Goodwin and Crook[149]. In this work, four mixtures of cement were pumped in large-scale cells of 16 m length constructed with 5,5-in (139.7 mm) tubing and 7 5/8-in (193.675 mm) casing. The annulus pressure was maintained at 35 bar during the curing, and leakage experiments were performed by injecting water into the annulus and changing the pressure inside the tubing. A five-step procedure was followed: first, at 0 bar of annular pressure the base leakage rate was measured. Second, an increase of the tubing pressure to 138 bar and measure the leakage of the annulus to water. Third, a decrease of tubing pressure to 0 bar, and measure leakage of the annulus to water. Fourth, repetition of steps 2 and 3 with tubing pressure increments of 138 bar to a maximum of 690 bar. Finally, the systems were cut for the final inspection. Results showed that considerable leakage rates were obtained when the pressure was released and not during the times when pressure was increased. Permeabilities were in the order of 10 to 70 mD [149]. One year later, in 1993, Jackson and Murphey published the results of leakage experiments using pipes of 5-in (128 mm) and 7-in (177 mm) with 1 meter length. Cement class G was placed in the annulus between the casing and two different experiments were completed. In the first, leakage measurements were collected while the internal tubing pressure was increased. In the second one, leakage was measured while the pressure was decreased. The procedures are similar to the Goodwin experiments, the difference being that the pressure was reduced in steps of 69 bar and the gas was used as a fluid instead of water. The results showed that flow through one meter of cement was measured when the differential pressure was 7 bar and casing pressure was 206 bar. If the casing pressure was reduced below 206 bar, the cross flow in the annular barrier was measured with differential pressures below 0.7 bar [150] . In the 2000s, Boukhelifa [151] developed a mechanical device to simulate changes in well conditions that cause expansion or contraction of the inner casing. Seven systems with slurries of class G cement and different additives were tested at room conditions. The leakage experiments were performed by pumping air through a cemented annulus. The cement test section had a length of 79 mm. The radial displacement, permeability and cement cracking were documented. According to the experimental results, the calculated permeability of uniform micro annuli of 60 μm should have a permeability of 500 mD. However, the measured permeabilities were lower in most of the cases, due to the creation of tortuous micro annulus. Later, Nagelhout et al [152] published a study evaluating

the leakage rates when two additives (Latex and Microgel) were included in the cement formulation to control gas migration. In the experiments, the plug cement was subjected to differential pressure and nitrogen gas flow rates were measured. Results from cells with two dimensions are presented: a large scale and a small scale test. The large test cells had an internal diameter of 173 mm and length of 125 mm, and small-scale cells with 50 mm of internal diameters and a length of 200 mm were presented. In these experiments, the cells and cement were not submitted to radial loading but after the comparison of results, the authors concluded that a large-scale test is a much more severe test for plugging ability than small-scale tests. More recently, annulus gas migration tests were performed by connecting four section to a nitrogen gas supply and the pressure control and flow measurement rig described by van Eijden et al. [153]. Four cells were used to reproduce a cement plug. The first has 0.38 m length and 2-in (50.8 mm) diameter, the second 1.14 m and 7-in (177.8 mm), the third 0.58 m and 4.25-in (107.95 mm) and the forth 1.90 m and 10.5-in (266.7). The rig for leak testing is equipped with different gas flow meters, covering a range of flow rates up to approximately 700 ml/min, with accurate inlet and outlet pressure control. Samples were cured under increased pressure-temperature conditions and the test allow the comparison of zonal isolation between the systems reconstructed in a laboratory environment. The goal was to avoid any disturbance to the test material prior to initiating the sealing test. An automated differential pressure was executed by lowering the pressure at the outlet, thereby preventing the metal pipe from additional ballooning. It was discovered that the size (diameter and length) of the sample has an effect on sealing performance. Furthermore, additions of metal oxide-based expansion additives to cement slurries resulted in improved sealing performance [153].

Studies in the last 20 years have provided valuable indications about how the cement sheaths may fail. However, some topics are still unanswered as for example the influence of tubing eccentricity in cement failure; the influence of type fluid (gas water or other) on the assessment of potential to flow using a positive or negative test; the type of leakage path and its relevancy to assess the severity of migration problems; the relation between the techniques for annular cement evaluation and hydraulic isolation. To have more insight, six assemblies are presented which were organized in 4 cases. Cells were constructed in full-scale, targeting the typical casing size used in Norway as casing (13 3/8-in, 9 5/8-in and 7-in) and all leak experiments were executed at the P&A laboratory at NORCE in Stavanger, Norway.

3.2 Theoretical background to evaluate leakage

The most general relationship between gradient pressure and effective permeability considers a non-linear behaviour. This non-linearity is attributed to viscous-inertial and inertial forces that are induced by fluids migrating at high velocities producing losses of energy or changes in geometries such as restrictions and constrictions that change the fluid behaviour. The non-linear behaviour of flow through a fracture has been defined as a quadratic function by Forchheimer [154] under the following expression:

$$-\nabla P = a\,Q + b\,Q^2 \tag{3.1}$$

with constants a and b defined as

$$a = \frac{\mu}{Ak} \qquad b = \frac{\beta\rho}{A^2}$$

$\nabla P = \frac{dp}{dz}$ is the pressure gradient along the direction of the flow. A is the area of the cemented wellbore annulus or cross-sectional area that can be expressed as $A = Wh$, W being the fracture width and h the hydraulic aperture. Q is the flow rate. k is the effective permeability. μ is the viscosity of the fluid and β is the non-Darcy coefficient. Equation 3.1 can then be rewritten as:

$$\frac{dp}{dz} = \frac{\mu}{A\,k}\,Q + \frac{\beta\rho}{(A)^2}\,Q^2 \tag{3.2}$$

When flow is not affected by viscous forces and the fluid is being transported by a sole fracture under a laminar flow regime, the quadratic component of the equation 3.2 is dismissed and the expression can be rewritten as follows:

$$Q_x = \int_0^W \int_{-h/2}^{h/2} Q_x(z)\,dz\,dy = -W \int_{-h/2}^{h/2} \frac{1}{2\,\mu}\frac{dp}{dz}[(z)^2 - (h/2)^2]dz = \frac{W\,h^3\,dp}{12\,\mu\,dz} \tag{3.3}$$

Equation 3.3 in some cases is written in terms of transmissivity, T, defined by $Q_x = -(T/\mu)(dp/dx)$ in which case leads to a cubic equation, $T = Wh^3/12$. Sometimes the equation 3.3 is call cubic law and relates with the transmissivity as per previous expression. The cubic law adopts the analogy of parallel planar plates to represent a fracture surface or microannuli. The equation assumes that the flow is steady and isothermal, inertial effects are neglected and the fracture is uniform and smooth. In the context of Darcy's law, the fracture permeability become $K = \frac{h^2}{12}$. A figure explaining how the approach is used for cemented sections is presented in Fig. 3.1.

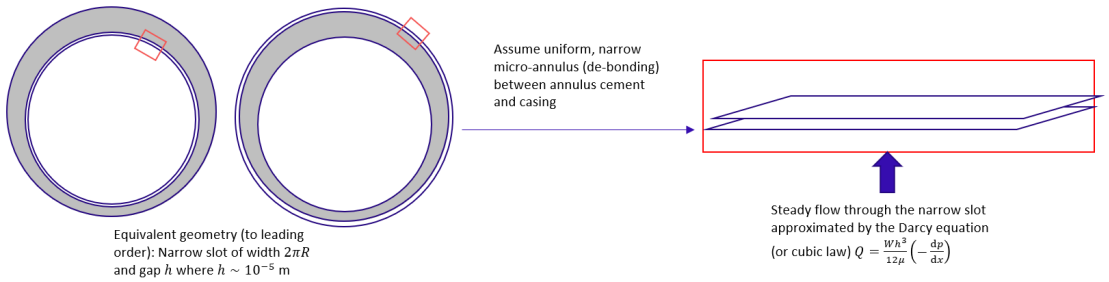

Figure 3.1: Current approach for estimation of effective size of micro-annuli or the permeability of a test section.

Studies in small scale have argued that migration paths through cement sheaths are rarely simple and that the equation 3.3 could be limited to model the migration of fluids occurring in migration paths [80, 155, 156]. However, the cubic law has been applied to model leakage through annular cement, assuming that the flow is mainly migrating through a specific fracture[157] or a microannulus [157–160]. Usually, when the leak test is done with water and the results are interpreted as a hydraulic aperture, the equation 3.3 is rewritten as follows:

$$h^3 = \frac{12\,Q\,\mu\,L}{W\,(P_o\,-\,P_i)} \tag{3.4}$$

Al Ramadam er al.[161] presented a model that combines the cubic law and the real gas law, to be used if specimens are tested with gases (air or nitrogen). The equation takes the following form:

$$h^3 = \frac{24\,\mu\,T\,R\,L\,\rho}{(P_o^2\,-\,P_i^2\,)\,2\,\pi\,r} \tag{3.5}$$

In equation 3.4 and 3.5 SI units are used, where $dz = L$ corresponds to the length of the cell in meters, P_i is the pressure in the inlet and P_o in the outlet in Pascal, T is the temperature of the fluid in Kelvin, R is the gas constant ($296.8\,\frac{m^2}{s^2K}$), ρ is the density of the fluid in the outlet in $\frac{Kg}{m^3}$, T is the temperature of the fluid in Kelvin and r is the radius where the microannuli is assume to occurred in meters.

For further investigation, equations 3.4 and 3.5 are used to evaluate the leaking behavior of six cells with different geometrical features as migration paths. Case 1: "uniform debonding cell", simulates a more defined geometry with a defect similar to a constant debonding of the casing/cement interface. While two cells in case 2, simulates a channel within the cement, which typically occurs when the cement job was unsuccessful and water is trapped in the cement. Case 3 (microannuli cell) and case 4 (Valhall sections) simulate a more realistic defect occurring in real downhole conditions, where the fluid migration paths through the cement sheath are complex

and difficult to map. The results presented in this chapter were collected with the injection of water and/or gas to evaluate the magnitude and severity of leakage on the cement sheath. The assemblies' permeabilities are compared with the equations to model leakage so that the correlation between microannuli size, hydraulic aperture and leakage potential can be discussed further.

3.3 Case 1: Uniform debonding cell

The cell was constructed with the objective of reproducing a uniform debonding between the casing and cement in the internal interface of the assembly. By assuming an ideal case where the microannuli is occurring as a well-defined migration path with a controlled aperture, the connection between effective permeability and hydraulic aperture is easier to define. Even though this geometry is very unlikely to occur in a well and it is very ideal for a downhole scenario, it is interesting as a study.

3.3.1 Construction

The cell constructed for this assembly uses a short sandwich cell of 500 mm in length. The design consists of two concentric casings 244.475 mm (9 5/8-in) and 177.8 mm (7-in), with nominal weights of 53.5 lb/ft and 23 lb/ft respectively. End caps were fabricated to center the 7-in casing within the 9 5/8-in casing. The details of casing dimensions and the scheme are presented in Fig.3.2.

Portland cement class G with a specific gravity of 1.90 was mixed and pumped in between the casings with the cell in a vertical position. The components included in the preparation of the slurry are listed in Table3.1.

Table 3.1: Cement Recipe for 300 L slurry. The volume capacity of the cell to be filled is 11 L

	Material	Amount	Unit
1	Fresh Water	161,3	L
2	SA-1015	0.061	Kg
3	NF-6	0.31	L
4	HR-5l	2.14	L
5	Dyckerhoff G HT Blend	412	Kg

The assembly was cured in a vertical position maintaining 150 bar of internal tubing pressure and around 6 bar of confining pressure in the cement sheath with free access to water. Pressures and temperature were monitored for 7 days and results are presented in Fig. 3.3

A temperature sensor placed on the outer surface of the outer casing shows an indication that the exothermic reaction of cement hardening is happening during

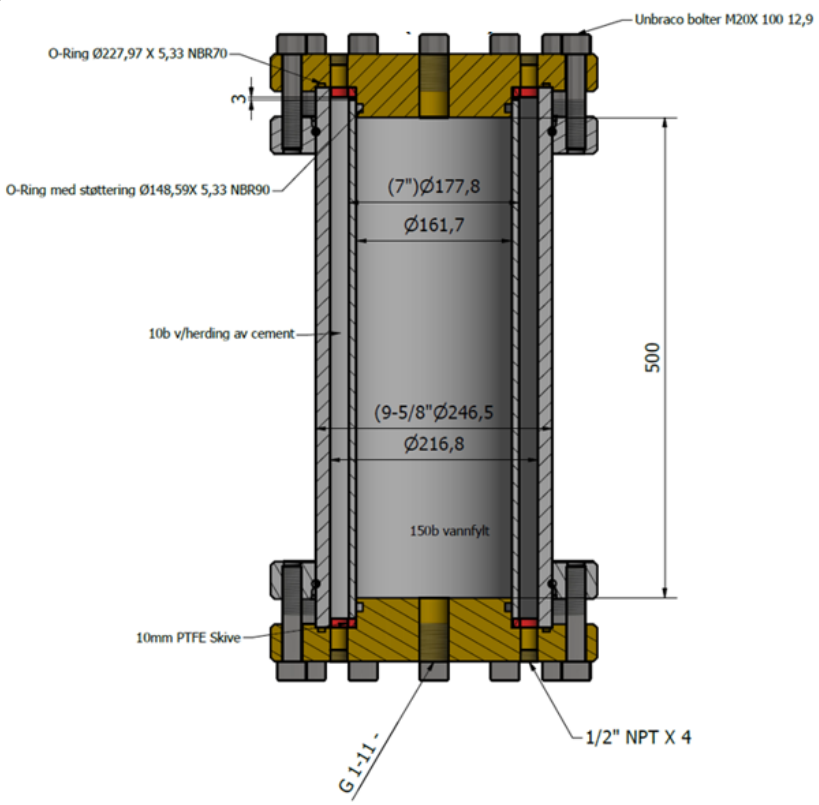

Figure 3.2: Details of fabrication of the uniform debonding cell. The end caps are presented in the figure in brown while the cell is represented in gray

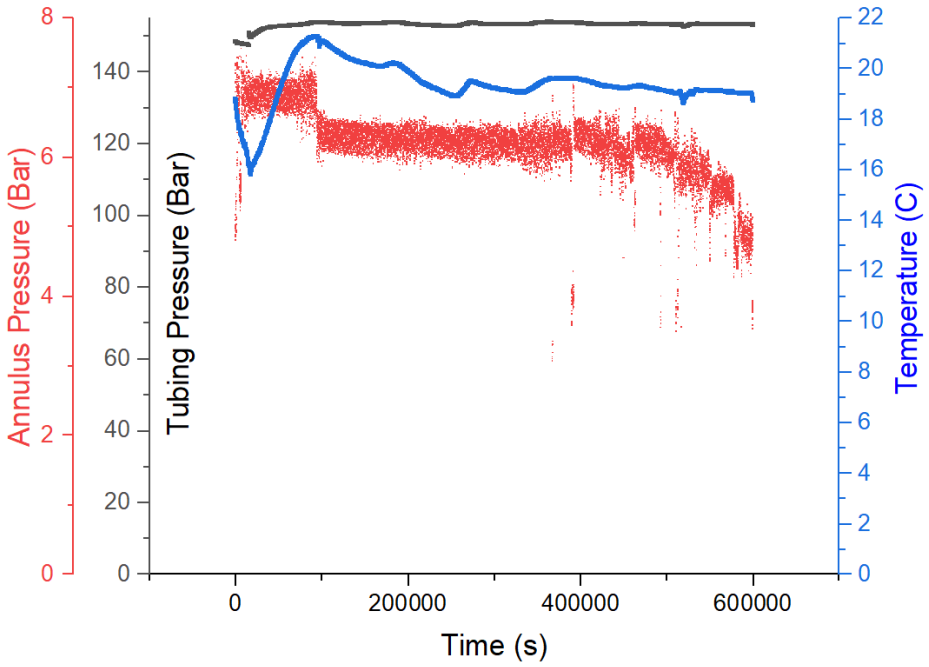

Figure 3.3: Pressure and temperature during curing for uniform cell

the first 15 hours (101700 s). This period is followed by the deceleration period to reach a more stable temperature. This is the typical development of the five phases of hydration of cement (pre-induction, induction, acceleration, deceleration and diffusion), where the saturation occurs when the heat reaches its maximum [89]. The temperature behaviour recorded can be an indication that the hydration periods of induction and acceleration are occurring before 15 hours of curing when the temperature reaches its maximum of 21 C°. After that, the deceleration and diffusion period take place and the hydration and changes in temperature are more stable. Note that variations of temperature observed can also be affected by the fluctuation of temperature in the curing room throughout the day.

The annulus pressure (in red) is the pressure of the water line connected and communicated with the cement sheath. Note that after the peak of high temperature at 15 hours the pressure in the line decay so that the saturation level is more stable after, and keeps dropping to 4 bars by the end of the curing. The confining pressure induced by the pressurization of the tubing at 150 Bar presents no variation. This pressure was set to mechanically expand the inner casing during cement curing to create the permanent microannulus.

3.3.2 Leakage testing

After 7 days of curing, the 150 Bar of pressure in the tubing was released and the end caps and ports were cleaned. Initially, a qualitative test with one open end was completed to verify the occurrence of migration paths. A film of soapy water on the end generated soap bubbles while the other end was connected to an air bottle at 1 Bar. The bubbles provide a visual trace of where the gas is migrating. Results of the soapy test and hydraulic aperture to water flooding are presented in Fig. 3.4. It is observed that the migration paths are well defined and concentrated in the interface between the 7-in casing and the cement sheath. No gas leakage through the external interface with the external tubing was observed.

Subsequently, the cell was instrumented with one temperature sensor and two pressure sensors (one on the top and one in the middle of the cell) while the vindum pump measured the injection pressure and controlled the injection rate. The outlet port was open to atmospheric conditions. The details of the rigging up and instrumentation is presented in Fig.3.5

The section was flooded with water to evaluate the permeability of the system with and without both end caps installed. The cell was tested, in both cases, with water at constant flow rates of 10, 20, 30, 40 and 50 ml/min and pressure was monitored to verify that the permeability is reaching steady state conditions at each flow rate step. Pressures measured at each flow rate tested are presented in

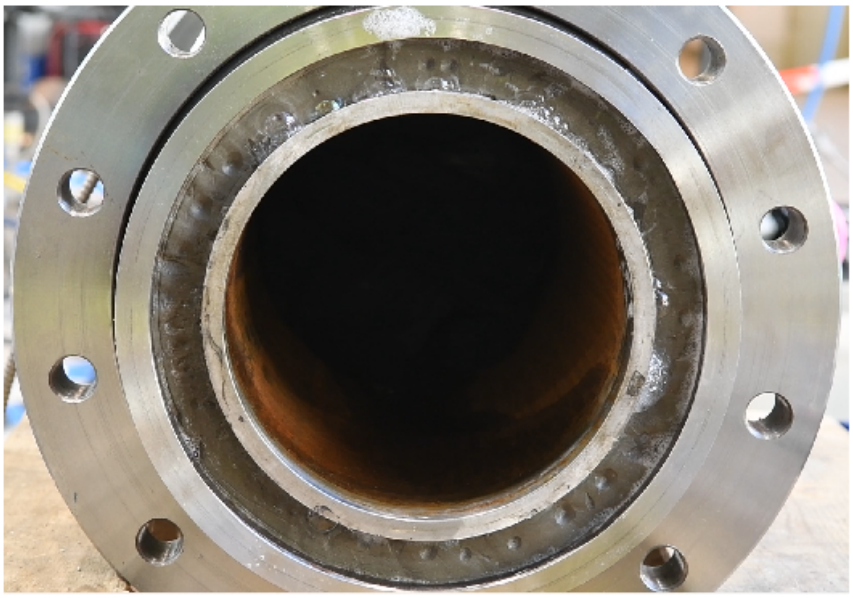

Figure 3.4: Soapy test presenting migration paths on uniform debonding cell

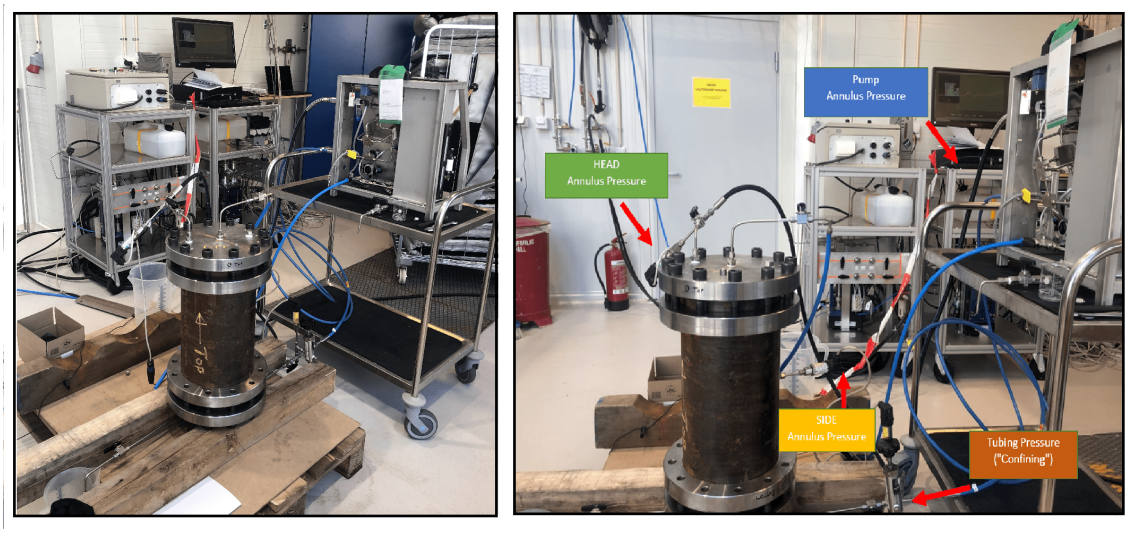

Figure 3.5: Picture of instrumentation and rig up for testing for the uniform debond cell

Table 3.2 and Fig.3.6. Solid lines on the figure denote the expected behaviour of a microanullus of 40, 50 and 55 µm using equation 3.4 and asuming a water viscosity of 0.00089 Pa s. Results show that most of the measurement collected fall in the range 45-50 µm of hydraulic aperture.

Using the water permeability measurements collected at steady-state, it is possible to estimate the effective hydraulic aperture of the microannulus, for each measurement, using the equation 3.4. The results show that the equivalent hydraulic aperture of the cell is around 50 µm on average and the effect of the installation of both end caps appears to be irrelevant when the flow rate is higher than 30 ml/min;

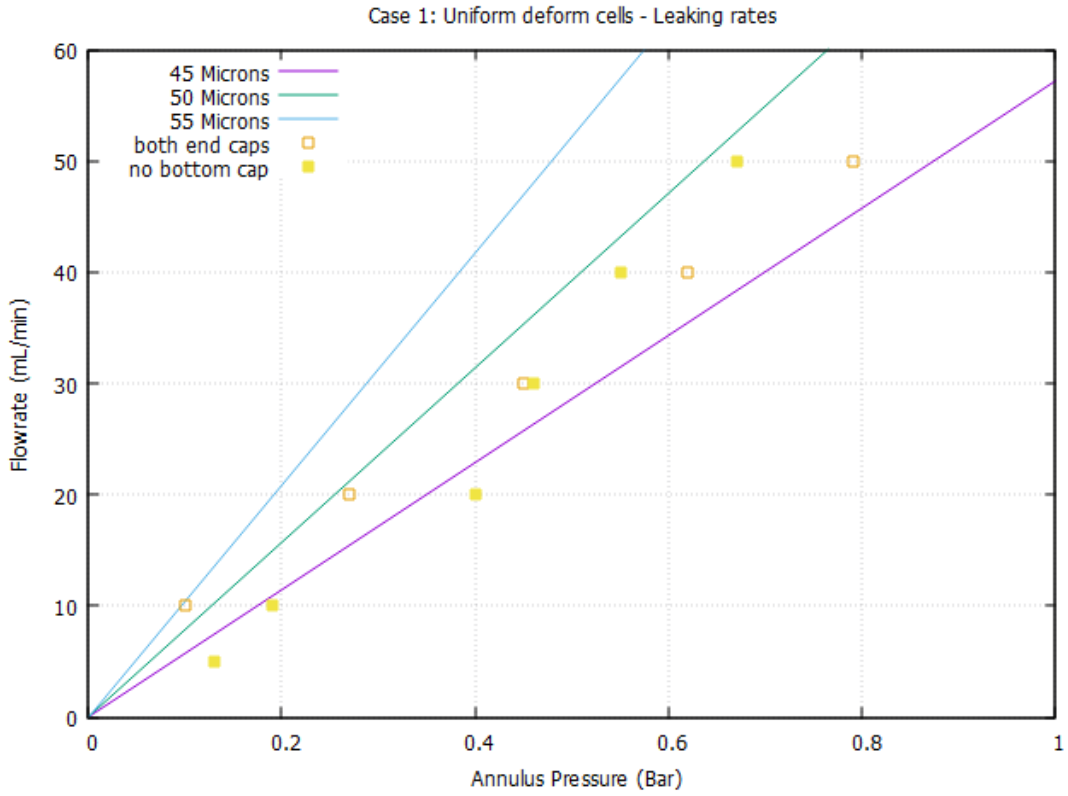

Figure 3.6: Flow rate and pressure measured for Uniform debonding cell

for lower flow rates, the results present a small mismatching. Data is presented in Table 3.2 and Fig.3.7

Table 3.2: Data of permeability test for uniform cell. No tubing pressure

Flow rate (ml/min)	Annulus Pressure (Bar)	hydraulic Aperture (µm)	Comments
10	0,10	55,01	
20	0,27	48,97	
30	0,45	47,47	with end caps
40	0,62	46,91	
50	0,79	46,64	
5	0,13	39,87	
10	0,19	43,46	
20	0,40	42,91	No bottom cap
30	0,46	46,89	
40	0,55	48,71	
50	0,67	49,11	

Additionally, the radial displacement of a closed-end cylindrical pressure vessel can be calculated considering linear expansion and assuming plane stress by the following equation:

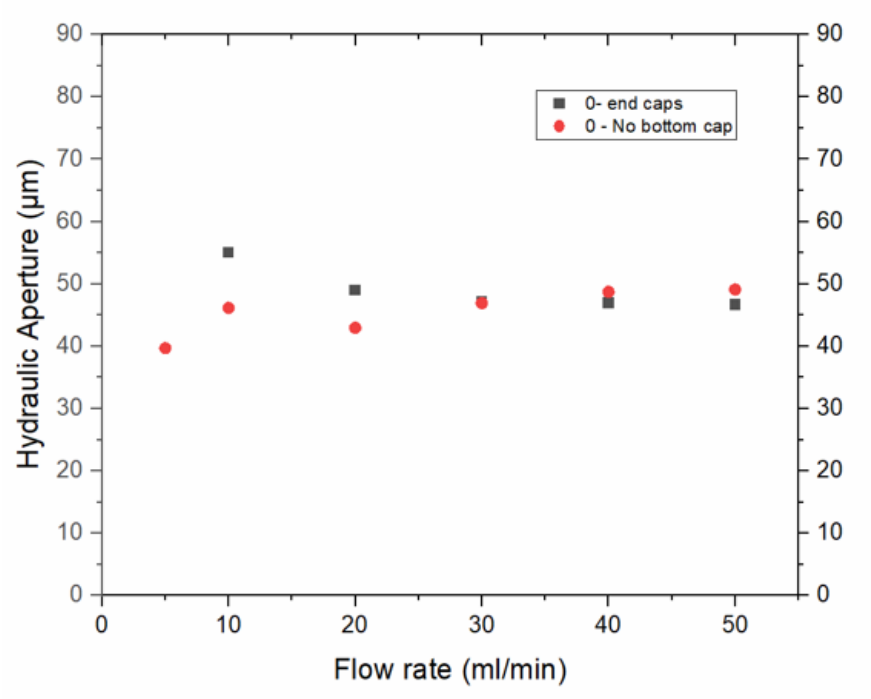

Figure 3.7: Computed equivalent hydraulic aperture for Uniform cell

$$U_r = \frac{P\,r^2}{t\,E}(1 - \frac{v}{2}) \tag{3.6}$$

where E and v are the Young's modulus and the Poisson ratio of steel, t is the casing wall thickness (0.317-in), P is taken to be the average of the tubing pressures during curing (150 Bar) and r is taken to be the radius of the inner casing (3.34-in). Assuming $E = 210GPa$ and $v = 0.3$ as representative values for steel. The radial expansion is estimated to be $U_r = 54,3\ \mu m$, which is slightly higher than the effective hydraulic aperture interpreted from results previously presented where $h \approx 50$ micrometre.

3.3.3 Confining pressure effect

The microannulus between casing and steel might respond to the loading conditions such as confining pressures. Such changes in loading can induce a closing or opening of the microannulus aperture with possible alterations in the permeability. In a downhole scenario, changes in confining pressures can occur, for example, when a fluid with a different density is placed into the wellbore, modifying the hydrostatic column. Another case is due to pressurization on the formations outside the cement sheath that increase the confining pressure. To evaluate the dynamic response of the microannuli, an experiment with a variation in loading conditions was planned.

The pressure in the inner casing was changed, compressing a fluid with a pneu-

matic pump connected to a port in the tubing. The permeability to water of the cement in the annulus was measured at constant flow rates of 3, 5, 10, 20, 30, 40 and 50 ml/min. Effective hydraulic aperture of the microannulus was interpreted using in equation 3.4 for confining pressures of 50, 100 and 150 Bar of tubing pressure. Results are presented in Fig. 3.8 and table 3.3. Note that a blue line of ideal closing is included in the plot, which assumes a symmetric radial expansion of the internal tubing that closes the gap between cement and inner casing (microannulus).

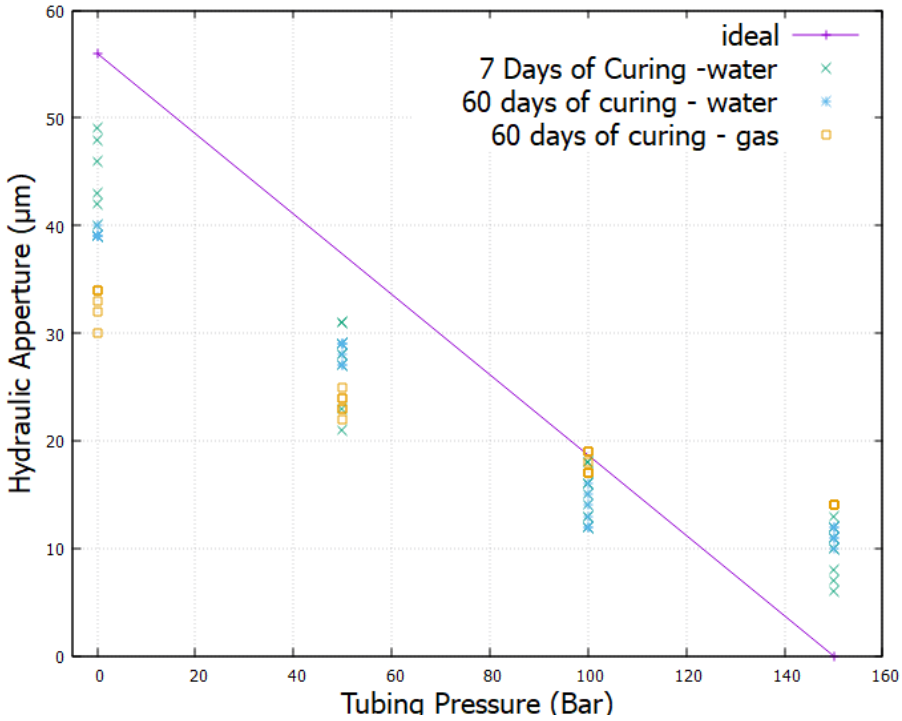

Figure 3.8: Results of equivalent hydraulic aperture when varying confining pressure at 7 days and 60 days of curing

3.3.4 Repeatability and aging effect

After 60 days of curing permeability measurements were collected, using the same procedure described in section 3.3.2 and 3.3.3 with the goal of evaluating changes in permeability over time. Results for both tests, after 7 days and 60 days of curing, are presented and compared in Fig. 3.8 and table 3.3.

The equivalent hydraulic aperture between 7 and 60 days presents slight variations but the data appears to be consistent. So, the results show that no significant changes have taken place in the cell between the two curing times. It is observed that the increase in confining pressure responds almost linearly with the reduction of hydraulic aperture but this behaviour does not follow the equation for ideal closing. This mismatch can be explained by the surface's roughness that always keeps a gap between the surfaces but also by the fact that pipes expand in a more oval way where

Table 3.3: Data of permeability test for uniform cell. Varying tubing pressure

		7 days of curing		60 days of curing	
Tubing Pressure Bar	Flow rate (ml/min)	Annulus Pressure (Bar)	Hydraulic aperture (µm)	Annulus pressure (bar)	Hydraulic aperture (µm)
150	5	20,09	7,35	-	-
150	10	24,20	8,70	8,42	12,37
150	20	27,90	10,45	26,03	10,70
150	30	32,91	11,32	33,86	11,22
150	40	32,88	12,47	38,08	11,87
150	50	35,77	13,06	41,51	12,43
100	5	3,51	13,15	4,43	12,16
100	10	9,04	12,08	7,76	12,71
100	20	7,73	16,03	11,79	13,93
100	30	10,26	16,70	14,54	14,87
100	40	10,48	18,25	16,67	15,64
100	50	12,23	18,68	18,36	16,31
50	5	0,65	23,05	0,30	29,77
50	10	1,69	21,11	0,78	27,30
50	20	1,27	29,25	1,45	27,99
50	30	1,96	28,99	2,02	28,70
50	40	2,05	31,45	2,53	29,30
50	50	2,58	31,36	3,06	29,63

gaps can be kept open in the smaller diameter of the expansion. The reduction in permeability looks to correspond to 36-41 % with 50 Bar, 61-66 % with 100 Bar and 13-81% with 150 Bar. Note the maximum tubing pressure applied of 150 Bar was also the pressure maintained during cement curing, so the initial debonding and closing were evaluated. The results demonstrate that after debonding occurs it is impossible to fully close the microannulus by increasing the confining pressure to 150 Bar. It is difficult to estimate when damage will occur if confining pressure is increase beyond that pressure.

3.4 Case 2: Continuous water channel

Four annulus test assemblies were constructed and cemented at a near-horizontal inclination in November 2017, as part of a full-scale fluid displacement and cementing experiment presented by Skadsem *et al.* [162]. After allowing the cement to cure, the test assemblies were found to contain free water channels along the top of the cement, a well-known defect that can compromise zonal isolation over long distances [89, 163, 164]. Due to their relevant and relatively well-defined defect, two of those test assemblies were subsequently selected for the study of leakage paths and fluid

migration potential in 2020 and are presented as part of this research. The results of the permeability experiments and characterization are presented in this section. The leakage paths in those two sections were late treated using a mechanical tool, called Local Casing Expansion (LCE); details about this tool, procedures and evaluation of leakage after treatment are presented in Beltran-Jimenez *et al.* [165] but are not included as part of this document.

3.4.1 Construction

Four test assemblies were each constructed of two joints of a 177.8 mm (7-in) casing (32 lbm/ft, 13CR80) placed inside a 244.475 (9 5/8-in) casing (53.5 lbm/ft, P110). A series of test ports were drilled through the top and bottom walls of the outer 9 5/8-in casing to allow monitoring of the displacement process, and to perform pressure testing of the cemented annuli after the cement had hardened. No attempts were made to centralize the inner tubing in these assemblies, so in most cases, the tubing rested on the low side of the casing, supported by its collar on the bottom wall of the annulus. Before cementing, the assemblies were inclined to 85° from the vertical, resulting in near-horizontal cementing conditions. The assemblies were wrapped in wool insulation to ensure protection from ambient temperature variations and stabilize elevated curing temperature by retaining some of the heat generated during curing. A view of the near-horizontal test sections is provided in Fig. 3.9.

Figure 3.9: View of the four test assemblies draped in insulation and plastic covers.

Cementing of the assemblies was performed sequentially. First, a 1.4 s.g. water-based spacer fluid, weighted using barite and viscosified using a polymeric additive, was circulated through the assemblies. Subsequently, a conventional Class G cement slurry with standard additives such as retarder, defoamer and stabilizer (see Table 3.4) was mixed and injected to displace the spacer fluid.

Table 3.4: Cement slurry composition.

Ingredient	Quantity
Class G cement	100 % BWOC
KCl brine (3% BWOS)	37.28 l/100 kg
Fluid loss additives	4.5 l/100 kg
Free water control additive	3.5 l/100 kg
Retarder	1 l/100 kg
Defoamer	0.1 l/100 kg

A KCl brine was used for the slurry mixing water in order to allow monitoring of spacer fluid displacement and cement placement using conductivity probes mounted at designated positions along the test sections. The cement slurry was mixed at the site of the cementing experiments using a standard offshore type batch mixer with two mixing compartments, each with a capacity of 8 m^3 fluid.

Fluid injection into the assemblies was pumped down the inner casing. A wiper ball was initially mounted at the upper end of the 7-in casing to ensure physical separation of the spacer fluid and the cement slurry during the injection down the assemblies. The wiper ball was captured at the bottom of the 9 5/8-in casing, allowing the cement slurry to flow back up toward the upper end of the assembly in the annular space outside the 7-in casing. Once a predetermined excess volume of cement slurry had been injected, pumping was discontinued and the injected cement slurry was pressurized to 5-8 bar by connecting the water main to the upper end of the assemblies. At this point, the assemblies were filled with the curing cement slurry both inside the inner casing and in the annulus between the casings. The assemblies were allowed to cure for 7 days before the first pressure test of the annulus cement was performed. Subsequent pressure and flow testing was performed several weeks later, followed by sectioning of the assemblies into shorter segments that had been stored at the yard for almost 3 years prior to performing the leakage characterisation experiments and treatment reported in Beltran-Jimenez *et al.* [165] and presented as part of this thesis.

3.4.2 Infrared Thermography (IRT)

To confirm that the flow is dominantly occurring through the channel at the top of the annulus, flow testing by injecting cold or warm water and imaging the external surface of the assemblies using infrared thermography (IRT) was performed. An infrared camera SEEK ShotPro (with a field of view (FOV) of 57 degrees and infra red chip resolution of 320x240) was used to take pictures to evaluate the temperature changes on the outer casing surface. The test was completed by first injecting warm water maintained at approximately 40 while monitoring the surface temperature of the outer casing using IRT. The warm liquid quickly heated the adjacent casing, and the resulting surface temperature profile provided another indication that flow was primarily through the distinct gap at the top of the annular cement. Subsequent cold water injection had the reverse effect of locally cooling the casing, initially along the migration channel. Fig. 3.11 presents three photographs of the experiment performed with assembly C6. Fluid flow was here from right to left, and a thin piece of metallic tape was placed at 1 m intervals to enable axial tracking of the temperature profile. The assemblies were rotated about their axis as part of the test to prove that the flow was only through the identified top annular channel.

For assembly C6, some uneven heating spots in the interval from 0.0 to 3 m were observed. These are indicated in Fig. 3.10 and are likely connected to the poor initial cement quality at this end of assembly C6. Fig. 3.10b) shows a side view of part of the assembly, showing that the surface heating of the outer casing occurred at the orientation of the top annular channel.

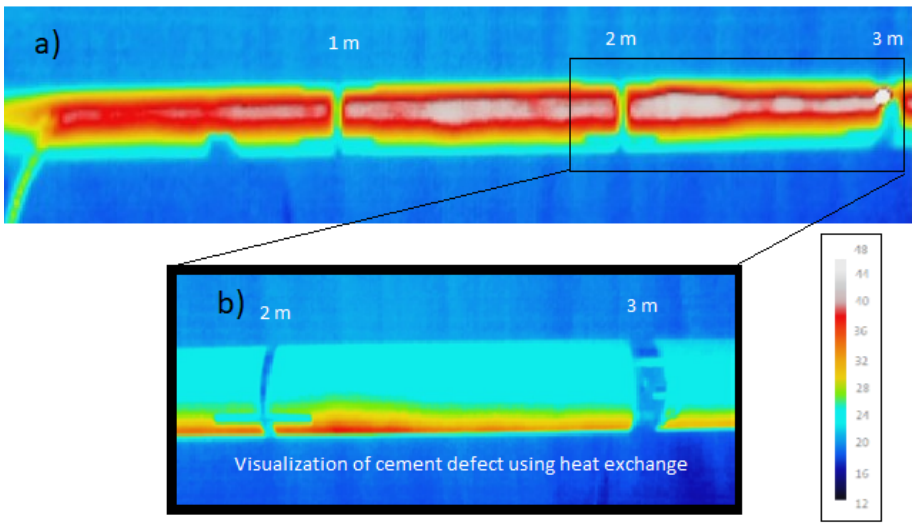

Figure 3.10: Warm water (40) injection in assembly C6. Water is injected from right to left. a) Picture of the interval between 0.0 m and 3 m after 30 minutes since the start of injection. b) Detail of a part of the assembly rotated by 90° showing that surface heating was limited to the region of the migration channel.

a)Test section C6 with metallic tape for position identification.

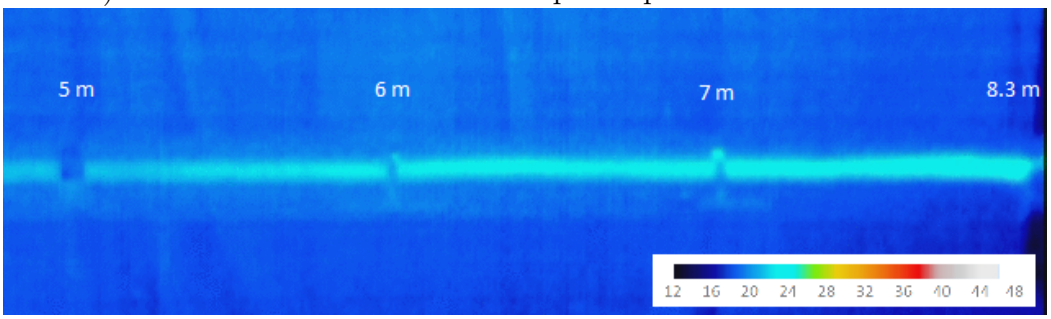

b) Initial stage of warm water (40) injection. Picture was taken 3 minutes after start of injection.

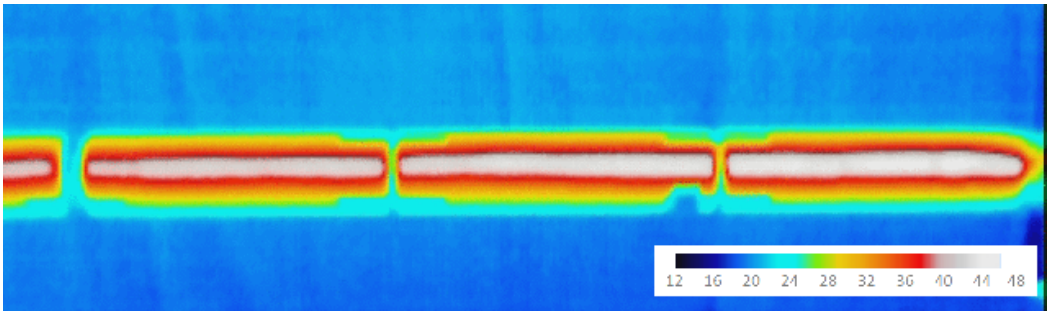

c) Final stage of warm water (40) injection. Picture was taken 30 minutes after start of injection.

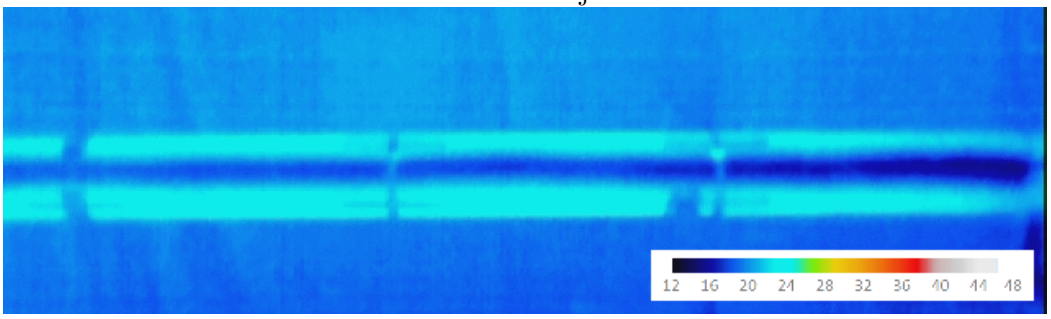

d) Final stage of cold water (10) injection. Picture was taken 10 minutes after start of cold water injection.

Figure 3.11: Sequence of images using infrared thermography during base line flooding test in section C6. The flow is from right to left. The photographs are from the interval between 4.8-8.3 m, at the right end of the assembly. Temperatures are in units of degree Celsius.

3.4.3 Leakage test assemblies A2 and C6

As part of the pressure and flow testing of the four assemblies mentioned above, it became evident that continuous fluid migration channels existed at the top of the annular cement. While pressure testing alternately through the test ports mounted along the top side of the assemblies and along the bottom side, it was concluded that the channels were located along the top side of the annulus and spanned most of the length of the test sections. At the time, the existence of the channel was attributed to either incomplete spacer fluid displacement or free water separation from the cement, promoted by the severe inclination of the test assemblies [89, 163].

Following the initial pressure and flow testing, the four test assemblies were sectioned into shorter segments for visual inspection of the cement quality across the cut surfaces. The sections A2 and C6 were labeled and provide photographs of the exposed ends of these assemblies in Fig. 3.12.

Assemblies A2 and C6 were 8.8 m long and 8.3 m long, respectively, and originated from two different, original full-length assemblies. Assembly A2 had a relatively smoothly varying channel at the top of the annular cement while assembly C6 had a similar channel at its far end (8.3 m), but particularly poor cement at its near end (0.0 m). Assembly A2 has an eccentricity of the inner 7-in tubing is approximately 0.45 at the left end (0.0 m) and close to centralised at the right end (8.8 m). In assembly C6, the eccentricity of the inner 7-in tubing is approximately 0.75 at the left end (0.0 m) and approximately 0.6 at the right end (8.3 m). Debris, voids and severely fractured cement occupied the annular space at the left end of the test assembly.

The existence of a migration channel along the top of the cement within the inner casing was also noted. This was particularly evident in assembly C6 but the channel was also present in A2. Since a wiper plug was used inside the inner casing to eliminate slurry contamination during injection down the test assemblies, the observed migration channels can be attributed to free water during curing and not slurry contamination [162]. For further characterisation of the annular channels, the cement inside the inner casing was removed by water jetting, leaving the two casings and the annular cement sheath.

The annular migration paths were characterized by 1) flow testing and 2) physical point measurements using a measurement stick inserted through test ports drilled in the outer casing. Based on the physical point measurements, the maximum gap width was estimated to be between 1 and 1.5 mm in assembly A2 and between 1 and 15 mm in assembly C6. These measurements agreed with the visual inspection of the exposed end cross-sections (Fig. 3.12). The largest gap width in assembly C6 was measured through a test port close to the near end at 0.3 m.

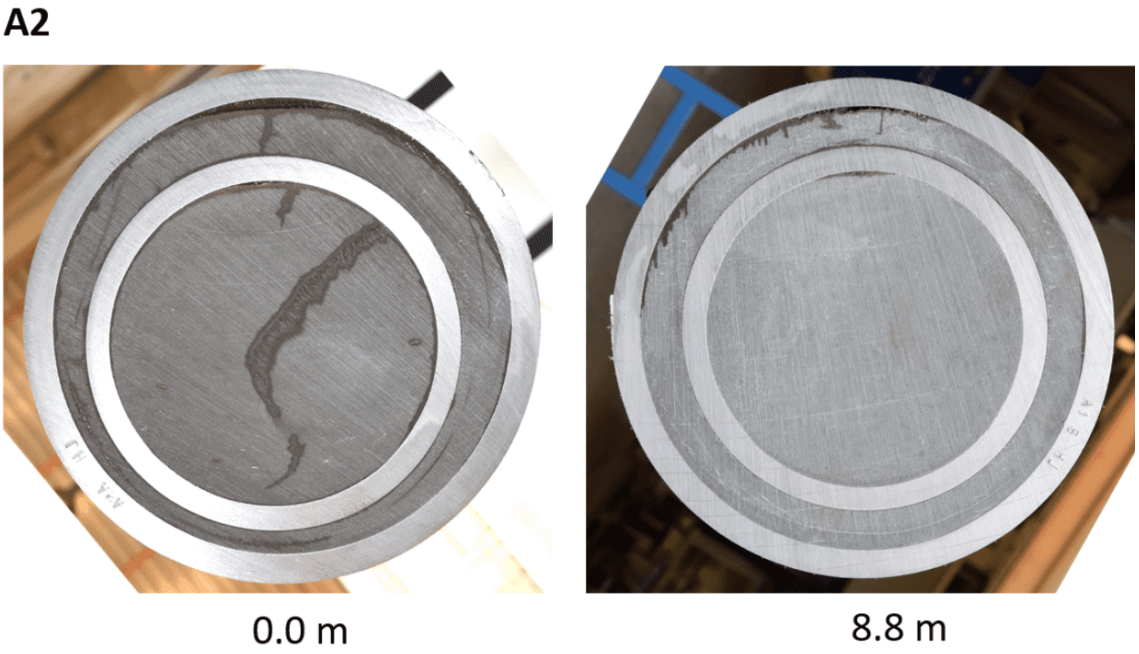

a) assembly A2. Continuous millimeter-sized channels were present on the top side of the cement in the annulus and in the tubing.

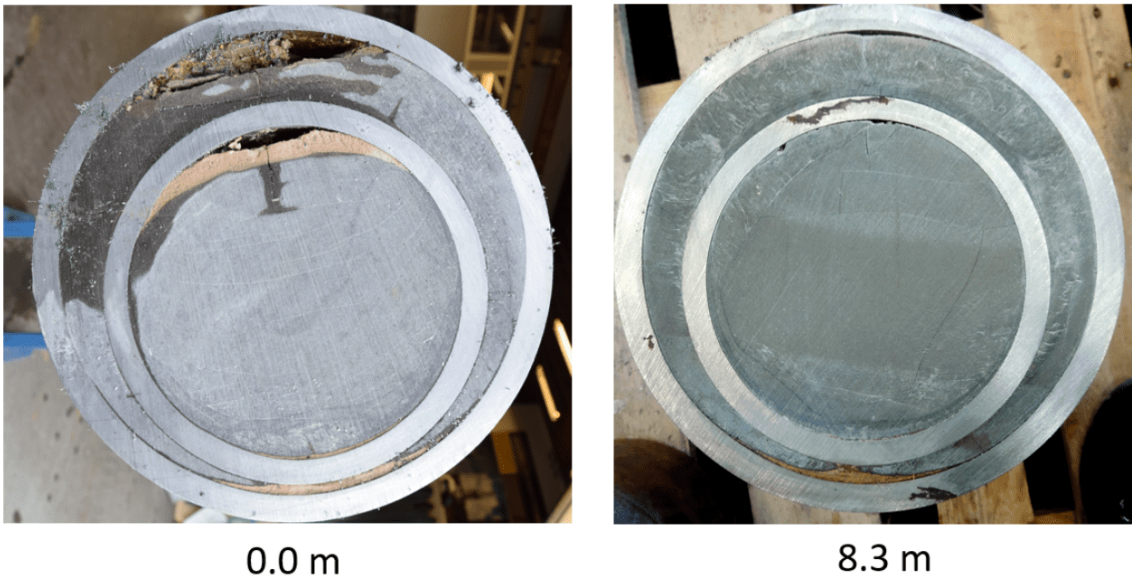

b) assembly C6. The condition of the annulus cement improved toward the right end where a millimeter-sized channel remained.

Figure 3.12: Ends cross sections of test assembles A2 and C6

Subsequently, flow tests were performed to confirm the physical measurement described above and connect the channel size to an effective annulus permeability. To this test, a pump was used to apply a constant water pressure, ΔP, to a test port at one end of the assembly. At the other end, the volumetric flow rate Q was measured, through an open test port a distance, ΔL, away from the inlet. The measurements were used in conjunction with the Darcy equation (See equation 3.3)

to estimate the effective permeability, K. Here, A is taken to be the cross-sectional area of the annulus between the 7-in inner casing and the inner wall of the outer 9 5/8-in casing, and μ is the viscosity of water, assumed 1 mPa·s in calculations. For the inner diameter of the 9 5/8-in casing, taking a nominal value of 0.2168 m.The flow measurements presented in Table 3.5 confirm that C6 has the largest free water channel and indicate initial permeabilities ranging from approximately 80 up to hundreds of darcy.

Table 3.5: Flow measurements on test assemblies established as baseline.

Assembly	ΔP (bar)	$\Delta L(m)$	Q (ml/min)	k (darcy)
A2	5.9	8.2	3960	77
	5.8	8.2	4080	80
C6	1.4	6	4080	243
	1.3	6	5580	364

To connect the effective permeability estimates to an effective channel gap width, considering the idealized geometry shown in Fig. 3.13. Here, the channel is bounded above by a circular arc of radius a within the angular interval $[-\theta^*, \theta^*]$, with $\theta^* = \arccos(1 - h/a)]$, and below by the horizontal line at a radial distance $\alpha(\theta)$ from the centre of the circular arc.

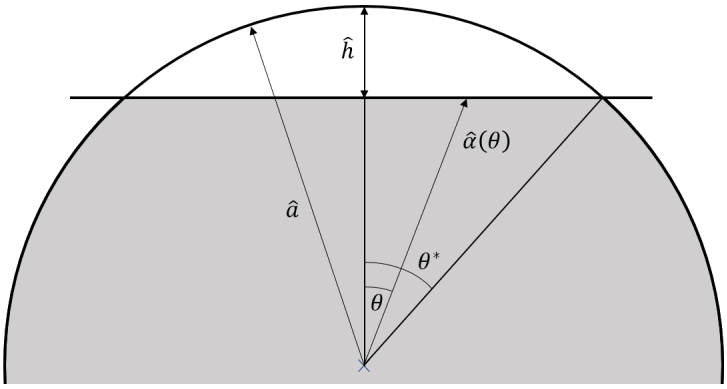

Figure 3.13: Geometric model to represent flow in a uniform free-water channel.

The circular arc corresponds to the inner wall of the 9 5/8-in casing, while the horizontal line is the top of the annular cement. By assuming fully developed, laminar flow, using the hydraulic diameter [166] of the geometry in Fig. 3.13 to approximate the volumetric flux as

$$Q = \frac{T(h)a^4}{\mu}\left(-\frac{\partial p}{\partial z}\right), \tag{3.7}$$

where

$$T(h) = \frac{\left(\theta^* - (1-h)^2 \tan\theta^*\right)^3}{8\left(\theta^* + \sin\theta^*\right)^2}, \tag{3.8}$$

and $h = h/a$. The constant friction pressure gradient is denoted by $-\partial p/\partial z$. Identifying the function $T(h)$ as a dimensionless transmissivity function and plot $T(h)$ as the solid line in Fig. 3.15.

To confirm the validity of the hydraulic diameter approach, numerical solutions of the exact momentum conservation represented by equation 3.9 is used.

$$\frac{1}{\mu}\frac{\partial p}{\partial z} = \frac{\partial^2 u}{\partial r^2} + \frac{1}{r}\frac{\partial u}{\partial r} + \frac{1}{r^2}\frac{\partial^2 u}{\partial \theta^2}. \tag{3.9}$$

Here, u denotes the axial velocity of the fluid and r is a radial coordinate measured from the center of the circular section in Fig. 3.13. The horizontal boundary is defined by $\hat{\alpha} = (a - h)/\cos\theta$, where h denotes the maximum channel width in the radial direction. Solving Eq. (3.9) using the Gauss-Seidel method and a finite difference discretisation of the equation; a sample dimensionless velocity profile for a channel of maximum width $h = h/a = 0.05$ is provided in Fig. 3.14. As before, the origin of the coordinate system is at the centre of the casing, and normalizing the coordinates x and y by a. Further, the velocity is normalized by $U^* = a^2(-\partial p/\partial z)/\mu$, *i.e.* $u = u/U^*$

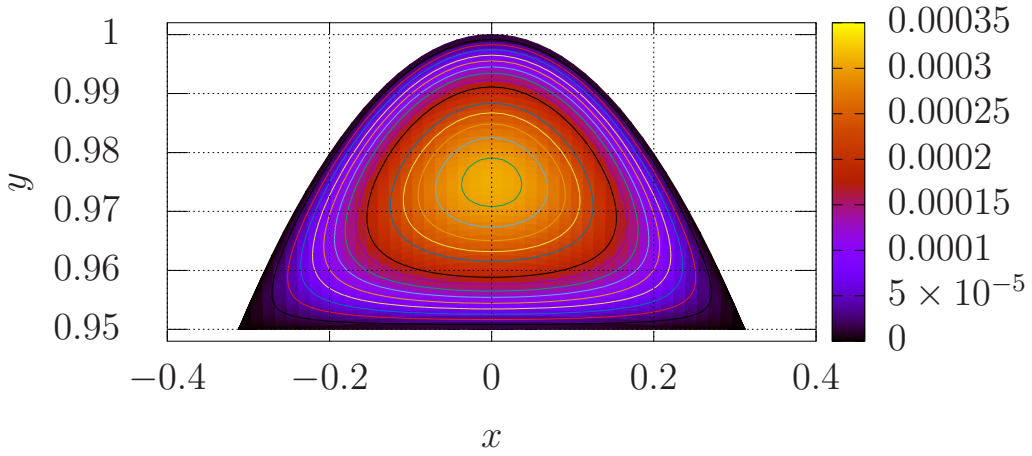

Figure 3.14: Dimensionless velocity profile for laminar flow along a continuous circular section channel.

A very good agreement between the hydraulic diameter approximation and the direct numerical calculation is observed. The close agreement between the two solutions confirms the validity of the simpler hydraulic diameter approach of Eqs. (3.7, 3.8) for relating the volumetric flux and friction pressure gradients to the water channel geometry.

For the two test assemblies A2 and C6, when the measurements in Table 3.5 to equating $T = kA/a^4$ it is find an average $T \approx 6.8 \cdot 10^{-9}$ for assembly A2 and $T \approx 2.6 \cdot 10^{-8}$ for assembly C6. As indicated in Fig. 3.15, these values of the transmissivity function correspond to $h \approx 0.009$ for A2 and $h \approx 0.013$ for C6. Converting to physical units, It was estimated a maximum gap width of 1 mm for

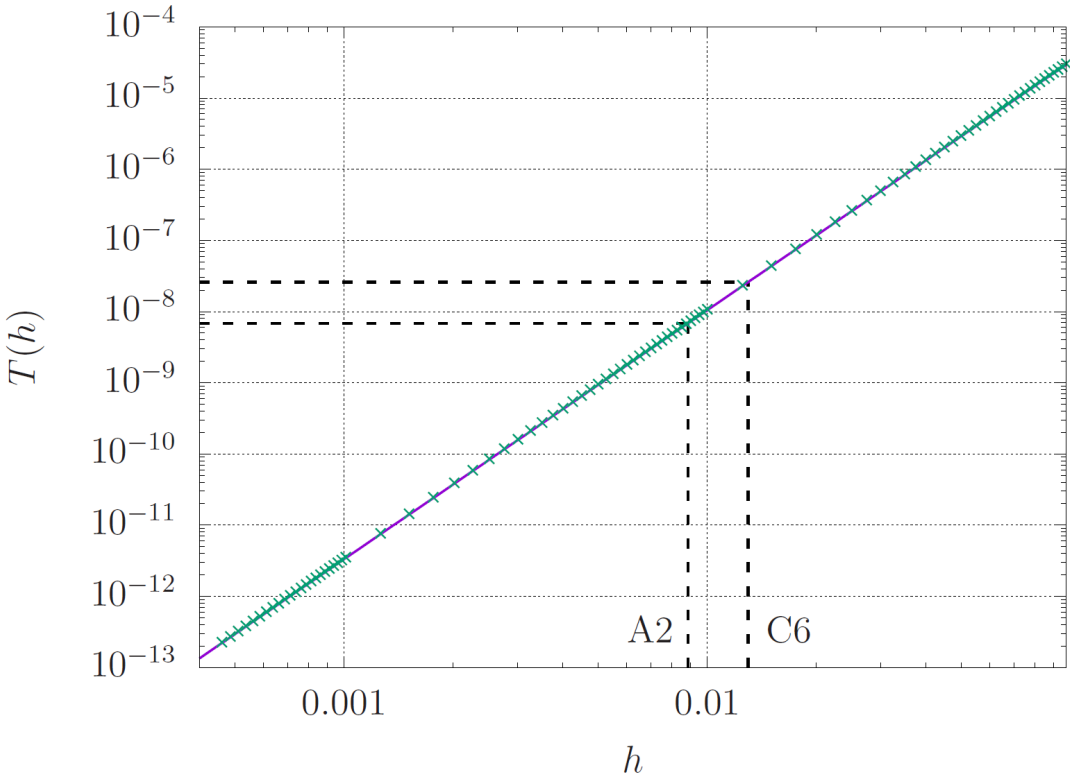

Figure 3.15: Evaluation of the transmissivity function Eq. (3.8) (solid line) for fully developed, laminar flow along a channel of circular section shape, previously presented on Fig. 3.13. Shown as points are numerical solutions to the exact axial momentum conservation equation.

assembly A2 and 1.4 mm for C6. These estimates agree well with the physical gap width measurements and suggest that, indeed, the leakage potential prior to treatment was largely determined by channel widths of 1 to 1.5 millimeters in either assembly.

3.5 Case 3: Irregular microannuli

Case 1 and 2 presented geometries where the migration paths are well defined. However, in downhole conditions the creation of migrations paths might present more complex geometries as a result of different causes, as loading, changes in temperature, changes in pressure and penetration of fluids of different natures inducing the creation of irregular defects. This hypothesis suggests that non-uniform apertures can be found and that the microannuli do not form completely in the interface, cement-casing (circumferential direction) or along the length (axial direction). The leak test on case 3 aims to evaluate the leakage rates when permanent a microannulus is already developed and its geometry appears to be non homogeneous around the circumference and along the axial direction.

3.5.1 Construction

An experiment to analyze the quality of the cement when the tubing is left in hole was designed in 2016 [52]. The test used two set-ups of 35 m of length using casings of 9 5/8-in and 7-in Conventional and expanding cement were mixed and pumped into the assemblies. After the curing phase, the sealing quality was tested using water at 50 and 100 bar of pressure. First, an increase of pressure was induced in the annulus, which follows a linear expansion that creates a permanent microannulus. The estimation of effective microannulus using the permeability test was calculated to be $59,3\mu m$ inside the casing wall and $97\mu m$ inside the tubing. Finally, the assemblies were cut into sections for visual inspection, finding perfect cement displacement at all points. No water channels or trapped fluids were identified [52]. Years after, the assembly Conv-B, which was constructed with conventional cement class G, was cut into sections, and the section 42B, from now "Microannuli cell", was preserved at NORCE facilities, see Fig.3.16. The Microannuli cell, was used for a new set of leakage experiments in 2018 and 2021; the results of those experiments are presented.

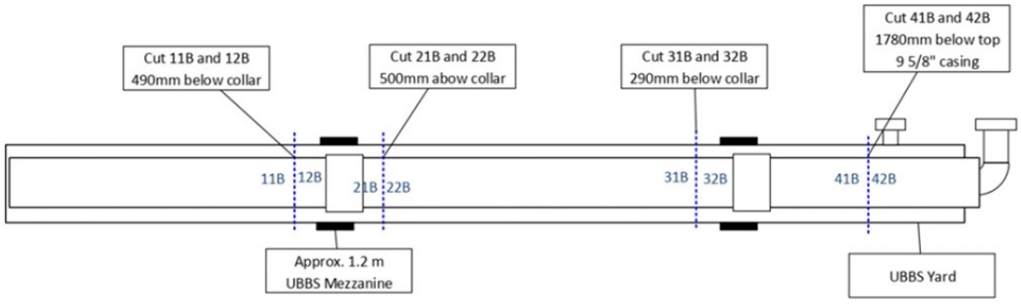

Figure 3.16: Assembly Conv-B, showing section 42 B on the right side

To prepare the cell, first, a cleanout of the inner tubing was done to remove the cement, so that the study of leak potential is completed only in the cement sheath between the 9 5/8-in and 7-in casings. Note that the length of the cement sheath is 1.8 m, while the 7-in casing is 2.5 m in length. The Microannuli cell was instrumented with six pressure gauges and twelve strain gauges type 3/350 CXY31. Fig.3.17 shows the dimension and position of the instruments in the cell body; pressure gauges are shown in blue (named P1 to P6), and the strain gauges are in purple (with numbers between 1 and 12). One particular characteristic of this cell is the tubing eccentricity of 10.5 mm of offset, the position where the thicker layer of annular cement is located will be called the wide side and has strain gauges 1 to 6 and pressure gauges P4,P5 and P6. The narrow side is positioned opposite, where the strain gauges 10, 11, 12 and pressure gauges P1, P2 and P3 are installed. Note

that the strain gauges and pressure ports were installed to record the response in the narrow and wide sides of the cell. Three additional strain gauges were installed in between them at 45 degrees of both (see strain gauges 7,8 and 9 on Fig. 3.17).

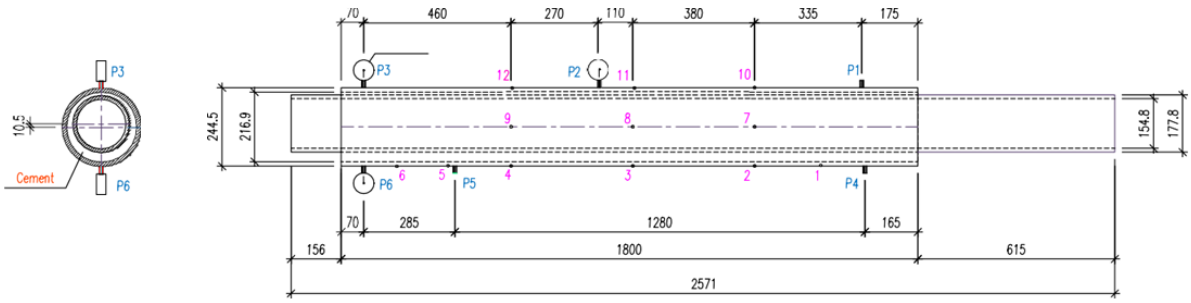

Figure 3.17: Microannuli cell schematic with dimension and instrumentation installed. Strain gauges numbered in pink and pressure sensors numbered in blue

3.5.2 Infrared Thermography (IRT)

The section has end caps welded, so it is not possible to do a qualitative inspection of migration paths by doing a soapy test. Instead, thermal imaging was used to identify the position and severity of defects, so changes in temperature on the casing surface were monitored during flooding. Tests were run initially injecting into the cement sheath (between the 9 5/8-in and 7-in) cold water at a constant pressure of 70 bar and 20 ° C. Followed by injecting hot water at the same pressure and a higher temperature of 45 ° C. The maximum fluid temperature was limited by the test pump capacity specification.

The infrared camera SEEK ShotPro used previously was used with the same set ups to take pictures and evaluate the temperature changes on the outer casing surface. The test duration was 90 minutes to achieve homogeneous heating along the cell. Every 5 minutes pictures were taken and the section was rotated from the initial position to 90, 180 and 270 degrees to cover the evaluation of heating of the whole circumference. Fig.3.18 shows pictures at elapsed times of 0, 30, 60, and 90 min. Snaps shots are presented in two columns where the left side show 90 degrees rotation and the right side shows snap shots at 270 degrees of rotation.

To facilitate the discussion of observations the cell was divided in 3 zones, see labels on Fig. 3.18. The heat diffusion in each zone presents different patterns, being that after 30 min of injection, the radial heating around the injection point (P1) located in zone 1 shows that the water is migrating through external micro annuli between the cement and casing; however, in zone 2, the heat diffusion stops,

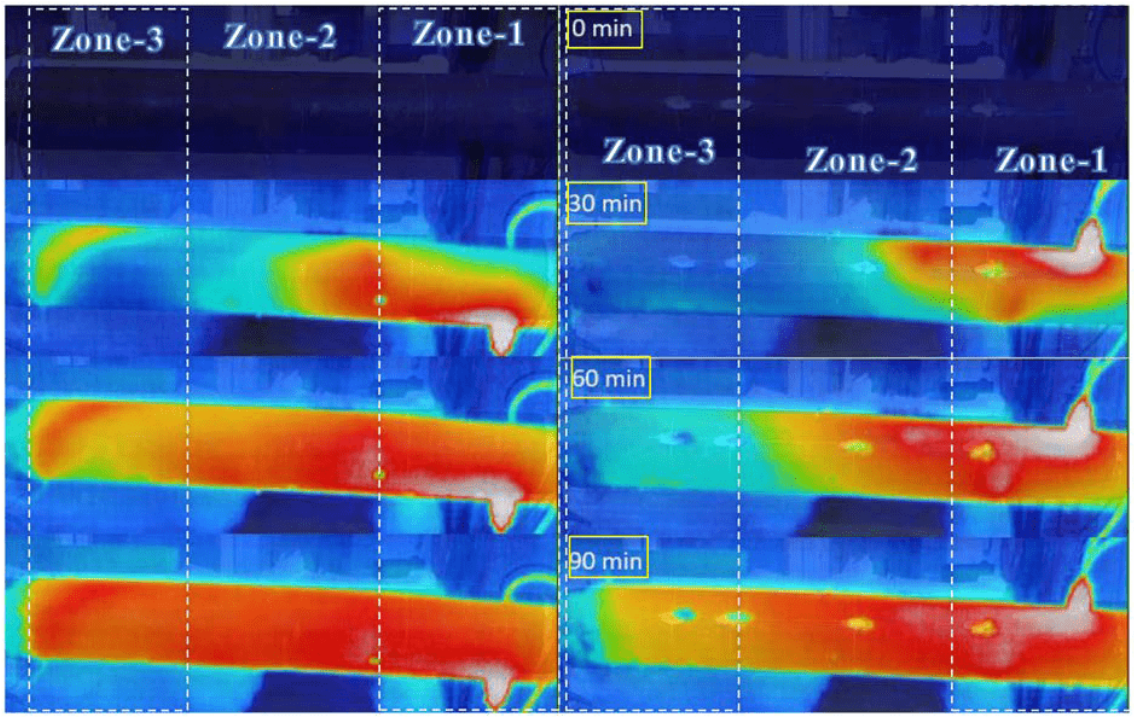

Figure 3.18: Thermal imagining sequence recorded in micro annuli cell when injecting hot water from left to right (using ports P1 as injection point and P3 as outlet)

and the fluid is probably moving deeper inside the cemented annulus and away from the outer casing. Subsequently, a hot spot appears further along the surface in zone 3, indicating that the fluid is coming out from the external interface between cement and casing. This behaviour is observed mainly for the snaps taken at 270 degrees rotation on the leften side column on Fig.3.18. Note that while the heating on the zone 3 appears at 270 degrees after 30 min, for 90 degrees rotation (pictures on the righten side) warm spots only appear after 90 min where the heating is more even in the cell, this suggests that the microannuli is not covering the complete circumference at zone 3. The evolution of the heat in the pictures shows that the hot fluid is moving (from right to left) through the migration paths along the axial direction. The observations of this experiment indicate that a complex migration path is present where tortuosity might be relevant. Such migration path looks like a microannulus, mostly caused by debonding between casing and cement, radial fractures are apparently also presented allowing flow in the radial direction. The water migrates between the internal and external interfaces of the cement sheath within the casings.

3.5.3 Leakage testing

Initial water flow measurements were made in the cell in 2017 and 2018. In both tests leakage was measured in the assembly by connecting a pneumatic piston pump

to the inlet port, see P1 on Fig3.17, and the outlet port was open to atmospheric pressure, See P3 on Fig. 3.17. A picture of the experimental set up used in 2018 is shown in Fig. 3.19. Experiments were conducted at a constant pressure at the inlet and leakage rate was measured at the outlet.

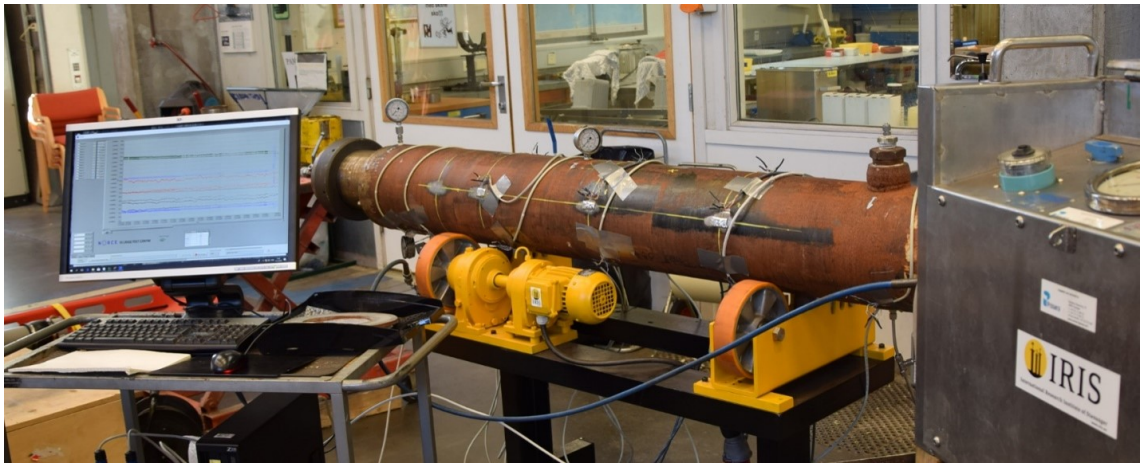

Figure 3.19: Initial instrumentation for testing in 2018

At the time, simple sampling of flow volume was collected using a baker container. The stable value of permeability was defined when the volume of three samples collected were repeatable in the same period of time. Results of flow rate and pressure collected from experiments are presented in Fig. 3.20. The solid lines show the expected flow rates assuming a constant microannuli width and using the Darcy equation (3.3). The measurements collected show that the equivalent a microannulus width in the cell varies between 30-40 µm.

Observing the results of leakage presented on Fig. alone, it is not possible to conclude that a heterogeneous microannulus was present, as it was observed when using infrared thermography. So, later on in 2019 inlet and outlet ports were exchanged to compare permeability when the fluid was injected in the opposite direction to see if the heterogeneity in the microannulus will affect the path and leakage when the direction is changed, the leakage results are presented on Table 3.6. Note that two new direction were tested, P3 to P1 (opposite to the original measurements) and P5 to P4.

High leakage rates were observed when the flow was injected from port P1 as inlet and port P3 as outlet, this direction also corresponds to the previous direction tested in 2017. When the fluid was injected in the opposite direction P3 to P1, the permeability of the system was reduced considerably. Finally, P5 was used as injection port and P4 as outlet, in this case the permeability was even lower, note that this is also the wider side of the annular cement sheath where the eccentricity makes the cement ticker. As a conclusion, the permeability in the narrow side of the annular cement was high in comparison with the wide side. This might suggest that

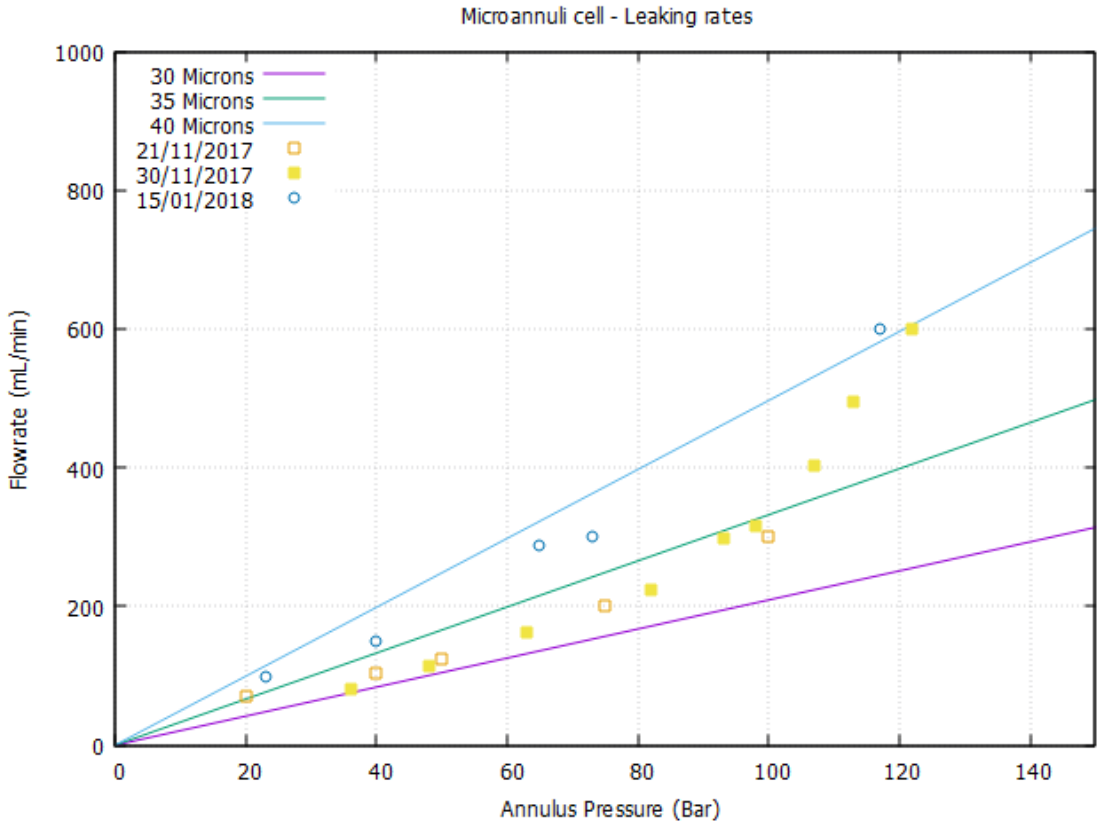

Figure 3.20: Flowrate obtained during experiments in 2017 and 2018. Inlet port P1, outlet port P3

Table 3.6: Flowrates when inlet and outlet are change

Inlet Port	Outlet port	Pressure (Bar)	Flowrate (mL/min)	Position of ports
P1	P3	50	340	Narrow
		75	820	side
		100	1520	
P3	P1	50	220	Narrow
		75	400	side
		100	680	
P5	P4	50	0	Wide
		75	52	side
		100	125	

the tubing eccentricity can have an influence on the development of a permanent microannulus and leak paths.It is likely that this cell has a preferential migration path along the narrow side of the annulus.

A final experiment of leakage was completed in August of 2021, this time more sophisticated equipment and instrumentation were used for testing. A picture of the layout in the lab is presented on Fig.3.21. Every port was instrumented with pressure gauges and a Coriolis flow-meter was installed on the outlet port; so that the steady state conditions were verified using measurements monitored by an ac-

quisition system. Also an advance piston pump, which is pulse-free, was used to deliver a precise flow rate of filtered water into the cement sheath. The pump was set to provide small flow rates of 10, 20, 30, 40 and 50 mL/min. Pressure and flow measurements were monitored to evaluate steady state condition, which were reached after approximately 7-10 minutes of flow at the same flow rate. Results of flow rate and annulus pressure for 2021 are presented in Fig. 3.22 together with data from 2017-2017 data.

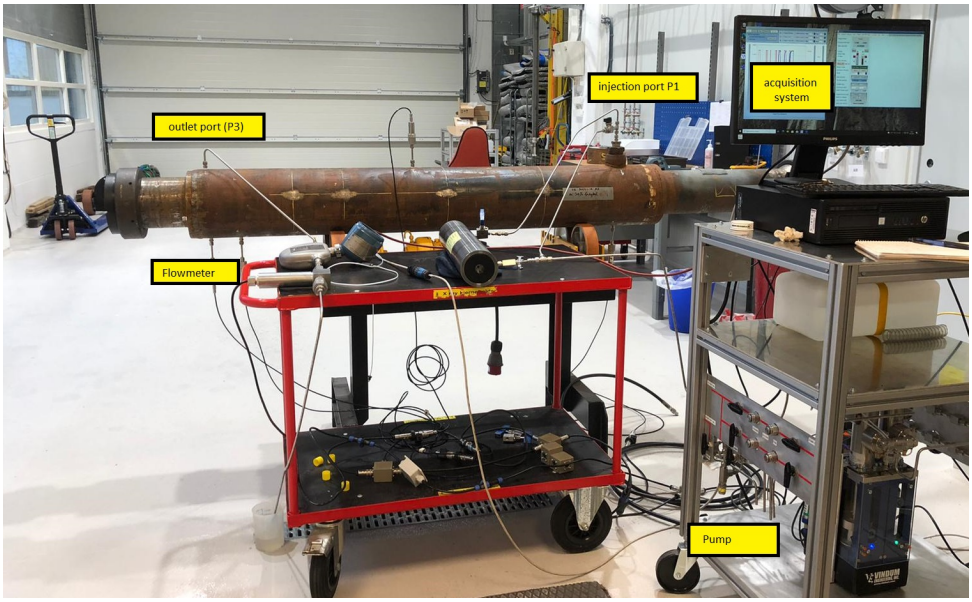

Figure 3.21: Experimental set up used in 2021 for leakage experiments on microannuli cell

While the early measurements in 2017-2018 were done with a pneumatic pump where bigger flow rates needed to be used the last experiment was planned at lower pressures/flow rates. Surprisingly, both ranges of measurements still fall within the range of 30-35 µm of equivalent microannuli aperture, even when 4 years had passed and different equipment was use. It is also observed that in 2021 experiment at lower pressures the linear correlation is stronger. It is possible that the variation away from a linear relation observed in the 2017-2018 data was due to errors induced by measuring with a baker flask.

3.5.4 Logging

The cell was logged using a wireline commercial ultrasonic tool due to collaboration with a service company. Logs were acquired at three annulus pressure of 0, 100 and 150 bar. Fig.3.24 presents the Puls Echo Acoustic impedance on the first 4 tracks, followed by the Flexalone acoustic impedance (on track 5 to 8), the Solid-Liquid-Gas Map- SLB (on track 9 and 10) a figure with ports referenced with depth

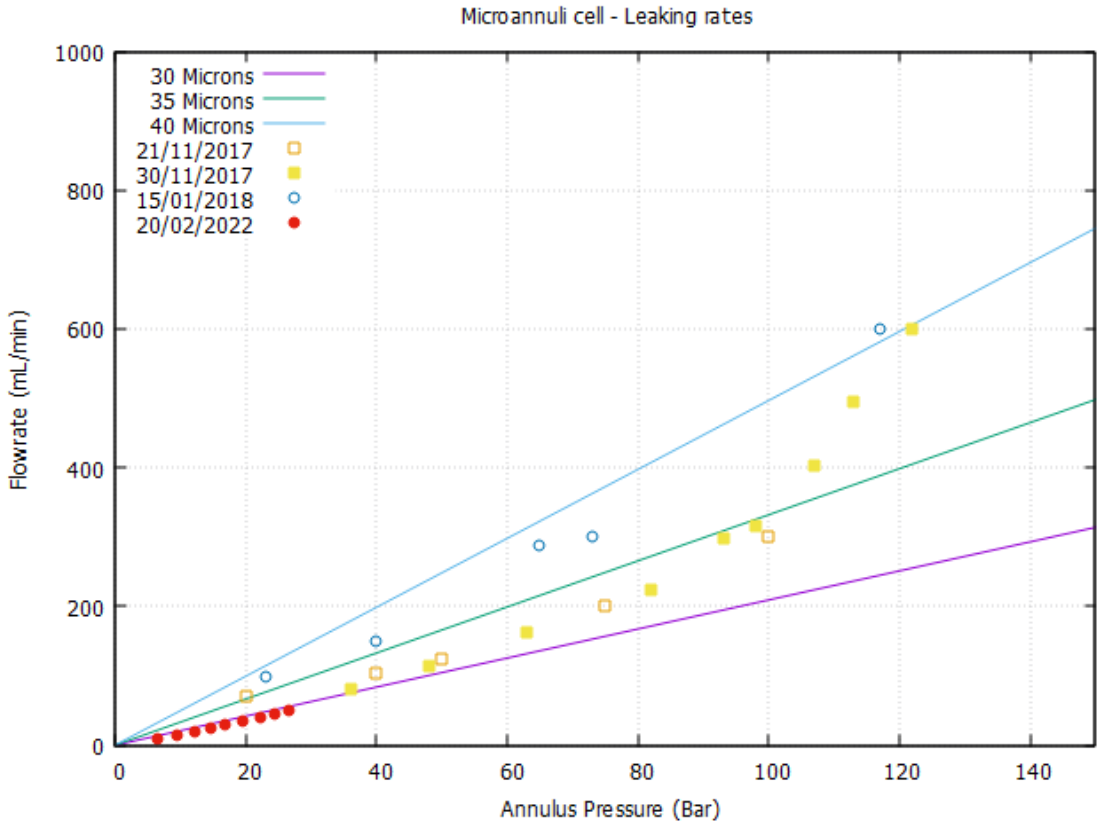

Figure 3.22: Flow rate obtained during experiments in 2017 and 2018

(on track11), and the flexural attenuation map on the last 4 tracks (13-16). The processing of log results was completed by an expert, who identified 3 main regions along the cell, indicated in Fig.3.24 as Zone 1, Zone 2 and Zone 3.

Log interpretation done by experts is discussed in depth in a published article [2], but findings regarding log features across the 3 main zones are briefly presented here:

- Zone 1: Presents major ultrasonic map disturbances, understood as a degraded bond quality between the 7-in casing and the cement sheath, are noted approximately between 300 mm and 600 mm. The location of this microdebonded or microannulus zone is noted almost azimuthally around the casing. This zone is also where the more significant differences are observed between different log passes for the average values measurements of acoustic impedance (AIAV) and, to a certain extent, flexural attenuation (AIFAV). At the higher annulus pressure (150 bar), both passes (with different vertical resolutions) revealed slightly lower acoustic impedance values when compared to the first passes done with atmospheric pressure, or 100 bar. This could be explained by the possibility that the extra pressure appeared to have created a bigger microannulus around this short zone.

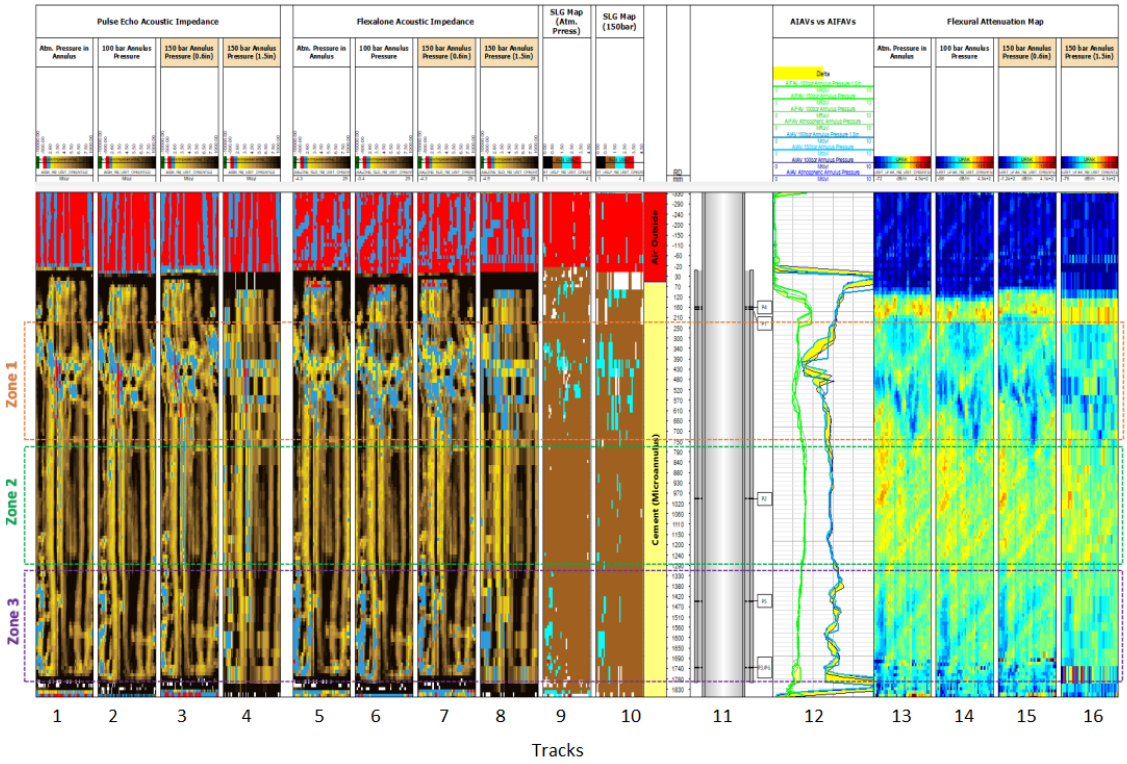

Figure 3.23: Logs recorded in microannuli cell in 2019, first published in Govil et al.[2]

- Zone 2: The region appears mostly undisturbed in terms of bond quality across different passes. Ultrasonic measurements such as acoustic impedance and flexural attenuation show similar values between passes. In the acoustic map, a frame appears to show signs of minor microdebonding as the test increases in pressure. This might indicate a channel (with reduced dimensions) across which upper and lower zones might communicate when annulus injected pressures are increased.

- Zone 3: Some bond quality disturbances (reduction of acoustic impedance) are noted across zone 3; however, zone 3 is different from zone 1 because the poorer bond quality is noted to be located mostly towards the narrow side. This can be identified as the blue spots located longitudinally within the acoustic maps for all the passes, which likely represent a microannulus channel created across the interval.

The Logs presented in Fig. 3.24 present the quality of the cement bond between the inner 7-in casing and cement while the thermal images present the bond quality between the outer 9 5/8-in casing and cement in Fig.3.18. Both results, however, are consistent in finding that the better quality of cement is present on the zone 2 of the cell.

3.5.5 Confining pressure effect

The experimental set up rigged up in 2018 allowed measurement of the leakage trough micro-annuli varying the internal pressure in the tubing. By changing the pressure in both the tubing and annular independently. In this experiment, the annular cement was saturated with water, and all of the ports in the cell were kept closed. Twelve Strain gauges were installed to measure the deformation, position of strain gauges can be found in Fig. 3.17. Six strain gauges were placed on the wider side, aligned to the axis formed between ports P5-P4. While 3 were installed on the narrow side, aligned to the axis P1-P3. All strain readings were acquired at a fixed sampling frequency throughout the experiments of 1 hertz.

The goal of the experiment was to evaluate the radial expansion of the outer casing when the pressure inside the tubing is kept constant at and the annulus pressure is increased between 0 and 125 bar in steps of 25 bar. this was designed to simulate a combined loading. Fig. 3.24 shows the results of radial deformation for the four tubing pressures used. As informative, a figure in the bottom indicated the two regions in the assembly. In purple and labeled as 1 is the region which corresponds to the tubing, while the region on blue, labeled as 2 correspond to the annular space.

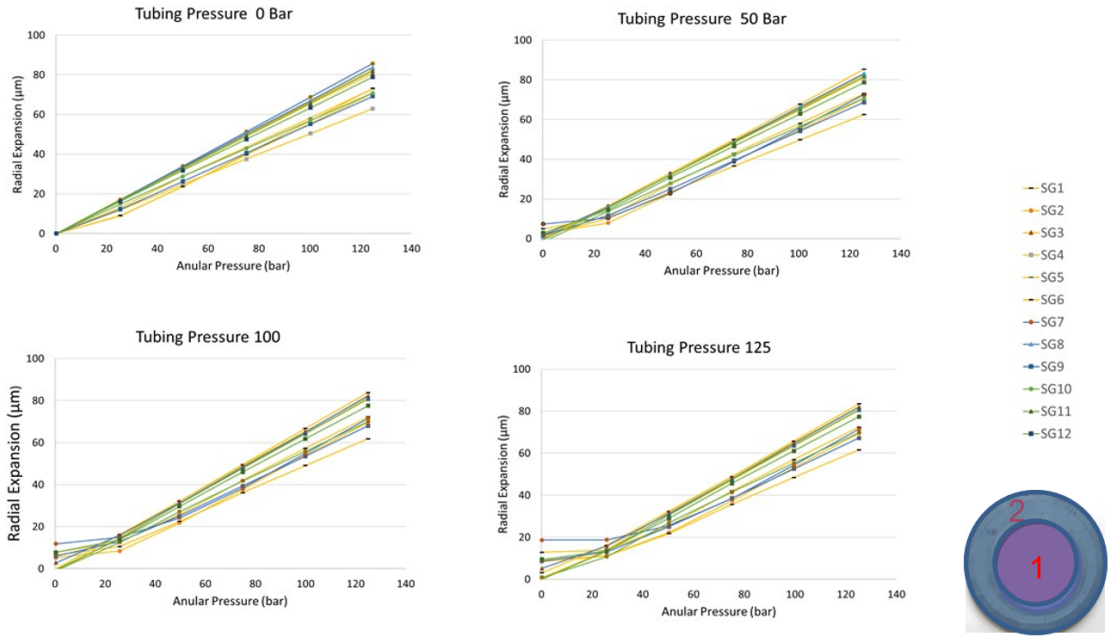

Figure 3.24: response of strain gauges when confining pressure in the tubing and annular pressure is increase.

To facilitate visualization, strain gauges placed on the wider side are plotted in yellow in Fig 3.24, while those installed in the narrow side are plotted in green. The strain gauges in blue were installed in the region in between. Please see the installed

position of strain gauges as marked in purple in Fig. 3.17.

As the annular pressure is increased, with 0 bar of tubing pressure, the outer casing surface responds with an almost linear radial expansion that reaches approximately 83 µm at 125 bar. Note that all strain gauges respond linearly to the loading. When tubing and annulus pressure is applied, the response on deformation indicates that the microannulus can be closed only in some cases where high pressure in the tubing is combined with low pressure in the annulus (see the flattening on some of the strain gauges response). Here, when tubing pressure is applied and the microannuli is small or absent, the loading will expand the inner tubing and the annular cement together, creating better contact between the annular cement and the outer casing. This can be observed by the lack of radial deformation of some strain gauges at relatively low annulus pressures, as for example on strain gauges 1, 2 and 7. After the annulus pressure exceeds approximately 50 bar, the radial deformation of the outer casing surface is linear again for all the strain gauges, indicating that the radial deformation is mainly due to the applied annulus pressure and the microannulus is open again. Additional details of this experiment can be found in an additional publication presenting this experiment in detail [38].

Comparing the deformation response behaviour with the observations done by logging in zone 1, 2, and 3. It can be conclude that a good correlation is observed for zone 1 (with strain gauges 1, 2, and 7 installed), where the results of the ultrasonic log show a larger microannulus in the interface between the tubing and cement that can relate with the observations of a lack of radial expansion.

3.6 Case 4: Field Sandwich Sections

The Valhall field is located in the southern part of the Norwegian sector of the North Sea, approximately 290 km offshore and at 69 m water depth. The presence of exploitable hydrocarbons was discovered in 1975, and the field started production in 1982 from an over-pressured, under-saturated Upper Cretaceous chalk reservoir [167]. The field produces paraffinic oil of 36 API gravity from the Tor and Lower Hod formations, having produced 500 MMSTB ($79.5 \times 10^6\,\mathrm{m}^3$) by 2002 [168] and doubling this volume by 2017 when a production record of 1000 MMSTB ($159 \times 10^6\,\mathrm{m}^3$) was achieved. Currently, the field consists of six platforms and has simultaneous activities including production, drilling operations and plug and abandonment (P&A) [169]. Up to now, 14 wells have been permanently P&A'd on the Valhall field, in accordance with the requirements of the Petroleum Safety Authority (PSA) [36, 37] and the guideline NORSOK D-010 [170]. When it comes to meeting the national requirements, what has proven challenging and time-consuming is the removal of casing sections in the upper part of the wells in order to place cross-sectional surface

barriers. This procedure is required for wells recorded to have Sustained Casing Pressure (SCP) records and/or poor cement quality behind the casing.

One well, originally drilled and completed in 1985 and in production for 33 years, was submitted to well integrity assessment prior to the abandonment operation. Cement evaluation was performed using acoustic logging tools, which indicated poor bond quality in the upper interval and moderate to poor quality in the lower intervals [171]. The well records showed 50 bar of SCP and $CaBr_2$ brine trapped and stationary for more than 2 years in the annulus between the 9 5/8-in (0.244 m) and 13 3/8-in (0.339 m) casing. Based on the log assessment, the operator chose to cut and recover sections of 13 3/8" and 9 5/8" casing strings with class G cement in between. Additional details describing the well logging, retrieval operation and surface re-logging are presented in Obando et al. [171]. In total, twenty-six sandwich sections were recovered (over the interval of 47 to 376 m well depth), enabling the subsequent installation of the surface barrier between 138 and 222 m. The location in the well from which the sandwich sections were recovered is shown in Fig. 3.25.

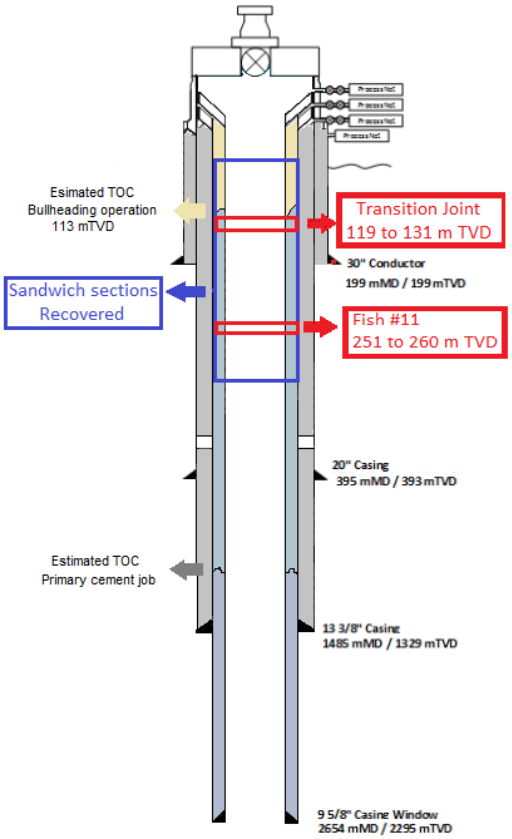

Figure 3.25: Well design showing the location of sections. In blue, location of the twenty three recovered sections and, in red, the two sections donated and object of study

The well reports were consulted to understand better the cement contained in the sections. The 13 3/8" casing section was cemented to the surface with 100%

returns, whereas the 9 5/8" casing was cemented in two stages. The first stage was a conventional job whereby the cement slurries were displaced down the inside of the casing and up into the annulus. Two slurries were pumped in this stage: A lead slurry with 15.5 ppg ($1857\,\mathrm{kg\,m^{-3}}$) density and a tail slurry with 15.8 ppg ($1893\,\mathrm{kg\,m^{-3}}$). The liquid phase was prepared with drill water, including additives for fluid loss control. The estimated W/C ratios were 0.48 and 0.45 for the lead and tail slurries. The first stage resulted in a cement job without returns to the surface due to the losses to a weak formation, so the second cement job was performed by bullheading cement through the annulus from the surface. For this slurry, the liquid phase was prepared with seawater, and the W/C ratio was 0.45, the slurry had 15.8 ppg ($1893\,\mathrm{kg\,m^{-3}}$).

3.6.1 The Valhall Cells

Two of the twenty-six recovered sandwich sections were donated for further study; see location on the well on Fig. 3.25. The sections were named Transition Joint and Fish # 11 and their location in the well and general specifications are presented in Table 4.1 and Fig. 3.26. Both sections were retrieved from the vertical part of the well where the slurry was bullheaded. It is generally assumed for the vertical section that the pipe hangs vertically due to gravity and the eccentricity between the casings is not an issue [172]. However, for both sections, a significant eccentricity of the 9 5/8" casing relative to the 13 3/8" casing was found. After receiving the sections, a visual inspection was performed, and the ends were dressed. The nomenclature of the bottom and top was maintained according to the originally recorded placement of the sections in the well, where the top is the shallowest well depth.

Transition Joint

The shallowest section, called the Transition Joint, was recovered from 119.2 to 131.5 m well depth, see Fig. 3.26. The overpull applied during retrieval was 310 Klbs. This section contains the top of cement (TOC), the region where the interface between the original fluid in the well and the cement pumped into the annulus is found. The position of this interface can be challenging to locate, especially when washouts are present or substantial losses occur during the cementing job. Estimations based on the volume of cement slurry that was pumped into the well predicted that the TOC should be found at 113 mTVD, whereas the results of surface re-logging using ISBL/VDL indicated that the true TOC was at 123 mTVD [171]. For the rest of the documment, we will use the depth of 123 mTVD when referring to TOC as indicated by the logs. Just above the TOC, the Cut # 3 was made; see Fig. 3.26. Here the annular space was filled with a brown coloured material from mud solids,

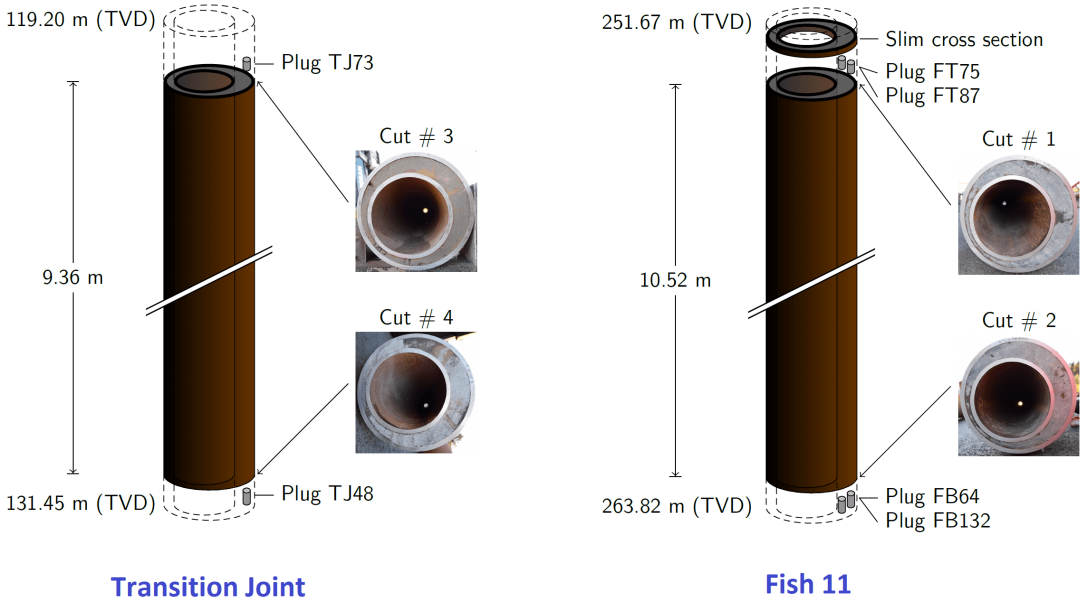

Figure 3.26: Transition Joint and Fish # 11 diagram including pictures of the ends (Bottom and Top)

and empty spaces were observed on the narrow side of the annulus. At the bottom, the Cut # 4 was made; cement fully covers the annular space, and yet there was evidence of intrusions of brown material, see Fig. 3.26.

Fish # 11

The deepest section, called Fish # 11, was recovered from the interval 251.7 to 263.8 m well depth, 140 m below the TOC, see Fig. 3.26. The over pull applied during retrieval was 500 Klbs. In this section, a 9 5/8 casing collar was present 4.2 m above the bottom. Cut # 1 was made at the top and Cut # 2 at the bottom. Cement covered the full annular space at the top and bottom. Local defects were present but were filled with mud solids; however, the regions with mud intrusions looked smaller and less significant compared to the Transition Joint. At both ends, there was evidence of cement debonding at the inner and outer casing surface, which appeared to be worst on the narrow side of the annulus.

3.6.2 Soapy test

A qualitative investigation of the leakage potential of the two sections was performed with open ends and before the sections were dressed with welded end-caps. The plan for this initial testing was to apply low gas pressure to pressure ports in the middle of each section and to visually observe where gas migrated out through the open ends. Each end was kept covered by a thin film of soapy water and as gas would

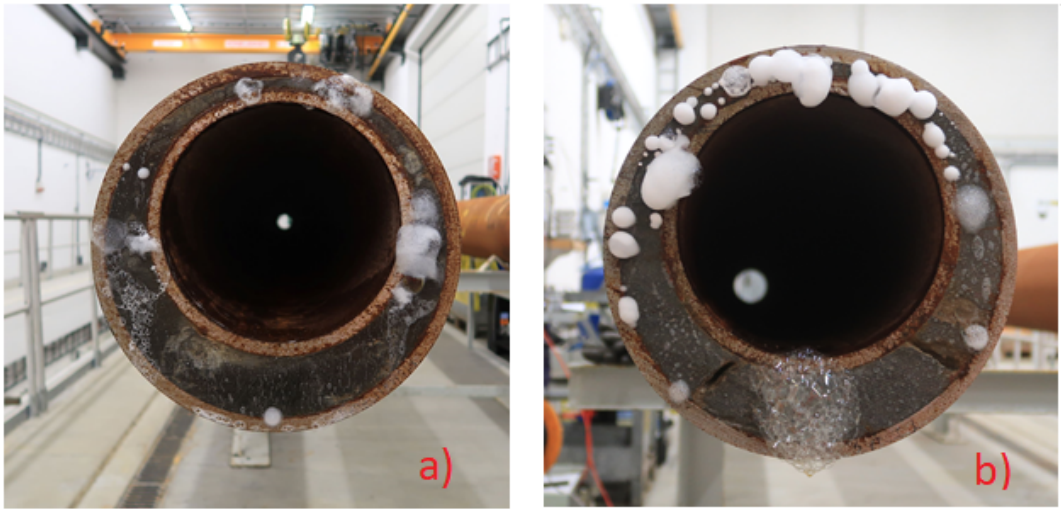

Figure 3.27: Qualitative gas leakage experiment aiming at detecting where gas escapes from the open ends of the test sections. a) migration through the bottom part of the Transition Joint. b) Leakage paths on the Top end of Fish #11

percolate through the open ends and the film of soapy water it would generate soap bubbles as visual traces of where gas is predominantly leaking. The purpose of this initial test was to provide a qualitative and visual impression of where gas is mainly flowing out of the test cells before welding on end-caps at the top and bottom of each section. The tests were performed by mounting the two sections horizontally inside a test hall and applying up to 5 bar of N2 gas at pressure in the middle of the sections. Gas pressure was maintained at a fixed level while the gas flow rate into the assemblies was measured with a low-range Coriolis flow meter.

Fig 3.27 shows a comparison of two images taken when testing Fish #11 and Transition Joint. Visual observations and Coriolis flowmeter measurements of injected gas volume during these tests suggested significantly less flow on Fish #11 compared to the Transition Joint. For the Fish #11 section, see Fig 3.27b, soap bubbles occur primarily at points along the cement-steel interfaces, with a few bubbles originating at points in the bulk cement. The majority of soap bubbles originate from roughly the narrow half sector of the annulus.

For the Transition Joint, see Fig 3.27b, the highest density of soap bubbles along the narrow side of the annulus is observed, with most soap bubbles occurring at the cement-steel interfaces of the inner and the outer casings. This appears to be the predominant direction of leakage in the lower part of the Transition Joint. It was also observed soap bubbles generated at the inner casing-cement interface in the wide sector of the annulus and also a few bubbles originating at locations along the bulk cement, but most "activity" occurs in the narrow sector of the cemented annulus. No gas was observed to leak through the top part of the Transition Joint. The

Transition Joint contains the top-of-cement nearly midway along the test cell: Above the TOC, the annular is filled with a brown, plastic material that may originate from the drilling fluid and/or spacer fluid from the original cementing operation. This material may be primarily settled solids (e.g. weighting material). No gas leakage was visually observed through the top part of the test assembly which contained this plastic material for test pressures up to the maximum test pressure of 5 bar. Note that even if the material above the top-of-cement restricted gas flow at pressures up to 5 bar test pressure, subsequent water flooding and leakage testing with water resulted in breakthrough and the opening of a flow path through to the top cross section of the test assembly. Subsequent testing indicated that the material above the top-of-cement has been irreversibly changed due to water flooding and has lost its original sealing ability.

3.6.3 Logging

In January 2018, before the cut-and-pull operation, the uppermost portion of the well (47 to 260 m) was logged for annulus and cement evaluation with the latest-generation ultrasonic tool, along with a conventional sonic cement-bond log/VDL. The logging objectives were to examine the 9 5/8-in casing/cement bond and identify the TOC to choose the optimal cutting depth for retrieving the 9 5/8-in casing. The 9 5/8-in-casing inner borehole was reported to contain a 1.51 specific gravity (s.g.) calcium bromide brine, which had been stationary for nearly 2 years and was not circulated before logging. Segregation of the inner fluid was noted with a clear change in fluid slowness over approximately two-thirds of the logged interval. The slowness values did not match expected theoretical values for the reported brine. This prompted the original data to be processed using a novel technique called R+ inversion, which helps to eliminate, to some degree, the dependence of borehole-mud properties such as fluid acoustic impedance and fluid slowness used in traditional ultrasonic processing [2, 173]. The logs and processing results are shown in Fig.3.28.

The interpretation of the original logs revealed that the uppermost interval within the zone deemed to have a poor bond quality contained original fluids in the annulus between the 9 5/8-in casing and the 13 3/8-in casing. Log interpretation of the lower intervals with moderate and moderate-to-poor bond quality revealed the presence of solids in the annulus, initially topped by barite segregation from original mud, followed by a contaminated cement and then lower down by dry microdebonded cement. Based on the log result in Fig.3.28, the 9 5/8-in casing was cut above the TOC at 119.2m and retrieved without overpull. Thereafter, the 9 5/8-in 13 3/8-in casings were simultaneously cut using long cutter blades at each joint from a depth of 276m and up to the first joint below the 9 5/8-in free point at 131.4 m. The

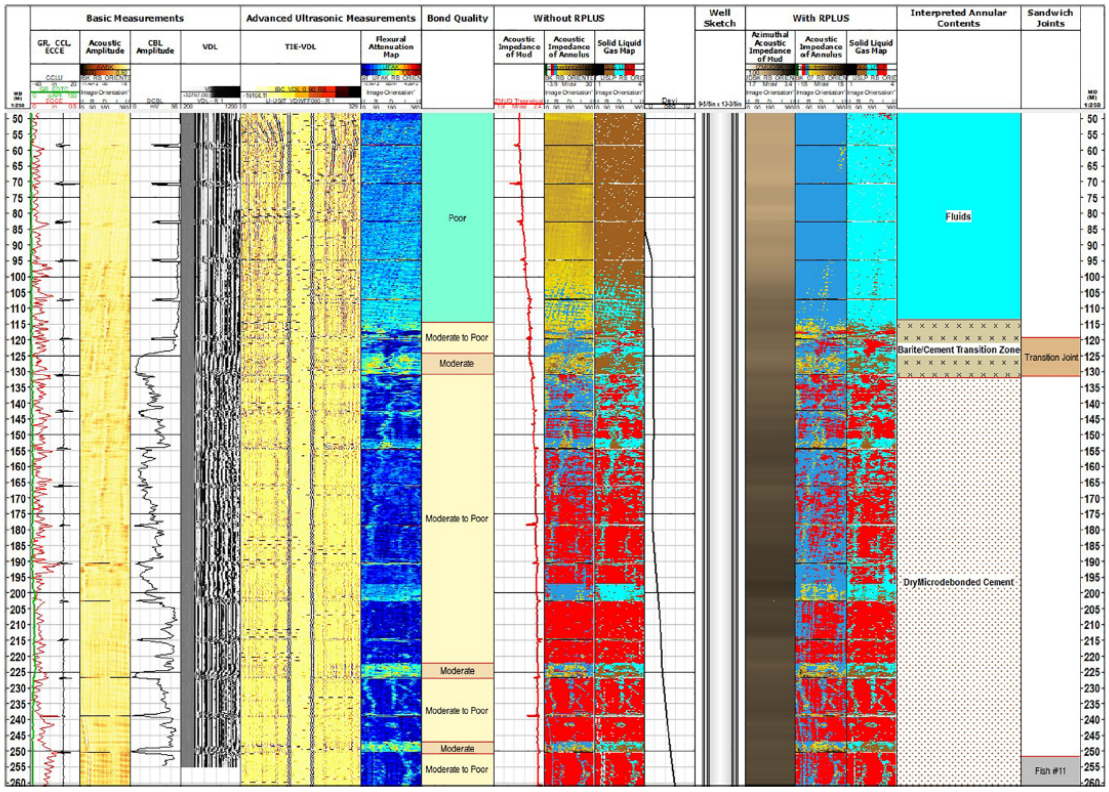

Figure 3.28: Original log from January 2018. The original position of both sections in the well is shown on the Right-most track. Figure was previously published in Skadsem et al.[3]

13 3/8-in casing was cut at 58.7 and 106.3 m, and these sections were pulled with the assistance of a downhole jacking tool. There were 26 sandwich joints retrieved individually. Each joint consists of the 9 5/8-in casing, annular cement, and the outer 13 3/8-in casing. The joints were numbered by order of retrieval. Importantly, two of these joints were retained by the operator for further studies, and these were subsequently referred to as the Transition Joint and Fish #11. According to the interpretation of the in-situ logs, the Transition Joint covers the TOC transition zone where cement and barite sagging are indicated. For the Fish #11 joint, the log interpretation indicates mainly dry microdebonded cement.

Following the initial examination of the joints described previously, preparations were made for onshore relogging using pulse-echo method, pitch-catch configuration, and VDL, per the log shown in Fig. Fig.3.28. An important purpose of relogging the joints onshore was to confirm that the annulus cement is in the same condition as when it was logged in the well. Another reason for the onshore test was to study the effect of dry and wet microannuli on the log response, as well as the potential effect of inner casing pressure on the bond between the 9 5/8-in casing and the cement. Because ultrasonic cement-evaluation tools are sensitive to the type of fluid that is present in the annulus, it was decided to first log the joints with the annular

cement in the original condition as received onshore. In the following, this state is labeled as "dry." Subsequently, and after completion of dry logging passes, the joints were waterflooded in an attempt to saturate the annular cement with water. We will refer to this state as "wet." To investigate the sensitivity of the log response to inner casing pressure, logging passes were made at 20-, 30-, and 40-bar casing pressure for both dry and wet conditions. Pressure-test ports were machined at various points along each joint to provide access to waterflood the annulus and perform interval leakage testing. To allow logging under internal pressure, pressure-tight bulkheads were installed on both joints. Finally, a blind flange sealed the bottom of the section, and a lubricator fabricated from a 9 5/8-in casing joint was connected to the top with a stuffing box allowing logging with pressure.

Two logging resolutions were selected for logging passes; referring to azimuthal and vertical resolution, these resolutions were 5 and 1.5 in and 5 and 3.0 in, respectively. Thus, the entire logging procedure yielded 24 passes for analysis, with 12 for each sandwich joint. For this paper and comparative simplicity, only the passes with the higher vertical resolution (5 and 1.5 in.) are used. In the following sections, the logging results are displayed graphically and compared. All the acoustic-properties maps use the same color scale for the respective measurements at each pass and condition. Scale is also respected and kept equal for the average curves. This is to allow a quick graphical assessment and comparison of the tests and logging results. Fig.3.29 shows the acoustic-impedance maps for the Transition Joint at different borehole pressures and under dry and wet conditions. The lower portion of the logged interval (5 to 9m) exhibits relatively higher acoustic-impedance values where cement is expected. The upper 5m reveal a more contaminated type of annular solid containing wider liquid pockets and channels. Varying the borehole pressure appears to have a negligible effect on the acoustic properties of the material in the annulus as measured by the acoustic impedance for both wet and dry conditions. However, there is a very clear difference in the response of the acoustic properties between wet and dry conditions, evident by the marked color contrasts between the maps for acoustic impedance. Also, when comparing the acoustic impedance from pulse-echo (AIAV), the difference in their responses is highlighted by the blue shading between the two curves (Track C in Fig. 3.29). This response might be explained as the originally existing cavities and dry microdebonding were now filled with water after flooding the joint, thus enhancing to a useable level the measurements sensitivity to the properties of the solid material in the annulus and potentially enabling an estimation of its true acoustic properties.

Logging results for Fish #11 are shown in Fig. 3.30. A minor difference in acoustic impedance between pressure passes is noted, especially under dry conditions (see Track D in Fig. 3.30). This small difference appears to be associated with

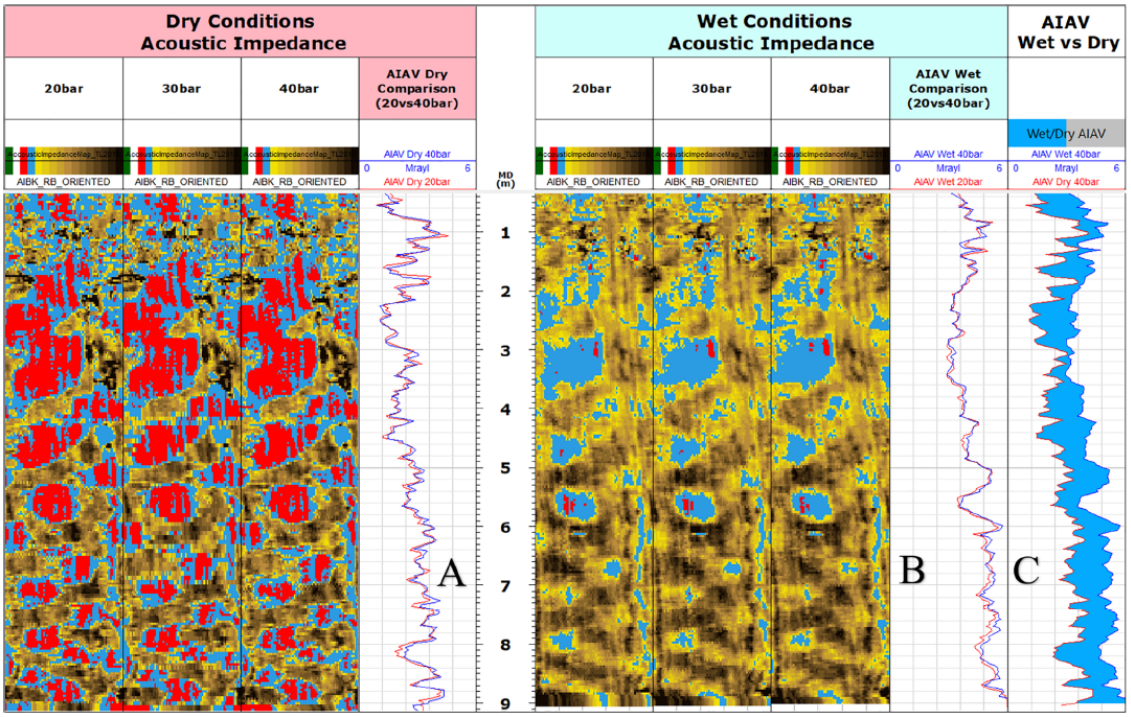

Figure 3.29: High resolution log for Transition Joint, collected on surface for dry and wet conditions. Log shows acoustic impeadance and AIAV [4]

the presence of microdebonded cement or cement with a microannulus [174]. The poorest bonding quality appears to occur again across the azimuthal side where the annulus-cement sheath is thinner, likely because of casing centralization, revealing a significant liquid channel. Per the results from the Transition Joint described previously, comparing wet and dry conditions reveals clear differences for acoustic impedance and flexural-attenuation response. In this case, this is mostly noted in two zones: one across the top interval (0 to 6.5 m) and another one at the short bottom section (9 to 10 m) where the passes run at dry conditions revealed the presence of microdebonded cement. The interval around the casing collar, and in fact above the casing collar in the well (6.5 to 9m in the log; see Track E in Fig.3.30), showed no major difference between wet and dry passes. This suggests better cement-bonding conditions that have remained undisturbed after the injection tests were attempted along the joint.

Note here that observations made during injection of water between dry and wet logging passes are in qualitative agreement with the results of the surface relogging, specifically the right-most tracks in Figs.3.29 and 3.30. First, for the Transition Joint, logging outputs suggest the ability to inject water across the annulus, and the flow tests confirmed this observation by the different flow rates measured at the outer ports installed across the joint. Note that during low-pressure testing with gas, as discussed previously, the settled solids on TOC provided a seal, resulting in no discernible gas escaping the joint through the settled solids. As part of the water

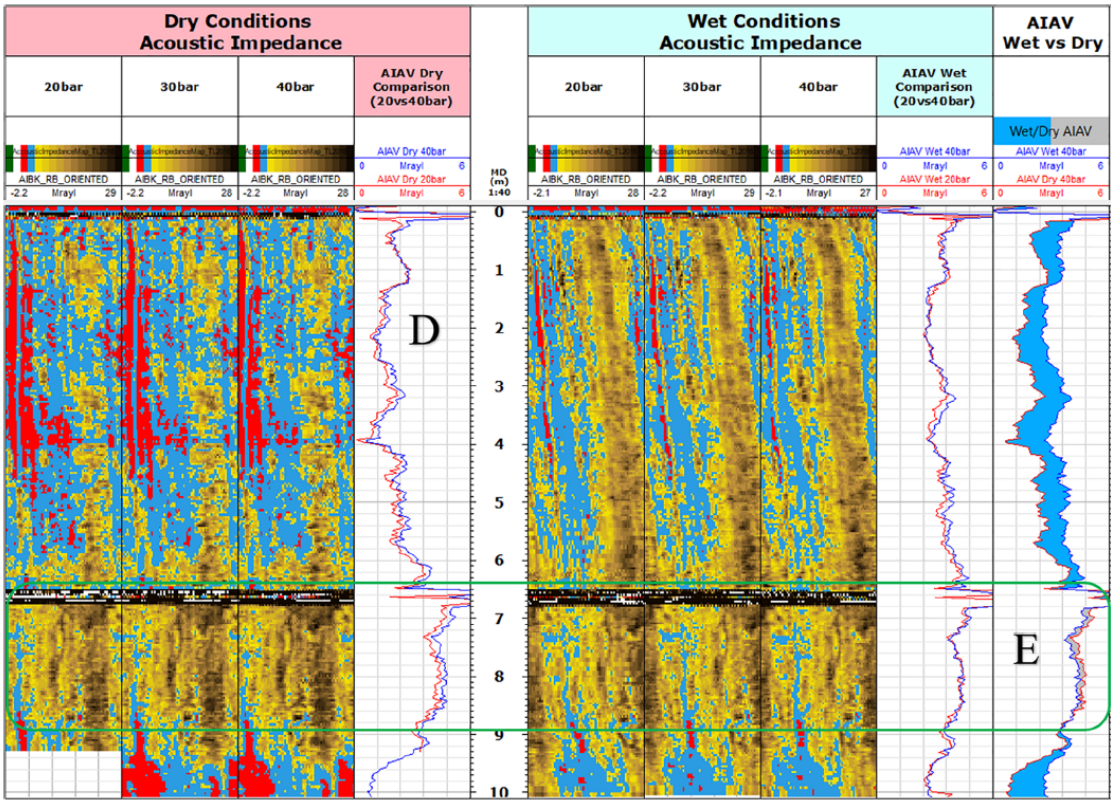

Figure 3.30: High resolution log for Fish #11, collected on surface for dry and wet conditions. Log shows acoustic impeadance and AIAV [4]

flooding operation between logging passes, this part of the joint ceased to provide a seal, and water flowed through the entire joint. The spatial resistance to flow will be discussed in more detail in the following section. Further, in Fish #11, the top-most interval (0 to 6.5 m) as well as the lower 1m (9 to 10 m) of the section showed a marked difference for acoustic properties between dry and wet conditions (Fig. 3.30). The injection tests corroborate this assessment by allowing water to flow and the rate to be measured, but with the notable exception of the short interval around the 9 5/8-in casing collar. According to the injection-test results, this cement with its nearly complete azimuthal coverage around the casing appears to have blocked the water flow through the annulus because the outflow rates were too low to be measured.

3.6.4 Leakage testing

For flooding tests on Fish #11 and the Transition Joint, a number of test ports have been mounted along and at the end of each test section. Short segments of the annulus cement have been removed at the ends to allow access to the entire annulus cross-section through ports P1 and P8. The other six ports are drilled radially through the 13 3/8-in casing and the annulus cement and to the outer wall of the

Figure 3.31: Typical instrumentation during leak testing on Transition Joint.

inner casing. This allows us to apply pressure at different positions along the test cells and to measure leakage rates specifically through different ports as required. The available test ports for leakage testing of each section are listed in table 3.7. Ports P1, P2, P4, P6 and P8 are in the wider side of the sections while P3, P5 and P7 on the narrow side. Fig. 3.31 shows the Transition Joint instrumented with pressure gauges on the wide and narrow sides and insulated covers to reduced the effects of a change in temperature.

Table 3.7: Position of test ports along the two sections.

Section	P1	P2,P3	P4,P5	P6,P7	P8
Transition Joint	0.0 m	2.4m	4.7 m	7.1 m	9.4 m
Fish # 11	0.0 m	2.7 m	5.3 m	8.0 m	10.6 m

Gas testing involving the sandwich sections was performed by first closing all pressure ports and connecting the test assembly through port P8 to a nitrogen source to pressurize the annulus to 20 bar. Once the pressure recorded at all ports appeared stable, the back-pressure at the designated outlet port was reduced step wise, while measuring at each step the stabilized gas flow rate injected into the assembly. The equipment used to control flow injection is equivalent to the one used by van Eijden et al. [153].

The normalized flow rates (volumetric flow rates for N2 at atmospheric pressure) through Fish #11 from inlet port P8 to the four different outlet ports are shown in Fig. 3.32 as functions of the applied pressure differential. The pressure at inlet port P8 was maintained at 20 bar throughout the tests. It was not possible to measure leakage through Fish #11 between the inlet port P8 and the lower ports, P1, P2 or P3. This suggests a segment of cement close to the bottom of the joint which is highly effective in restricting the gas flow. This is also consistent with the initial gas testing with open ends, where no visible gas or soap bubbles were generated at the bottom cross section.

Starting with the results from Fish #11, It was observed that the flow restriction introduced when setting P4 and P6 as outlet ports result in nearly identical effective

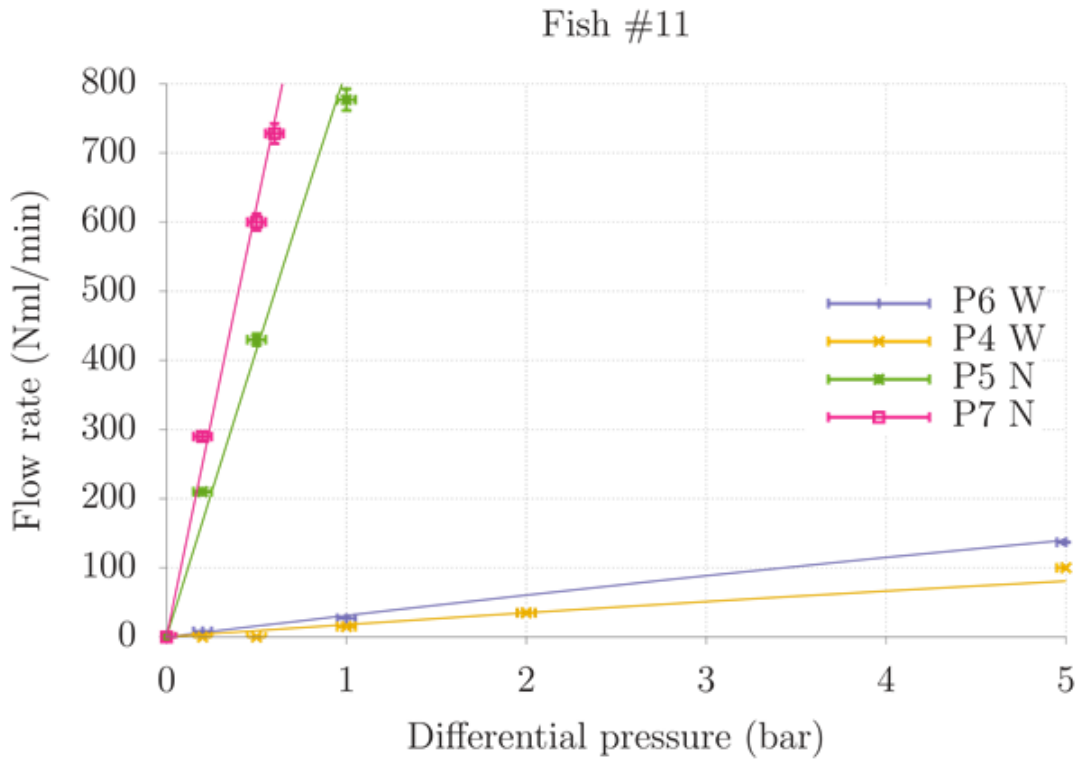

Figure 3.32: Measured, normalized gas seepage rates through the annulus of Fish #11 to different outlet ports

micro-annulus sizes. As discussed above, it is likely that gas migrates from the inlet P8 and down the annulus through the narrow side, before flowing toward the outlet port on the wide side. Such a flow path is clearly in violation with a micro-annulus assumption. Leakage rates through the narrow side ports P5 and P7 correspond to effective micro-annuli of between 15 and 17 µm.

Table 3.8: Fish #11 gas leakage results

Inlet port	Outlet port	Permeability (mD)	Microannulus (μm)
P8	P7 (N)	9.9	15.4
P8	P6 (W)	0.2	4.5
P8	P5 (N)	13.5	17
P8	P4 (W)	0.3	4.8

The corresponding leakage measurements through the Transition Joint are shown in Fig. 3.33. Using the same procedures described above, port P8 is used as the inlet port and maintained at 20 bar throughout the tests. Differences between the leakage rate measured when the outlet port is varied between the wide and narrow side are less than for Fish #11. The flow rate at a certain differential pressure increases as the outlet port is moved closer to the inlet port. The outlet ports P4 and P5 are close to the top of cement and gas migration rate through these ports

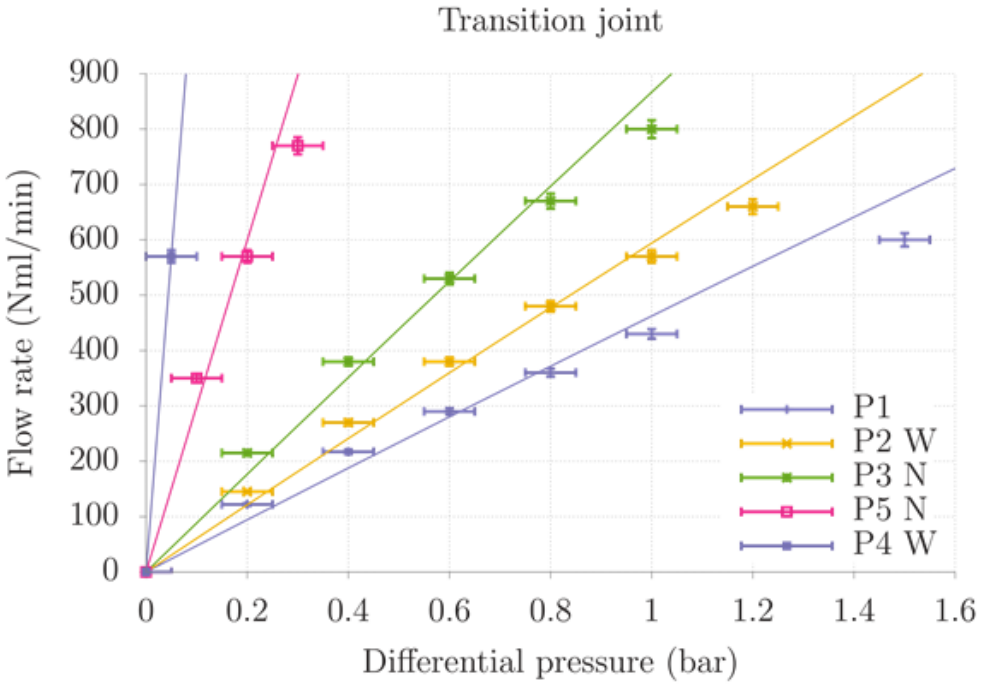

Figure 3.33: Measured, normalized gas seepage rates through the annulus of Transition Joint to different outlet ports

appear significantly greater than the rate through the ports closer to the bottom of the assembly. While the initial, qualitative gas testing indicated a low-permeable material above the top-of-cement, the material appeared to lose its sealing capability during subsequent experiments, as remarked above. At the time of the gas tests shown in Fig.3.33, the material above the top-of-cement had already (apparently irreversibly) lost its sealing capability.

The solid lines drawn in the Fig.3.33 correspond to a theoretical relation between flow rate and pressure difference when assuming laminar, steady state, single phase (dry), isothermal flow through a material of constant permeability, k, or equivalently along a constant and uniform micro-annulus located between the inner wall of the outer 13 3/8-in casing and the annulus cement. Measurements can be related either to flow through bulk permeability or through a conduit such as a uniform micro-annulus; the conversion between the two is performed by applying Equation 3.5. The resulting effective permeabilities or micro-annulus model gap widths are listed in Table 3.8 and Table3.9 for the two sections. Note that since the test assemblies are maintained at absolute pressures close to 20 bar throughout the tests (21 bar absolute pressure at the inlet port, up to 5 bar lower at the outlet port), the flow rate is a nearly linearly proportional to the pressure difference for the pressure range in these experiments.

Similar effective microannuli sizes are found in the Transition Joint when the

outlet port is taken as P1, P2 or P3, i.e. when the outlet port is within the cemented part of this joint. The two ports P4 and P5 are within the "transition" zone of the joint, close to the top of cement. Here, leakage rates and effective micro-annuli gap widths are larger compared to the lower ports in this joint and when compared to Fish #11.

Table 3.9: Transition Joint gas Leakage results

Inlet port	Outlet port	Permeability (mD)	Microannulus (μm)
P8	P5 (N)	42.9	25
P8	P4 (W)	162.5	39
P8	P3 (N)	18.8	19
P8	P2 (W)	12.9	16.6
P8	P1 (W)	13.5	17

As these tests were performed at test pressures close to 20 bar, it is relevant to compare the measured "effective micro-annulus" to the outer casing expansion caused by the pressure applied to the annulus. To approximate the linear elastic expansion of the outer casing, using Equation 3.5 and assuming $E = 210$ GPa and $v = 0.3$ as representative values for the casing steel. The radial expansion is estimated to be between 14 µm and 16.5 µm for the test pressures in Tables 3.8 and 3.9. This is close to the effective micro-annulus values estimated for leakage through the cemented part of the Transition Joint and also the narrow side of Fish #11, suggesting that elastic deformation of the casing has an influence on the measured leakage rate. The slight tendency for the flow rate measurements to fall below the solid lines drawn in Fig.3.33 is also consistent with the pressure-induced deformation affecting the net flow rate. Compression of the annulus cement and the inner casing would increase the elastic gap opening further but is not accounted for in this analysis.

3.6.5 Confining pressure effect

To further assess the effects of the inner casing pressure on gas permeability a new test was devised. To test Fish #11, a constant nitrogen-gas differential pressure of 5 bar was applied at Port P8 on the end, while port P5 in the middle of the cell was open to the atmosphere. Inner casing pressure was increased in steps while gas injection was measured. Fig.3.35 shows the measurements acquired during this test.

At approximately 12:30:00, the injection flow rate had stabilized close to 120 normal millimeters per minute (Nml/min) in the absence of casing pressure. The casing pressure was then increased in steps of 10 bar, up to a maximum pressure of 40 bar within one hour and twenty minutes, the interval is indicated by the dotted vertical lines at 12:30:00 and 13:50:00. We observed an immediate response in the injection flow rate while maintaining a constant injection pressure, indicative

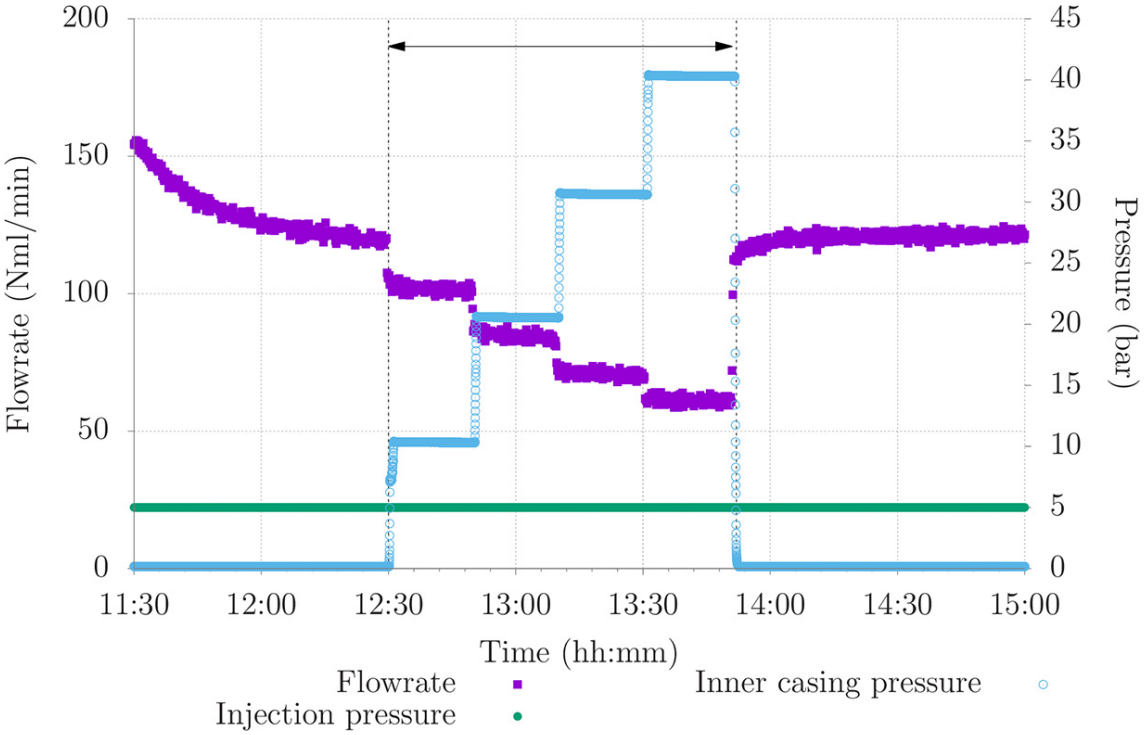

Figure 3.34: Measurement of flow rate at constant injection pressure, varying the casing pressure inside Fish #11

of increased flow resistance caused by the inner casing pressure. After the casing pressure was relieved, the injection rate reverted to its original level at approximately 120 Nml/min. The response observed in the test sequence shown in Fig.3.35 suggests a fracture-like response of the annulus-seepage path, similar to how a hypothetical uniform microannulus would respond to an inner casing pressure.

Assuming linear elasticity and perfect bonding between cement and inner casing, we expect the microannulus gap width at the inner wall of the 13 3/8-in casing to decrease linearly with applied casing pressure, i.e., $h(p_c) \approx h_0\ \Delta h\ P_c$, where h_0 is the effective gap width in absence of casing pressure (P_c), and δh is a constant that converts casing pressure to radial displacement of the outer face of the cement. Assuming a Darcy cubic law for the flowrate, we expect a behavior $Q(p_c) \approx (1\ p_c)^3$ with $\alpha = \Delta h\ /h_0$. As shown in Fig. 3.35, a good fit is observed between measurements and this scaling with casing pressure for a fitted value $\alpha \approx 0.0051/bar$. This suggests a fracture-like response in the effective channel size, as found previously by other researchers [175, 176]. A similar plot with measurements from the Transition Joint, but this time using water as the test fluid, and 35 bar pressure difference across the test cell is also presented in Fig.3.35. The internal casing pressure is varied up to 30 bar, and once again a reduction in flow rate with increasing casing pressure was found. The response can be represented through the Darcy cubic law and an assumption of a fracture-type behavior of the channel. The curve in Fig.3.35

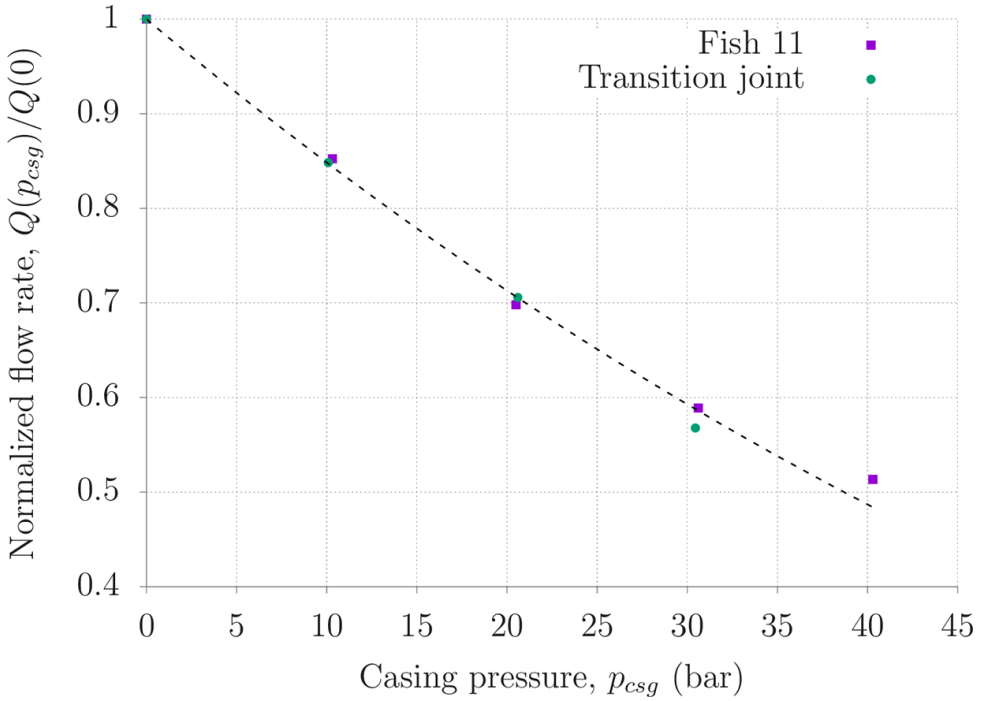

Figure 3.35: Normalized Leakage rates as a function of internal casing pressure for Fish #11 and the Transition Joint.

corresponds to a value of $\alpha \approx 0.0061/bar$.

3.7 Discussion

In general, when the leakage rate from annular cement barriers is analysed, to simplify the complexity, it is frequently assumed that the leakage is a long microannulus with a constant width, for example, between annulus cement sheath and the inner/outer casing wall. This assumption is not only common in field application, when evaluating annular cement barriers [126, 177–179] but is also accepted by the scientific community [80, 156, 157]. Logging technologies are sometimes limited to investigating the debonding occurring in the first and second interfaces, which makes this assumption particularly applicable to the data available. These interfaces normally correspond to the first contact between casing and cement. An additional factor is that the hydraulic tests (positive and inflow test) used in the field to estimate the hydraulic isolation also assume that the migration path goes through a unique fracture with a defined aperture. Even though this is far away from reality, at least from a geometrical point of view, the experiments conducted in this research and presented in this chapter suggest that the simplification of the equations, popularly known as the cubic law, present good approximations with theoretical models and experimental data and consequently could be used to evaluate the leakage potential in primary well barriers. This appears to be aligned with the findings of a

paper recently published by Wise et al.[180], which compare experimental data from small scale specimens with the cubic law. The results show that the difference in the magnitude of the leakage computed from the cubic equation when compared with experimental data does not appear to be significant, but the cubic law is not accurate when the differential pressure is greater than 1 bar or the flow is bigger than 5 mL/min. All the experiments conduct in this research were executed at pressure and flow rates bigger than the ones defined by Wise et al.[180], contradicting such affirmation.

Leakage rates for all four cases were consistent with flow measurements using the theoretical, single-phase flow equation. We found annulus leakage rates one to two orders of magnitude larger than the bulk permeability measured for intact cement that is normally assumed to be 0,001 mD. In all of the experiments presented, this is consistent with the view that the net permeability is governed not by bulk cement permeability but by flow along interfaces and/or through defects in cement as concluded by other studies [157, 181]. Additionally, results show that in cases where eccentricity was found, such as the cases 2, 3 and 4, the leakage rates are substantially larger when the outlet port is on the narrow side of the annulus compared to the wide side. As the entire annulus cross-section is exposed to pressure in those experiments, this suggests that fluids tend to migrate preferentially along the narrow side of the annulus. When the outlet ports are taken on the wide side of the annulus, the flow rate is markedly lower at the same pressure differentials. This suggests effective choking or restriction of the flow from the narrow side to the outlet port on the wide side. This observation, however, can suggest that the orientation of the perforations on a section downhole can have an impact on the way that hydraulic test downhole are collected and interpreted.

An additional finding when comparing the test sections recovered from the wells was that the deeper Fish #11 has lower leakage rates compared to the upper Transition Joint which contains top-of-cement. The plastic mass above the top-of-cement did initially hold pressure and did not allow gas to escape; during subsequent testing, however, the sealability of this material was compromised and it is now allowing fluid flow with little restriction. This result supports the hypothesis of other authors [182–184] who have investigated the potential of barite as a complementary annular barrier, when settle on top of annular well cement. However, the results also show that the settle of barite has a limited capability as a complementary barrier.

3.8 Conclusions

In this chapter, the experimental work completed in six full-scale cells is presented. The cells were organized in four cases, where the main difference between them is

the type of defect present on the annular cement sheath. All cells were instrumented and tested in a similar way to analyse leakage path characteristics, leakage rates, pressure build-up and casing radial strain.

The soapy test was shown to be a simple but powerful method to visualise the location of preferential leak paths in the specimens. The application of a soap film over the cross sections revealed qualitative information about where gas percolates from the cement sheath: through the inner interface, the narrow sector, the wide sector or both. However, the technique has clear limitations in terms of quantifying and comparing the magnitude of leakage, so permeability studies are still necessary.

For the permeability experiments, two testing protocols were established. The first one considers the injection of fluid at constant pressure (Case 2, 3 and 4) while monitoring the flow rate through the annulus. The second one considers fluid injection at a constant flow rate while monitoring pressure (Case 1 and Case 3). Both methods appear to be adequate to evaluate hydraulic conductivity. In case 3, both methodologies were used and no difference in the interpretation of results was evident. It seems relevant to define stabilisation criteria to consider steady state conditions, considering all the cases and the fluid used for the test. Permeability tests on Case 1, Case 2 and Case 3 used water, while Case 4 used gas.

As a general conclusion for all cases, it was observed that the flow rates show a direct relation with pressure; when the pump pressure is increased high leakage rates were measured. The effect of the annular eccentricity appears to be relevant to the development of leakage flow rate. In experiments where eccentricity was observed (Case 2, Case 3 and Case 4) we have consistently observed differences in the leakage rate produced using ports at the narrow and wide parts of the annulus. The results might suggest that it is more likely to have higher permeability on the narrow side of the cemented annulus sheath.

Regarding radial expansion, the results show that increased tubing pressure induces changes in the micro-annulus, hence provoking variations along the leakage paths. Such variations affect the local gap width of the micro-annulus channel which shows a clear relation with permeability. When the tubing pressure is increased, the microannulus is closed and as a consequence, the leakage measured is reduced, as presented in case 3 and case 4. The inclusion of strain gauge measurements in this type of experiment was a useful tool to observe the response of the aperture of the microannulus and variations in the radial expansion. Moreover, the experiments presented might indicate that micro-annuli apertures vary along the length of the test cell and between the wide and narrow sectors of an eccentric annulus.

The results of complementary techniques such as logging and infrared thermography appear to be in agreement with the general observations collected from the permeability tests. However, they are still limited in their ability to quantify the

hydraulic isolation of a cement barrier, and so these techniques alone are insufficient to evaluate annular cement quality. It still remains an open question of research how large is the volume of gas/water that can cross a barrier when it is classified as "poor" compared with a barrier classified as "good".

Chapter 4

Long term integrity - durability and barrier failure

After well construction and throughout the well's life cycle, cement is normally exposed to gases and fluids from different sources. It is also subject to changes in pressure and temperature. These could negatively affect the cement properties with adverse consequences concerning its effectiveness as a barrier in a long-term perspective. The recognized factors that potentially affect cement properties include: water penetration, gas migration, chemical attack and variations in pressure and temperature that are able to generate thermo-mechanical failures such as shrinkage, cracking and debonding [82, 155, 185]. Mapping the consequence of these factors with a long-term perspective is a challenging and complex task but three main processes are identified as the most critical: increases in porosity and permeability, reduction of mechanical resistance and the creation of fluid migration paths that can allow the migration of fluids through a barrier creating well integrity problems such as Sustained Casing Pressure (SCP) [148, 186].

The cement properties for early age cement have been extensively investigated in the laboratory, see e.g. [187]. However, studies related to durability are sparse but the recent increased interest in projects for Carbon Capture and Storage (CCS) have improved the understanding of cement degradation mechanisms such as carbonation and bicarbonation occurring when CO_2 reacts with cement. As a consequence, the degradation due to CO_2 exposure is nowadays relatively well understood based on contributions from different researchers who have analyzed the changes in cement properties, phases and micro-structure in the laboratory [188–194]. Degradation due to H_2S exposure and brine penetration have been less studied but a few authors have published some findings from laboratory experiments concluding that leaching and calcium loss are the main degradation mechanisms [81, 195–198]. The studies of hydrocarbon penetration for aging and reaction with cement have been sparse and the results did not show alterations in the mechanical properties [81, 193].

The studies of durability of cement recovered from oil wells after exposure to downhole conditions are limited. The effects of degradation on oil field recovered samples were studied by Duguid et al. [181] and Scherer et al [199] with analysis limited to petrophysical properties and SEM. A few studies present the results of the combined effect of aging and degradation due to exposure to CO_2 [200, 201]. In this context, a durability study of cement samples recovered from the Valhall cells presented in section 3.6 was a unique opportunity to complete a pioneer study of cement characterization after 33 years of exposure to downhole well conditions.

4.1 Caracterization of well cement after 33 years of downhole exposure

An in-depth characterization (including petrophysical, mechanical properties and compositional analysis) of class G cement samples recovered from an offshore wellbore system is presented in this chapter. The results provide a unique opportunity to establish a baseline to assess the effect of ageing on cement properties and composition, whereas most of the previous studies of cement durability for field samples combine the effects of ageing and CO_2 exposure making it difficult to address the alteration due to age effects alone.

4.2 Material Characterization and Methods

The studied materials are divided into two parts. The first part corresponds to an in-depth characterization of core plugs drilled from the off-cuts removed when dressing the sandwich sections' ends. Cores were cut from the wider side of the sections, as shown in Fig. 3.26 and 4.1. Table 4.2 presents an overview of the methods used to characterize the core plugs, and the results allow comprehension of the material bulk properties. The second part includes the characterization of a slim sandwich cross-section cut from the top of Fish # 11, see Fig.s 3.26 and 4.10, where it was possible to study the variations in cement properties around the annulus, not only on the wider side (as per core plugs) but also on the narrow side.

Table 4.1: Sandwich sections under study

	Transition Joint	Fish # 11
Well depth (m)	119.2-131.5	251.7-263.8
Final length (m)	9.36	10.52
Min. Stand off (m)	0.01057	0.01250
Max. Eccentricity %	70	64

Table 4.2: Overview of methods used to characterize the cement core plugs. CT: Computer Tomography Scanning, E:Young's Modulus, UCS: Uniaxial compressive strength, SEM: Scanning Electron Microscopy, EDS: Energy Dispersive Spectroscopy , XRF: X-Ray Fluorescence, XRD:X-Ray Diffraction

		Petrophysical Properties			**Mechanical properties**		**Compositional Analysis**		
Section name	Core plug	Porosity	Permeability	CT scan	E	UCS	SEM- EDS	XRF	XRD
Transition Joint	TJ48	✓	✓	✓	✓	✓	✓	✓	✓
	TJ73	✓	✓	✓			✓	✓	
Fish# 11	FT 75	✓	✓	✓	✓	✓	✓	✓	✓
	FT87	✓	✓	✓	✓	✓	✓	✓	✓
	FB64	✓	✓	✓				✓	
	FB132	✓	✓	✓					
Results can be consulted in:		Table 4.5	Tables 4.4, 4.3	Figure 4.3 Table 4.6	Table 4.7	Table 4.7	Table 4.8 Fig.4.6,4.7	Table 4.9	Table 4.10

4.3 Part 1 - Core Plugs analyses

A total of 6 core plugs were drilled from the wider part of the annular space (as illustrated in Fig. 4.1a) and recovered in satisfactory conditions. Four core plugs were recovered from the Fish # 11 section: two from the bottom (FB 64 and FB 132) and two from the top (FT 75 and FT87), as shown in the right panel in Fig. 3.26. From the Transition Joint, two additional core plugs were recovered (left panel in Fig. 3.26): one from the bottom (TJ 48) and the other one was taken from the material found above the TOC (TJ 73).

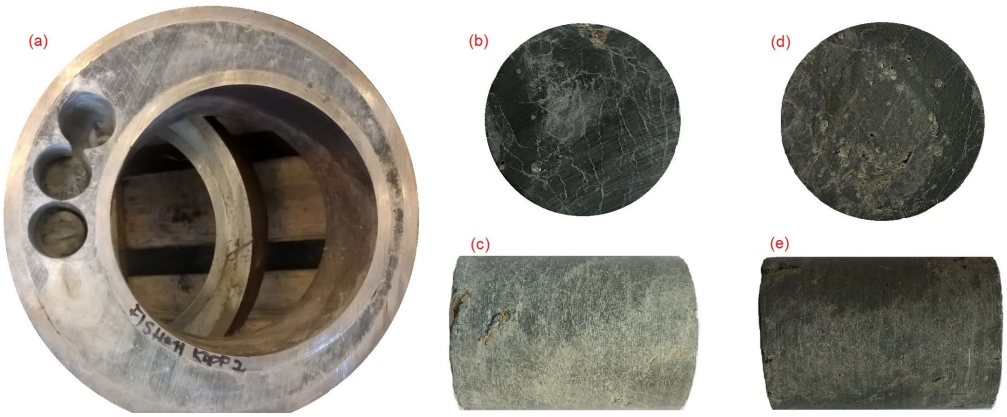

Figure 4.1: Core plugs obtained from Fish 11 (Bottom). (a) Drilling of core plugs, (b) FB 64 top view, (c) FB 64 lateral view, (d) FB 132 top view and (e) FB 132 lateral view

4.3.1 Petrophysical Analysis

The core plugs were weighed in their initial condition (as drilled from the sandwich sections), cleaned with soxhlet extraction and subsequently dried at 60° C for several days until the weight was observed to stabilise, indicating that pore fluids had been removed prior to gas permeability measurement. To measure the matrix volume, matrix density, pore volume and porosity, gas was allowed to enter the pore space of the cores from a container with a known volume at an initial pressure of 0.7 MPa. The calculations were made applying Boyle's law.

Gas permeabilities reported were measured by flooding the core plugs with nitrogen at a constant flow rate of 5 ml/min and measuring the obtained differential pressure drops across the cores. Most of the measurements were conducted at 2 MPa confining pressure. For each flow rate studied, permeability was defined using stabilisation criteria, which were reached when the differential pressure change across the cores was less than 10 Pa in a timeframe of 30 s. Stabilisation time varies between 1 and 6 hours.

The liquid permeabilities were estimated using the Klinkenberg correlation [202]. This method is used for tight porous mediums where the permeability is in the range of millidarcy and gas permeability measurements are feasible and accurate [203, 204]. Flow rates of 1,5 and 10 ml/min were used. By plotting the gas permeability versus the reciprocal of the mean pressure, it is possible to estimate the medium's liquid permeability (or permeability at infinite pore pressure) from the intercept using a linear fit,

$$K_g = K_l(1 + \frac{b}{P}), \tag{4.1}$$

where K_g is the gas permeability, K_l is the permeability of the medium at infinite pore pressure, P is the pore pressure and b is the gas slippage factor.

For the core FT 87, gas permeability was measured for different confining pressures 2, 5, 10 MPa to evaluate the effect of confining pressure. For one of the cores (FT 75), the liquid permeability was also measured directly by applying 2 MPa of confining pressure and pumping deionised water at 20 °C (273.15 ° K).

Core plug weights (initial and after drying), pore volume, matrix volume and density are presented in Table 4.5. Core plugs from the Fish # 11 section show small variations in the pore and matrix volumes. The matrix density is also similar for all core plugs and cement density is estimated at $2.6\,\mathrm{g\,cm^{-3}}$. For the Transition Joint, the measured properties are significantly different compared to Fish # 11. The core TJ 73 has the highest matrix density of all the cores ($3.3\,\mathrm{g\,cm^{-3}}$ and the core TJ 48 has the lowest one ($2.57\,\mathrm{g\,cm^{-3}}$). These results appear to be consistent with the CT scan images for those core plugs, see Fig. 4.3. The plug TJ 73 is composed of higher density materials, while TJ 48 has a lower matrix density and a larger porous volume. Table 4.4 lists measured porosities plus gas (Kg and Klinkenberg (Kl)) and water (Kw) permeabilities. The porosity of the cement core samples varied from 46.7 % in the bottom of the Transition Joint to between 35.9 % and 41.1 % for the core plugs retrieved from Fish # 11.

The gas permeability was measured at 2 MPa of confining pressure for all cores. For the Transition Joint core sample TJ 48, the gas permeability was estimated to be 0.32 mD ($3.15 \times 10^{-16}\,\mathrm{m^2}$). Three of the four cores from Fish # 11 had gas permeabilities slightly lower than that from the Transition Joint, in the range 0.18-0.29 mD ($1.77 \times 10^{-16}\,\mathrm{m^2}$ to $2.86 \times 10^{-16}\,\mathrm{m^2}$). The core FB 132 has values of permeability two orders of magnitude higher than the other core plugs. Some authors suggest that mud contamination can increase the effective permeability of cement samples [181, 205]. This observation agrees with the results of permeability and CT scans for the core plug FB 132, see Fig. 4.3, where core FB 132 exhibits higher contamination (with high and low density features from the CT scan) and the highest permeability of the core plug samples.

Table 4.3: Measured gas permeability (Kg) for core plug FT 87 varying the confining pressure. Results are presented in milidarcies, for SI units use conversion factor ($1\ \text{mD} = 9.869\,23 \times 10^{-16}\,\text{m}^2$)

	Permeability (mD)		
Core plug	at 2 MPa	at 5 MPa	at 10 MPa
FT 87	0.18	0.04	0.03

Table 4.4: Petrophysical properties: Permeabilities. Kg: Gas permeability, Kl: Liquid permeability-Klinkenberg, Kw: Measured Water permeability. Results are presented in millidarcy, for SI units use conversion factor ($1\ \text{mD} = 9.869\,23 \times 10^{-16}\,\text{m}^2$)

Core plug	Porosity (%)	Kg (mD)	Kl (mD)	Kw (mD)
TJ 48	46.7	0.32	0.15	Not measured
TJ 73	1.6	≤ 0.001	≤ 0.001	Not measured
FT 75	38.4	0.29	0.21	0.02
FT 87	35.9	0.18	0.10	Not measured
FB 64	38.2	0.27	0.14	Not measured
FB 132	41.1	22.96	18.43	Not measured

Table 4.5: Petrophysical properties: Core plugs bulk properties

Core Plug	Length (cm)	Diameter (cm)	Initial Weight (g)	Final Weight (g)	Pore Volume (mL)	Matrix Volume (mL)	Matrix Density ($\text{g}\,\text{mL}^{-1}$)
TJ 48	5.08	3.75	99.49	76.58	26.15	29.81	2.57
TJ 73	4.60	3.75	159.77	Not measured	0.78	48.03	3.33
FT 75	4.92	3.75	105.76	89.04	20.93	33.53	2.66
FT 87	4.97	3.76	107.67	92.23	19.66	35.17	2.62
FB 64	5.14	3.75	103.75	92.01	21.66	35.01	2.63
FB 132	5.08	3.75	96.72	85.60	22.81	32.66	2.63

The additional analyses were done on the core FT 87 to measure the gas permeability at different confining pressures. The results suggest that the permeability decreased as pore pressure increased; see results in Table 4.3. These results highlight the importance of reporting the cement permeability along with the confining pressure applied.

Fig. 4.2 illustrates the estimation of liquid permeability (also known as Klinkenberg) for the core plug FB 132. Five gas measurements are used to obtain a linear regression, given by equation $K_g = 2.494(x) + 18.43$ with $R = 0.9965$, for which the intercept with the vertical axis corresponds to the liquid permeability.

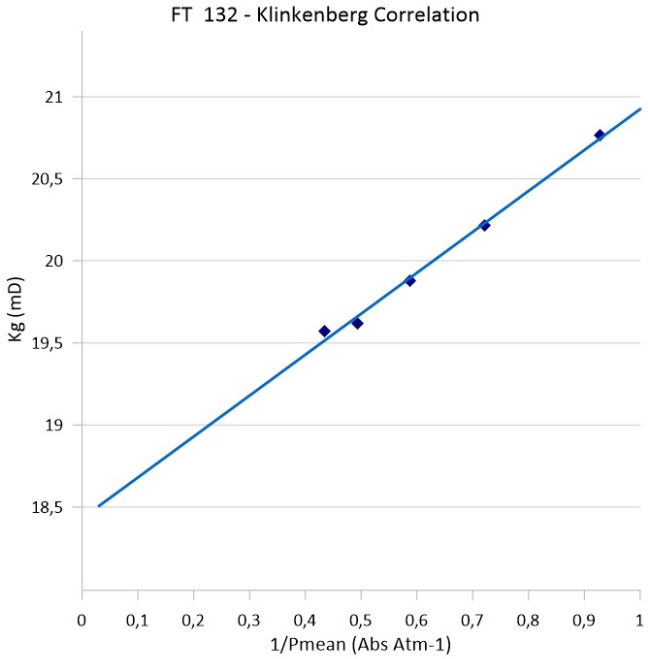

Figure 4.2: Klinkenberg correlation for core plug FB 132. All measurement at 20 bar of confining pressure

A similar procedure was performed for all cores. Estimated liquid permeabilities are between 0.1 mD and 0.21 mD (9.87×10^{-17} m^2 to 2.07×10^{-16} m^2) for most of the cores. The results are presented in Table 4.4 and suggest that liquid permeability is always smaller than the measured gas permeability in steady state conditions. Time to reach steady state conditions, considering the stabilization criteria of 10 Pa in 30 seconds, varied between 1 to 3 hours for the samples.

The Klinkenberg correlation for all the cores shows that the permeability to gas increases linearly with an increase of the inverse of pressure. This observation is consistent with the results obtained for tight reservoir rocks [206–210]. Klinkenberg permeability results for other samples of cement class G were not found in the literature for comparison. The results for FT 75, FT 87, FB 64 and TJ 48 are consistent with the results from gas, liquid and Klinkenberg liquid permeability obtained for

sedimentary reservoir rocks. Where gas permeability is 2 to 10 times larger than water on the same specimen and gas permeability decreases with an increase in pore pressure [206, 207]. The results of water permeability for the core FT 75 show that permeability to nitrogen is ten times larger than the permeability to water. The difference between the liquid permeability (estimated by the Klinkenberg correlation) and the measured water permeability may suggest the importance of fluid–structure interactions . Differences between both have been explained by heterogeneities in the porous media or phenomenons such as slippage effects [207, 211, 212], wettability [213], hysteresis and capillary forces[214]. This observation highlights the need to extend the study of the Klinkenberg effects in very tight porous media such as cement, as has previously been studied in concrete materials by Zhou et al [215] and Loosveldt et al [216].

4.3.2 Computed Tomography (CT) scanning

CT scans are widely used to characterise the distribution and connectivity of pores and fractures for reservoir rocks. However, more recently, CT scans have been used to investigate the petrophysical properties of early age cement [217–220]. The apparatus Toshiba Aquilion Prime 80 was used to acquire images with a resolution of 500 µm for the six core plugs.

The core density determines the degree to which X-rays are attenuated, which directly affects the brightness and contrast of the images. Materials with high attenuation (strong absorption) are shown as white, while those with low attenuation (weak absorption) are black. The Hounsfield Unit Value (HUV) is used to quantify the attenuation. For rock samples, low HUV due to pore space and fractures is represented with a dark colour, whilst components with high density have high HUV and a light colour.

CT scans for the six core plugs taken from both sections are presented in Fig. 4.3. The images shown are for the middle of the core plug in the radial and longitudinal directions. The maximum and minimum values of the Hounsfield scale for the plugs are presented in Table 4.6.

Table 4.6: CT Scan. Hounsfield Unit Value (HUV) for core plugs

Core plug	Hounsfield Unit Value (HUV)	
	Min	Max
TJ 48	795	1766
TJ 73	3314	5446
FT 75	1207	1836
FT 87	112	1655
FB 64	941	1595
FB 132	518	1714

The core plugs from the top of Fish # 11 section (FT 75 and FT 87) show a similar response with few intrusions of high-density material. Surprisingly, the CT scan for cores obtained from the bottom part of the section (FB 64 and FB 132) showed more heterogeneity and with significant differences between them especially considering that the core plugs were cut adjacent to each other. The core FB 64 showed sparse intrusions of material with high attenuation. The material with low attenuation (pore space or low density material) was apparently interconnected and more present in the upper part of the plug. The core FB 132 showed a considerable content of high-density material, partially agglomerated.

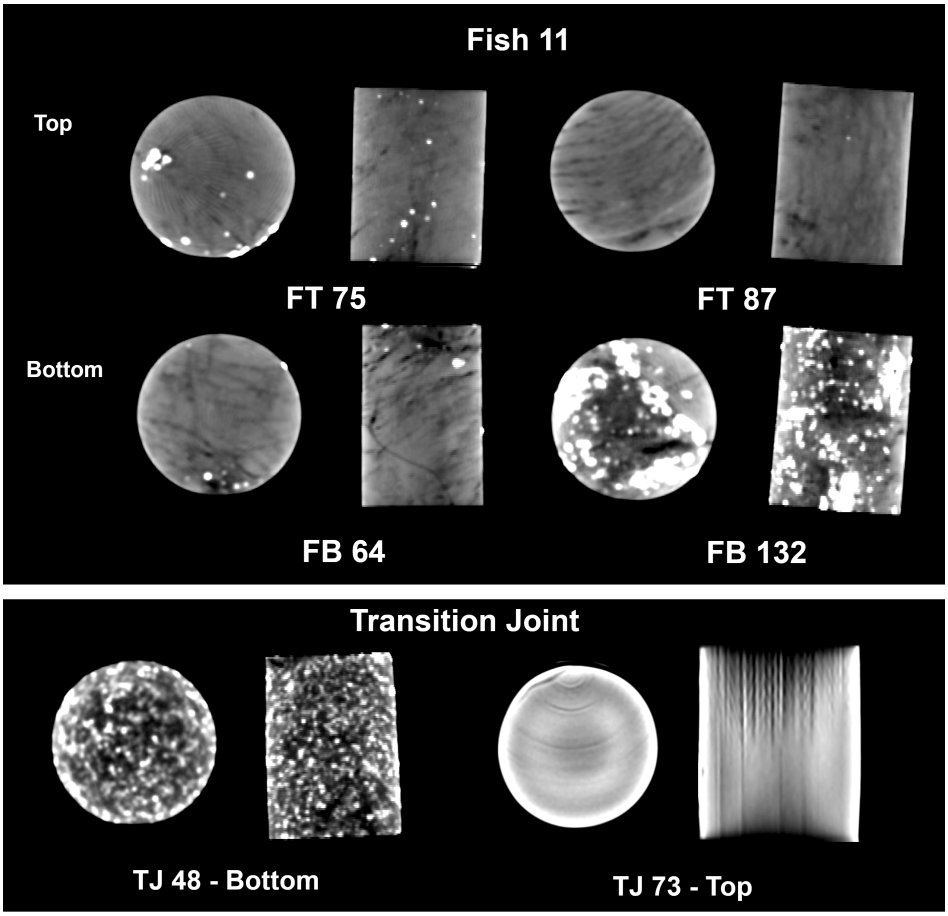

Figure 4.3: CT scan for Fish # 11 and Transition Joint core plugs

For the Transition Joint, the core plug from the bottom part (TJ 48) also showed a significant content of both high and low-density materials, but it appears less aggregated than FB 132. The core plug TJ 73, above the TOC, is comprised of high-density material.

HUV is a scheme for scaling the attenuation coefficients. Since there is no standardization, comparisons of results from different instruments and measuring conditions are difficult. However, predictions can be made based on the densities of the materials. Some authors published typical values of the Hounsfield scale for some

mineral components [221]. According to them, calcite, one of the main components of cement, typically shows 1861 HUV when the density is 2.71 g/mL. This number appears congruent with the upper limits of HUV obtained from the cores studied and the density reported in the previous section. The CT response for the core TJ 73 was associated with the presence of barite (also known as barium sulfate $BaSO_4$), which is a dense mineral used to increase the drilling mud density. The white spots in the cores FT 75, FB 64, FB 132 and TJ 48 represent intrusions of barite in the cement slurry, which was confirmed by the compositional analysis.

4.3.3 Mechanical Properties

After evaluation of petrophysical properties and CT Scans, three of the core plugs were exposed to uniaxial monotonic loading to determine the uniaxial compressive strength (UCS). The UCS and Young's modulus were determined for two core plugs from the top of the Fish # 11 section (FT 75, FT 87) and one from the bottom of the Transition Joint (TJ 48). The experiments were performed at the University of Stavanger (UIS), using an *Instron 5985* with a force capacity of 250 kN. A constant displacement of 0.2 mm min^{-1} was set for the load cell, and the core plugs were loaded until failure whilst recording the load with the Instron machine and the deformation using an Instron long-travel extensometer for a single-column model Instron AUTOX750 as illustrated in Fig. 4.4. Note that the dimensions of core plugs do not follow the ASTM D 2166-00 standard recommendation, where the suggested length should be 2 - 2.5 times the diameter of the core sample, but the strain rate used complies with the ASTM recommendation for standard core sizes.

The results for UCS and Young's Modulus for core plugs FT 75, FT 87 and TJ 48 are presented in Table 4.7. The values suggest that the cement in the Transition Joint has a lower resistance to compression, whilst the cement in Fish # 11 can support higher loading before failure. The curing conditions for FT 75, FT 87 and TJ 48 were estimated to be a pressure of 1.28 MPa for the Transition Joint (TVD of approx. 130 m, and a column of water above). For Fish # 11, considering a TVD of 260 m and assuming that the slurry below 130 m has 1.92 sg, the pressure on site was approximately 3.70 MPa. The curing temperature is more difficult to establish. However, the temperature at the sea bottom is around 4 °C and the thermal gradient for the North Sea is estimated to be 4 °C per 100 m [222, 223]. That, at the depths of the sections, indicates a temperature around 10-12°C. So, for practical purposes, a value of 10 degrees Celsius might be assumed for both sections. Nevertheless, the temperature after the well started production may be higher.

A comparison between the Valhall samples and the results published by other authors, see Table 4.7, shows that the measured Young's modulus falls between the

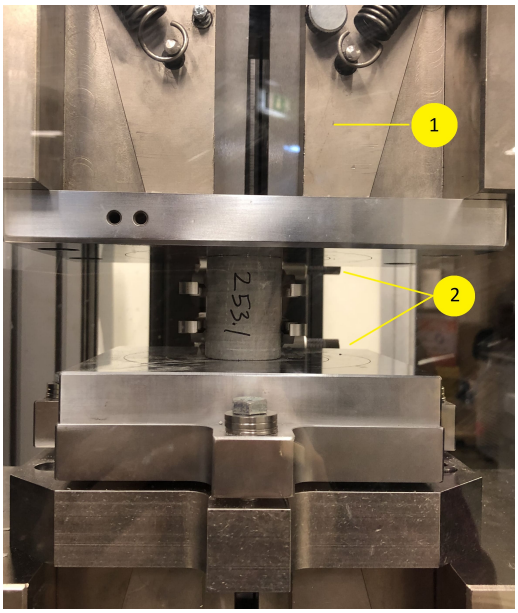

Figure 4.4: (1) Testing machine model *Instron 5985*. Picture shows core plug FT75 sample positioned for testing, where instrumentation with a deformation indicator of type single column extensometer is indicated (2).

Table 4.7: Mechanical properties from core plug and reference values reported by Teodoriu and Asamba [5]. *Values were assumed

Sample	Maximum UCS (MPa)	Young's Modulus (GPa)	Curing Time	In situ Conditions Temp (C) - Press (MPa)
FT 75	26.9	6.74	33 years	10 - 3.7 *
FT 87	42.8	7.45	33 years	10 - 3.7 *
TJ 48	17.1	6.08	33 years	10 - 1.2 *
LeRoy- Delange[224]	37	6.6	3 days	77 - 27
Morris et al. [225]	40	4.4	3 days	84 - 27
Teodoriu et al. [226]	60	17	60 days	75 - 0.1
Lesti et al. [227]	45-60	17	6 months	90 - 40

values reported for other samples with curing times between 3 days and 6 months. The compressive strength for FT 87 is also comparable with the references, suggesting a cement with good structural integrity.

The UCSs for the cores FT 75 and TJ 48 show a reduction of 32.75 % and 42.75 % compared to FT 87 and are lower than the reference values listed in Table 4.7 for Class G cement. This reduction in resistance may be associated with the mud contamination detected in the samples by the CT scan and the compositional analysis. This observation is consistent with other studies that have found indications that UCS decrease with the increase of OBM content [228, 229]. In a recent publication, Katende et al. [205] found that mud contamination of 10 % and 30 % reduced the UCS by 25 % and 72 %, respectively.

The core plug FB 132 (from the bottom part of Fish # 11) was used for additional petrophysical studies, and its mechanical properties have not yet been measured.

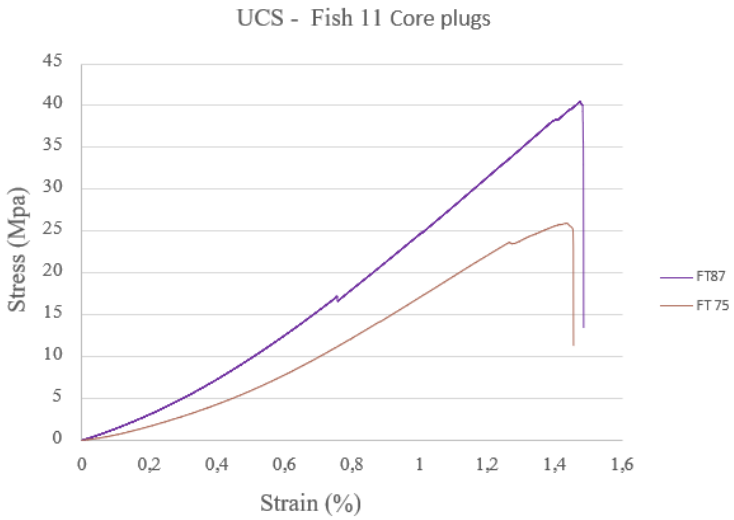

Figure 4.5: Strain- Stress curve obtained when core plugs from the top of Fish 11 were submitted to monotonic compressive load (UCS test). Note that FT75 and FT87 where recover from cement at 253 m well depth and cut beside each other. Large Deviation is observed.

The core FB 64 was fractured during transport, and the core TJ 73 is unconsolidated, so that neither was suitable for mechanical properties analysis.

4.3.4 Compositional Analysis

After mechanical analysis, fragments of the samples were used to evaluate the cement chemical composition using different techniques: Scanning Electron Microscopy (SEM) and Energy Dispersive Spectroscopy (EDS), X-Ray Fluorescence (XRF) and X-Ray Diffraction (XRD).

Scanning Electron Microscopy (SEM) and Energy Dispersive Spectroscopy (EDS)

SEM-EDS analyses were used to examine the cement microstructure and composition. SEM was used to study morphology, and EDS was used to perform a semi-quantitative analysis of the elemental composition. Fragments were analyzed using a Zeiss Supra 35VP field emission gun scanning electron microscope (FEG-SEM) fitted with an EDAX Octane Elite EDS system, located at UIS, Norway. The unpolished samples were coated with a thin layer of palladium to avoid charging of electrons during analyses and the equipment was set to an acceleration voltage of 15 kV,the aperture size of 30 µm and a working distance of 12 mm.

Elemental compositions for 4 core plugs were obtained: for two core plugs from the top of Fish # 11 (FT 75, FT 87) and two cores from the Transition Joint

(TJ48, TJ73). For each core, two fragments were selected for high-resolution imaging at magnifications of 500 X, 1 kX and 10 kX. Fig. 4.6 shows the comparison of microstructure for samples with 1 kX magnification in the upper panels and 10 kX in the lower. Cement hydration products were identified as an homogeneous matrix with some angular morphologies that can be associated with the presence of calcium carbonate. In the images, the bright matrix is typical for Portland cement hydration products (C-S-H and CH) with a medium to light grey colour.

EDS was used to identify the elemental distribution using spot and area modes. A total of 6 areas and between 65-70 spots per sample were analyzed. Typical elements in hydrated cement were found (Ca, Si, Al, S, C, O). Barium (Ba) is one of the elements composing barite ($BaSO_4$), an additive used in Oil Based Mud (OBM) and Water Based Mud (WBM) as a weighting material. The presence of this element can be used as a tracer to identify whether the cement slurry was contaminated by mud or spacer fluid during the placement, as this element is not typically present in hydrated Portland cement.

Table 4.8 shows the results of elemental concentration by atomic weight percent from the EDS area mode. Only the average values are reported. The results show that samples FT 87, FT 75 and TJ 48 have a similar elemental mean composition and are rich in calcium phases. There are high amounts of carbon, associated with calcium to form calcium carbonate ($CaCO_3$). The sample TJ 48, however, has a richer content of Ba, Cl, Na, Fe, S, K, probably associated with mud contaminants and congruent with the CT scan. The sample TJ 73 shows a different elemental composition, rich in O, Ba and S and poor in calcium phases.

Fig. 4.7 shows the results of elemental concentration by weight percent using the EDS spot mode for 140 spots from each section. The distribution of elements for the Transition Joint appears to be more dispersed, mainly for the contents of Ca, C, O, S and Ba. The Fish # 11 and Transition Joint show barium (Ba) content, implying some level of mud contamination in the slurry that is more represented in the Transition Joint. Higher content of sulfur (S) was also found in the Transition Joint, which is associated with the presence of barium sulfate (barite).

X-Ray Fluorescence (XRF)

The fragments from one core of the Transition Joint (TJ 48) and two fragments from the top of Fish # 11 (FT 75 and FT 87) were used to obtain their elemental composition using X-Ray Fluorescence. Measurements were made using a commercial benchtop spectrometer, the M4 Tornado, located at the Universidade do Estado do Rio de Janeiro - UERJ, Brazil. This device has a Rhodium tube (air-cooled) and an energy dispersive silicon drift detector with a sensitive area of$30 \times 10^{-5}\,\mathrm{mm}^2$. The system also has a polycapillary lens that provides a micro beam size of 25 µm. The

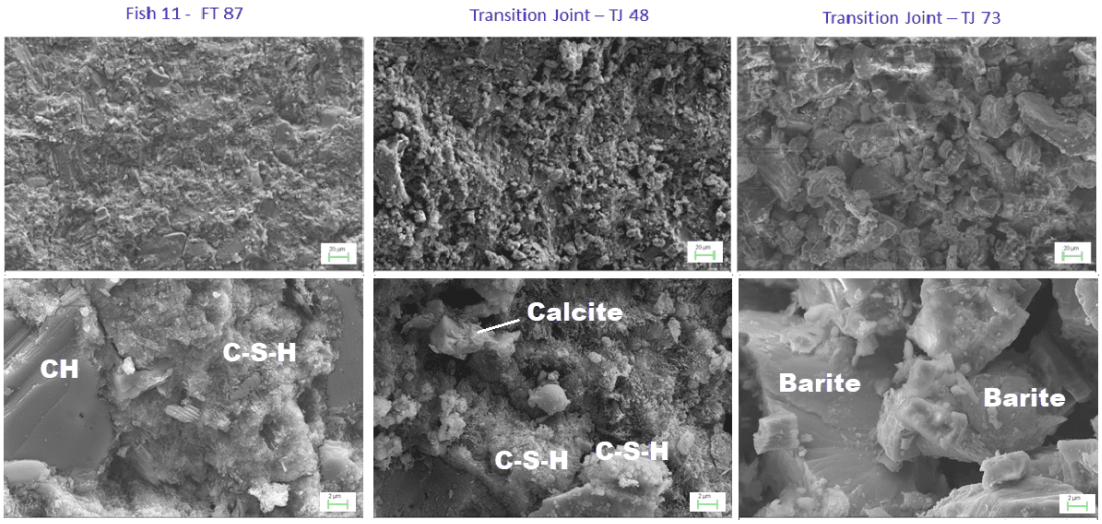

Figure 4.6: Comparison of SEM Images at magnifications 1.0 kX (upper panels) and 10.0 kX (lower panels) for material extracted from FT87, TJ47 and TJ 73 core plugs

equipment was operated at 35 kV and 600 µA with a 12.5 mm/Al filter. The acquisition time for each spectrum was 100 s, and a vacuum of 2000 Pa was applied during the measurement. The model for the elemental quantification assumes a matrix of Calcium Carbonate ($CaCO_3$), and the analysis was performed in 5 aleatory points for each sample.

The results of elemental composition were converted to oxides and normalized to 100 %, see Table 4.9. The results confirm the similarity in composition of samples FT 75, FT 87 and TJ 48 and imply a high content of Ca, Si and Al, consistent with the presence of cement phases such as calcium silicate and calcium aluminates. The core plug TJ 73 appears to be mainly composed of barium components, supporting

Table 4.8: Semi-quantitative results of elementary concentration using SEM-EDS (content in weight percent)

Element	FT 75	FT 87	TJ 48	TJ 73
C	8.66	7.55	8.0	24.57
O	53.58	54.67	49.16	43.35
Mg	0.63	0.67	0.46	1.06
Al	0.93	1.12	1.28	1.45
Si	8.63	7.65	7.88	2.12
S	0.73	0.55	1.74	10.87
K		0.1	0.26	0.1
Ca	26.88	25.15	31.12	1.32
Fe	0.70	0.67	1.44	1.25
Na			0.1	
Cl	0.6	0.5	0.7	
Ba			1.34	13.87

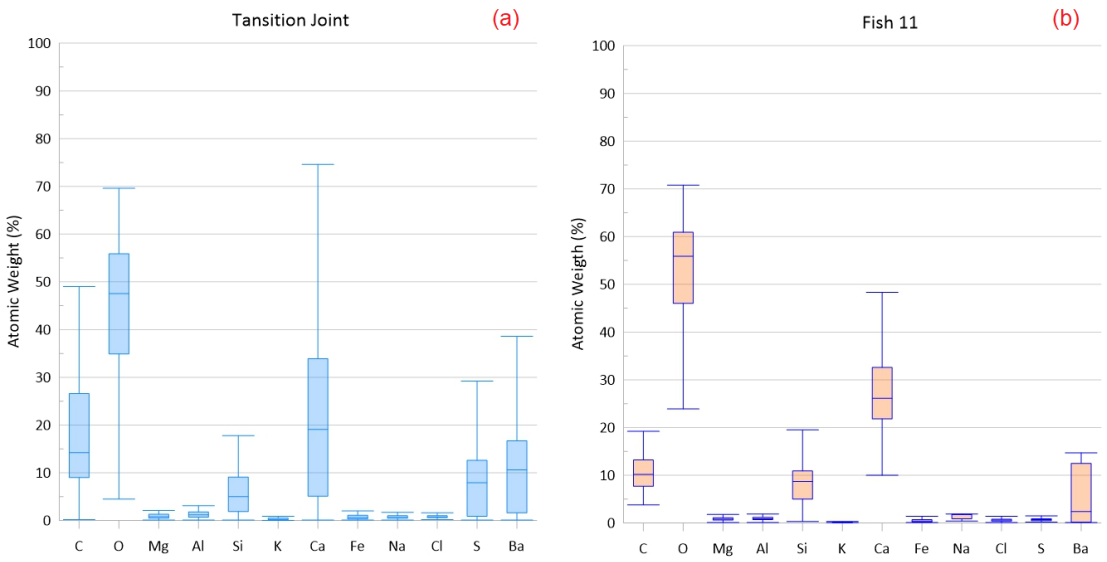

Figure 4.7: Box plot of elementary atomic Weight for (a) Transition Joint and (b) Fish # 11. Results based on EDS for 140 spots.

the findings from the CT scan and SEM/EDS.

Typical values from laboratory samples have been reported for Portland cement by Kosmatka and Panarese [230], Dueramae et al. [231], and Bahafid et al. [232]. For cement samples recovered from oilfield wells, Carey et al. presented the results of XRF for unaltered cement (which they named Gray cement 6545 and 6549) and degradated cement (named Orange cement 6549) [200]. A comparison of the values is presented in Table 4.9, and it is seen that the Valhall samples present a lower content of silicon dioxide (SiO_2) and aluminium oxide (Al_2O_3) and levels below detection for magnesium oxide (MgO). The content of calcium oxide (CaO) is still close to 60 %, comparable both with the laboratory samples and the unaltered cement, which indicates that only minor degradation (decalcification) has occurred in the cement over time.

Table 4.9: Quantitative results of oxides concentration in percentage normalized to 100 %. LOI: Loss of Ignition (mass loss after cement sample is exposed to 1000 $C°$), ** Values were normalized including LOI.

	Valhall samples				**Laboratory samples [232]**	**Samples from SACROC Unit [200]****	
Oxide	FT 75	FT 87	TJ 48	TJ 73		Unaltered cement	Degraded cement
SiO_2	12.28	10.04	13.28	2.40	19.1	19.09	19.40
Al_2O_3	1.05	0.90	1.91	1.88	2.90	3.95	3.87
Fe_2O_3	3.44	3.77	3.87	0.92	3.70	2.15	2.04
CaO	62.63	64.92	59.93	0.50	67.2	53.65	43.80
NaO_2						1.91	3.19
SO_3	0.55	0.95	1.43		2.5		
TiO_2	0.25	0.29	0.28		0.4	0.20	0.19
K_2O	1.48	0.75	0.77	0.18			0.14
MnO	0.05	0.06	0.05			0.09	0.07
MgO					1.4	2.95	1.01
BaO				94.17			
Others	0.12	0.15	0.12		0.5	0.09	0.07
LOI	18.15	18.43	19.62	9.82	2.4	15.92	26.22

X-Ray Diffraction (XRD)

The fragments from the core plugs were prepared in powder form and subsequently analysed at the University of Stavanger, using a Bruker D8 Advance with a Lynxeye detector (Cu-K α radiation 1.5406 Kα1, 40 kV 25 µA, 0.6 mm receiving slit). The measurements were obtained in the range of 2 θ, from 8° to 90° in steps of 0.05° and 8 seconds per measurement. The crystallographic analysis from the identified minerals was performed in the database PDF2 using the software X'pert Highscore, and the crystalline phase content was quantified using the Rietveld refinement method in the software GSAS.

Table 4.10: Crystalline phase quantification in percentage, obtained by XRD and Rietveld refinement

Phase	FT 75	FT 87	FB 64	TJ 48
Barite	1.58	3.88	5.21	5.46
Belite	4.44	10.56	18.29	16.22
Calcite	24.70	22.39	35.67	15.00
Portlandite	51.95	31.07	34.46	28.90
Vaterite	17.33	32.10	6.37	31.03
Katoite	0.00	0.00	0.00	3.40
Total	100	100	100	100
$\chi 2$	17.37	24.57	26.34	23.26
wRp	0.031	0.0595	0.0594	0.0567

The X-ray diffraction patterns confirm the presence of both crystalline and amorphous phases, see Fig. 4.8. The amorphous fraction, evidenced by a hump between 20 and 35 degrees (2 θ), corresponds to the short-range structures from the Calcium Silicate Hydrate (C-S-H), formed as the main hydration product of Portland cement. The crystalline fraction was found to be composed of belite (Ca_2SiO_4) from residual anhydrous clinker, portlandite ($Ca(OH)_2$), which is a byproduct of the C-S-H precipitation, katoite ($Ca_3Al_2(SiO_4)1.5(OH)_6$) from the hydration of calcium aluminates, and calcite and vaterite, two polymorphs of calcium carbonate ($CaCO_3$) from the carbonation process of portlandite. Barite was also identified, which confirms the intrusion of mud in the cement slurry. XRD analysis for TJ 73 mostly showed content of barite, and the results for this sample are not included in Table 4.10. Small amounts of barium bromide hydrate ($BaBr_2H_2O$) and Friedel's salt ($Ca_2Al(OH)_6Cl(H_2O)2$) were also identified in all samples; these can be associated with the presence of chlorine and bromine in seawater in the trapped brine. The FB 64 sample also contained some ettringite ($Ca_6Al_2(SO_4)_3(OH)_{12}\,26H_2O$), which can be associated with the calcium aluminates from clinker. Due to the small amount of these three salts in the samples they could not be quantified by the Rietveld refinements.

Regarding the phase quantification, presented in table 4.10, the results show a

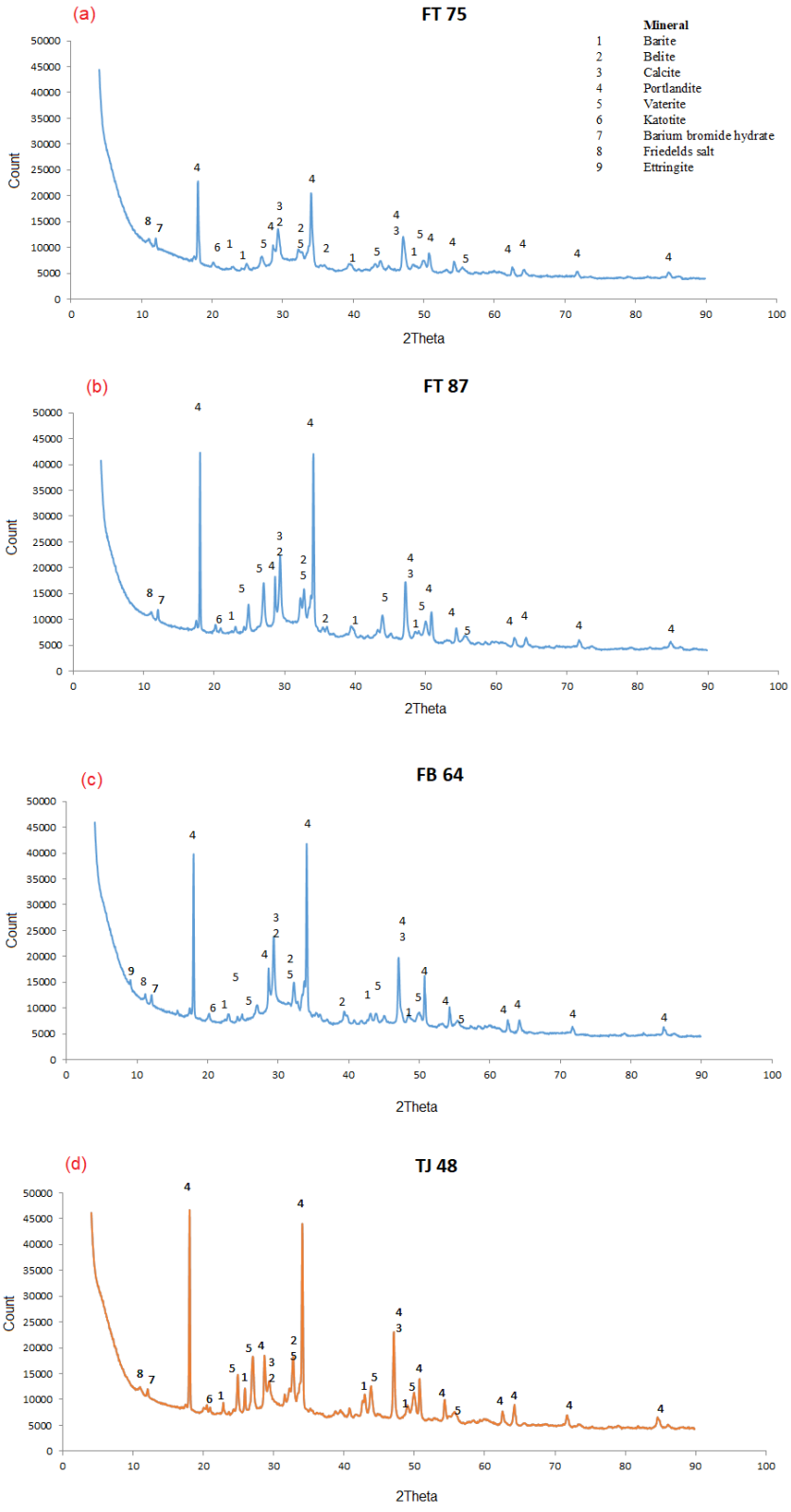

Figure 4.8: X-Ray Diffraction pattern phase identification comparison (a) FT75, (b) FT87, (c) FB64, (d) TJ 48

predominance of calcium carbonate, comprising between 42 and 55 % of the crystalline phases in the studied samples. This, together with the content of portlandite,

indicates the development of a slow rate of carbonation over the years and possibly a low temperature phase transition from vaterite to calcite, since the first is a metastable phase of the latter. Finally, the observed content of belite is consistent with an advanced hydration process, where all the more reactive phases of alite, C3A and C4AF have fully reacted, while the slow rate hydration of belite is still occurring.

Thermo Gravimetric Analysis (TGA)

Thermogravimetric analysis, known as TGA, is a complementary technique for material characterisation that is used to evaluate the portlandite $Ca(OH)_2$ content, measure hydration, and to identify amorphous hydrates, such as $C-S-H$. 10 mg samples from cores FT 87, FT65, FB64, TJ73 and TJ48 were analysed using a TG-DTA equipment and Alumina crucibles. The temperature was raised from room to 35 °C and maintained for 60 minutes to evaporate any water that may have adsorbed during storage and handling of the samples. Subsequently, the temperature was raised up to 1000 °C using a 10 °C/min heating rate. An empty crucible was used as a reference, and a constant 50 ml/min of nitrogen was used as a purge gas. Mass loss quantifications were performed using the tangent method, and $Ca(OH)_2$ and $CaCO_3$ contents were computed using the following equations.

$$\%Ca(OH)_2 = H\frac{MW_{Ca(OH)_2}}{MW_{H_2O}}$$

$$\%CaCO_3 = H\frac{MW_{CaCO_3}}{MW_{CO_2}}$$

Where H is the mass loss obtained from the thermogravimetric curve and MW is the molecular weight of the indicated compound. A similar response was observed for TG and DTG between most of the samples showing a very typical cement response. The results are plotted in Fig. 4.9.

For four samples (FT87, FB64, FT65 and TJ48), the Total Content of Water (TCW) was below 16%, while the portlandite $Ca(OH)_2$ varied between 12-18% and the calcium carbonate $CaCO_3$ was below 6%. Such results confirm a low level of alteration/degradation in the cement where the portlandite content is still representative and the carbonation has been low. The results for sample TJ73 show a different response where the peaks for cement phases are less representative; such a response is attributed to the high content of barite in this sample. Note that peaks at 580 and above 850 °C seem to be characteristic for barite. Such peaks were also observed for sample FT87 and TJ48, which well agrees with the detection of barite by other tecniques presented in this chapter.

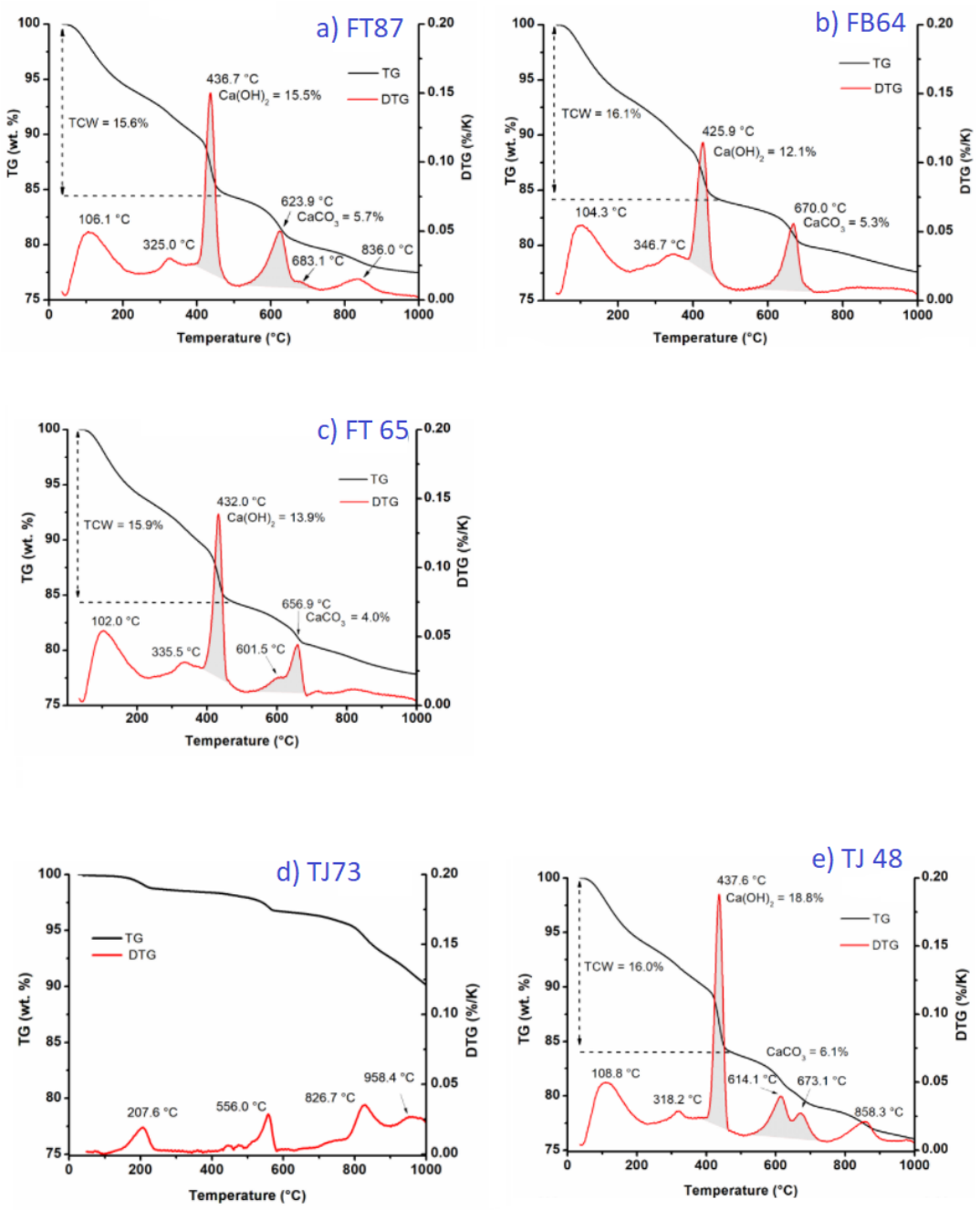

Figure 4.9: TGA peaks identification comparison (a) FT87, (b) FB64, (c) FT65, (d) TJ 73 and (e)TJ 48

4.4 Part 2 - Slim Sandwich Cross-section

A 3 centimeter thick slim cross-section was cut from the top of Fish # 11, shown in Fig. 4.10. Eleven angular segments of approximately 33° were defined and numbered 1 to 11 on the sample to perform additional analysis (see nomenclature on Fig. 4.10). The characterisation of this sample was performed in collaboration with the Museum

of Archaeology in Stavanger, Norway.

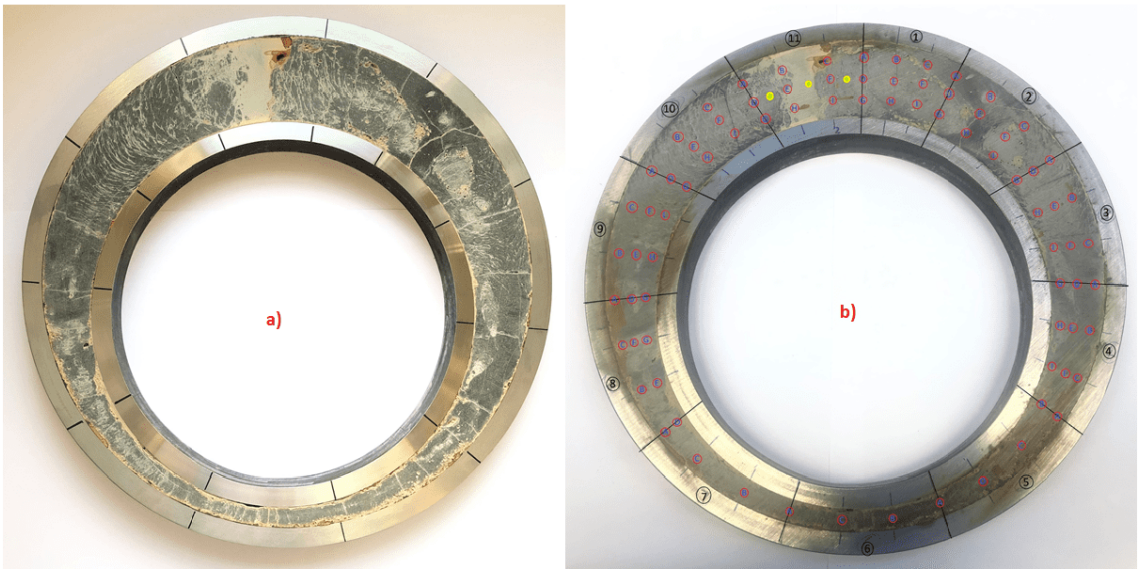

Figure 4.10: Slim section recovered from the top of the Fish # 11 Section. a) High-resolution picture b) section showing points of measurement for XRF in red (all points) and Rebound hammer in yellow (only points in angular section 11 are highlighted).

4.4.1 Compressive Strength by rebound hammer

The rebound hammer method is based on the principle that the rebound of an elastic mass is a function of the hardness of the material which the mass strikes against. The tool to perform the test is known as Schmidt hammer, which uses a non-destructive technique estimates the compressive strength of concretes based on the rebound index, the procedure of which is detailed in the ASTM C805 [233]. Other studies of the application of this technique for concrete mixtures have been reported by other authors [234, 235]. For this study, the measurements of rebound were made using a Schmidt hammer. The linear relation of rebound number with compressive strength was used to investigate the variations in cement strength around the cross-section. Thirty measurements were obtained holding the hammer vertically. Three measurements were made in the centre of the annular space for each segment, except for segment 6 due to the reduced area. As an example, the yellow circles in Fig. 4.10 show the location of the measurements for segment 11. A total of 30 rebound measurements were made holding the Schmidt hammer vertically. Results of the average rebound for each angular segment were computed to equivalent compressive strength range from 40 to 64 MPa. The results agree within an order of magnitude with UCS obtained for the core plug FT 87, see Table 4.7, and also with the values reported by Teodoriu and Asamba [5, 226]. In their results, the maximum uniaxial

compressive strength for pure cement class G mixed with freshwater reached 60 MPa while cement mixed with salty water gave a reduction to 30 MPa. Seawater was used to prepare this slurry and the cement contained intrusions of mud that reduced the mechanical strength.

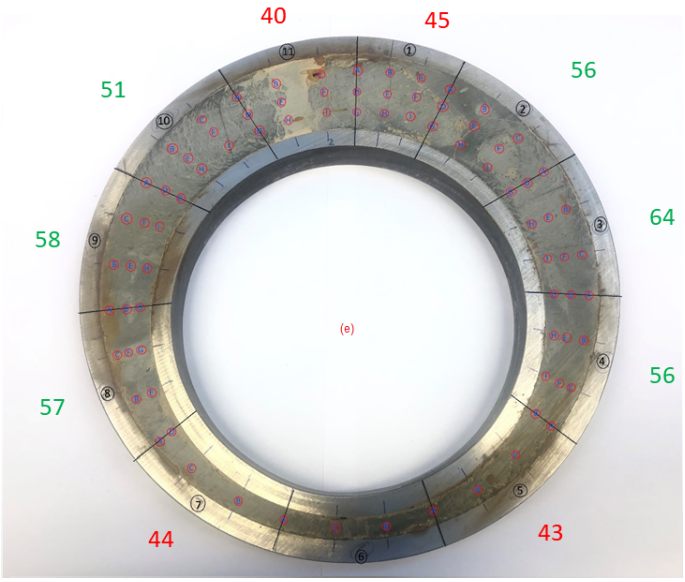

Figure 4.11: Average compressive strength (MPa) identified in the eleven angular segments (labeled in black) in the slim sandwich cross section

The results of equivalent compressive strength obtained with rebound hammer measurements can be useful to obtain an initial rapid estimation of mechanical properties. However, they may overlook the loss of strength due to local mud contamination that was observed in the UCS for the core plugs tested and discussed in section 4.3.3.

4.4.2 Elemental mapping using X-Ray Fluorescence (XRF)

A total of 80 measurements was made to characterise the composition using a Bruker Tracer III-SD handheld X-ray Fluorescence (XRF) spectrometer, as indicated by the red circles in Fig. 4.10. The instrument allows a non-destructive identification of elements from magnesium to uranium and semi-quantitive analysis. The measurements were carried out at 40 kV and 30 µA without using a vacuum system. Each measurement covers an area of 0.7 mm^2 and has a penetration depth of 0.7 mm below the surface. For the angular segments in the wider annulus region, numbered 1, 2, 3, 9, 10 and 11, nine measurements were taken (highlighted by red circles in Fig. 4.10. Three to five measurements were taken for the narrow annulus region segments, numbered 5, 6 and 7, due to the reduced area.

The elemental composition and their azimuthal and radial variations were measured and discussed. Elements such as Al, Ba, Br, Ca, Cl, Fe, K, Mn, S, Si and Sr

were detected in the sample. Vector analysis was performed using the results of the relative weight percentages of each element. Fig. 4.12 shows the distribution of typical elements present in cement. Calcium was the most abundant element detected, with relative percentages between 64 and 78 %. Aluminum and silicon represented less relative percentages with 0.4-0.5 % and 0.84-0.90 %, respectively. The results suggest that the distribution in the azimuthal and radial direction of those elements was mostly homogeneous. This agrees with the abundance of calcium phases found in the core plug results.

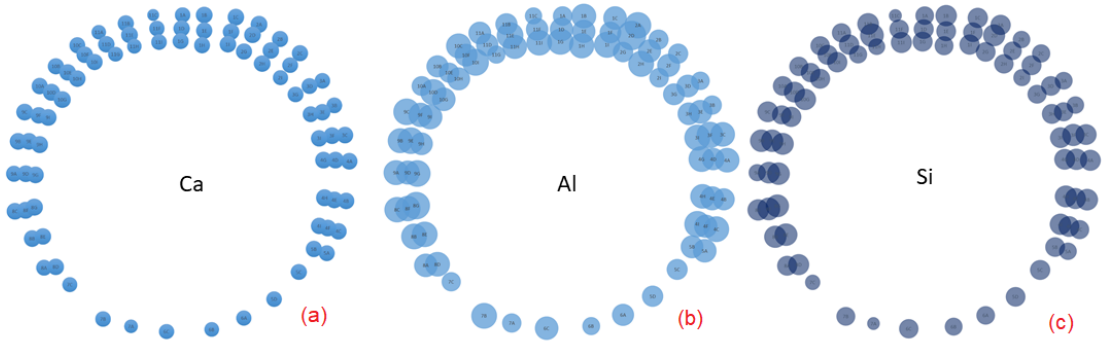

Figure 4.12: Distribution of (a) Ca, (b) Al and (c) Si on the surface of the slim sandwich cross section

A similar analysis for other elements is presented in Fig. 4.13. The distribution of nine elements such as bromine, chlorine, barium and potassium is presented. The results suggest that the distribution of these elements is more heterogeneous along the radial and azimuthal directions. Chlorine and bromine are elements typically present in seawater, and their presence in the sample is consistent with the fact that the slurry was originally prepared with seawater. However, the different patterns in the distribution of those elements might suggest the location of migration paths where the $CaBr_2$ brine was trapped between the 9 5/8-in and 13 3/8-in casings. The distribution of potassium is more complex to explain as this element is added to cement slurries and drilling muds through additives such as potassium chloride. However, it appears to be less abundant in angular segments 4, 8 and 9.

An important variation in the barium content was found for the adjacent angular segments 1 and 11. The richer content of barium in segment 11 and poorer content in segment number 1 can explain why the cores FB 64 and FB 132 have a very different response in the CT scan, see Fig. 4.3. This also agrees with the different barium levels detected by SEM, XRF and XRD analysis for both core plugs. The slim sandwich cross-section was cut just a few centimetres above where the core plugs were drilled in the top of Fish # 11.

Fig. 4.11 shows the results of compressive strength measured with the rebound hammer and indicated in red and green numbers around the cross section. The

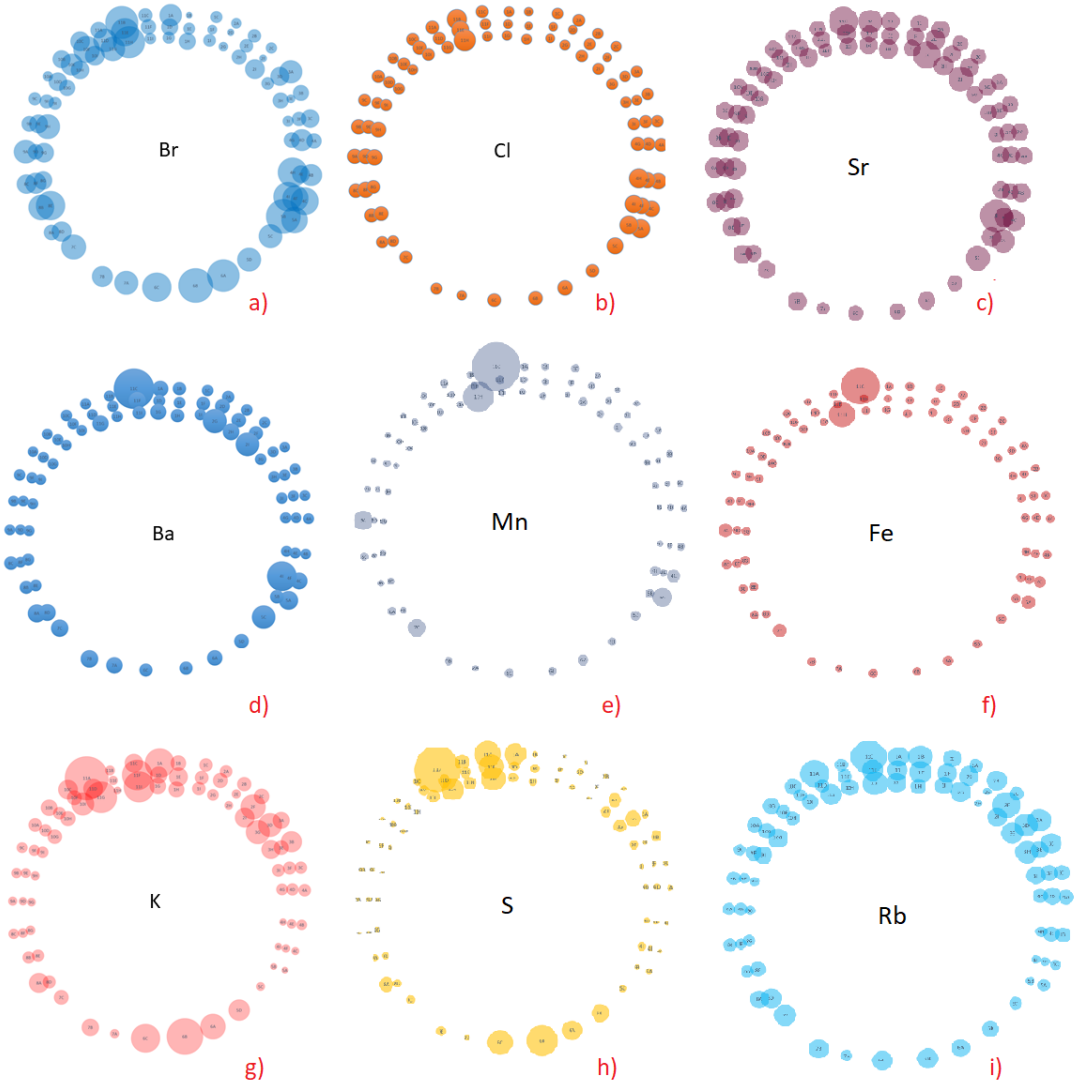

Figure 4.13: Distribution of elementary composition for (a) bromine, (b) chlorine, (c) strontium, (d) barium, (e) manganese, (f) iron, (g) potassium, (h) sulfur and (i) rubidium.

segments with lower resistance (sectors 1, 11, 5 and 7) correlate well with variations in levels of Br, Cl, K, and Ba presented in Fig. 4.13. On the other hand, segments 3 and 9 show lower amounts of these elements and lower intrusion of contaminats. This observation suggests that contamination of the slurry may have an influence on the compressive strength.

4.4.3 Principal Component Analysis (PCA)

Using the results collected by Elemental mapping using X-Ray Fluorescence (XRF), a Principal Component Analysis (PCA) was used to evaluate the data. PCA is a method of data analytics that enables the dimensional reduction of large data

sets identifying the dominant patterns and relations between the variables using the eigenvalues of a matrix [236]. A matrix of 960 values (80 measurement points and 12 elements per point) was constructed and analysed for four main components. The four principal components account for about 87% of the variation in the 12 elements selected for the PCA analyses. The results of eigenvalues are presented in Table 4.11. Subsequently, the three main eigenvalues were used to understand the relation between the elements, presented in Fig. 4.14.

Table 4.11: Results of eigenvalues in the PCA for 4 main components.

Component	Total	Variance (%)	Cumulative (%)
1	4.84	40.3	40.30
2	2.67	22.05	62.35
3	1.73	14.43	76.80
4	1.24	10.26	87.07

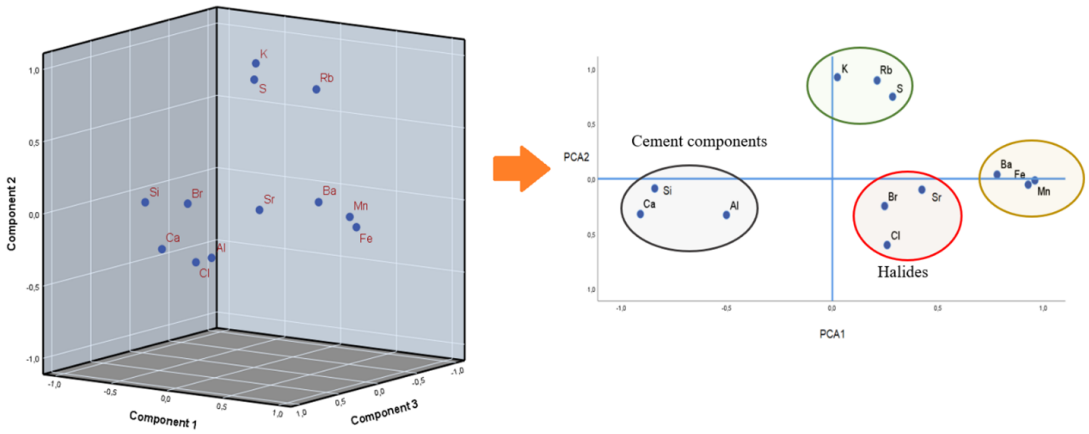

Figure 4.14: 3D and 2D visualization of the 3 and 2 main components for the PCA analysis based on XRF dataset

3D and 2D visualisation of the PCA components shows that the calcium (Ca) is highly correlated with silicon (Si) and aluminium (Al), as expected due to their association and importance in the cement phase. Typical salts (halides) present in seawater (used in the preparation of the cement slurry as reported in the cement job) such as chlorine (Cl) and bromine (Br) were also correlated. An interesting association that was observed was the relation between iron (Fe) barium (Ba) and manganese (Mn), confirmed through the mapping of the elements, in Fig. 4.13, and the visual inspection where the film of mud looks to be relevant in the presence of oxides. Sulfur (S) is correlated with potassium (K) and rubidium (Rb). The correlation between potassium (K) and rubidium (Rb) could be traced back to the feldspar aggregates that could have been used in the cement. The high degree of correlation between potassium (K) and Sulphur (S) could imply the possible

formation of potassium sulphate (K2SO4) in parts of the specimen analysed. This is further strengthened by the EDS spectra acquired from SEM-EDS analysis where potassium (K) and sulphur (S) do exit together in some grains of certain samples analysed.

4.5 Durability Discussion

Important indicators of well barrier failure due to cement degradation are the appearance of fluid migration paths, loss of cement mechanical strength, increases in permeability and porosity and aggressive changes in cement phases (such as reduction of portlandite and decalcification) [185, 237]. The appearance of these phenomena is normally difficult to track due to their interdependency and intercorrelation, as well as their variability as a function of the initial pore structure and curing conditions. The results presented in the previous section are discussed in light of the conceptual map for long term durability for cement well barriers presented in Chapter 1 - section 2.1. The discussion aims to understand signs of degradation or alteration and possible causes.

The loss of cohesion and mechanical resistance are important symptoms of cement degradation that can lead to barrier failure, as shown by item B in Fig.2.2. Other studies have suggested a decrease in compressive strength over time at high temperatures [195]. In the present study, at relatively low curing temperatures, mechanical properties such as maximum UCS and Young's modulus were comparable to early age cement (see Section 4.3.3), and the reduction in mechanical strength was shown to be affected mainly by localized slurry contamination. Consequently, the mechanical properties for the tested core plugs suggest only a low degree of degradation or alteration affecting structural integrity. This looks to be in agreement with the findings of other authors, where cement exposed to brine showed no critical alteration on cement [81].

High values of permeability and porosity are expected when the cement has been damaged or has integrity problems, as per item C in Fig. 2.2. Such alteration occurs especially when water penetration or aggressive ions (such as sulfate, chloride, magnesium, etc) intrude the porous structure, reacting with cement and leading to deleterious chemical reactions weakening the material. The results of petrophysical properties presented in this work, Section 4.3.1 do not indicate significant cement alteration or degradation. The porosity and majority of the gas permeability measurements agree well with comparable values from other cement samples recovered from fields, such as those reported by Carey et al. [200] and Duguid et al. [181], and the bulk permeability for early age cement recently reported by Yang et al. [220]. The field cement samples analysed and reported as "degraded cement" by

Duguid et al. [181] have porosity reaching 63% and permeability above 4.63 mD. Such values are almost twice the magnitude reported for the Valhall samples in the current work.

Changes in the contents of cement phases, such as the decrease in calcium (decalcification), decrease in portlandite (leaching) and increase in calcite (that forms as a product of the consumption of portlandite) are also strong evidence of initial material degradation. As the initial content of the cement phases in situ is unknown, the direct comparison of initial conditions with current conditions is difficult. However, as presented in items 18 and 19 in Fig. 2.2, these changes can be an early sign of alteration or degradation. This can later lead to material weakening and an increase in permeability. The results of chemical characterisation (SEM, EDS, XRF and XRD), Sections 4.3.4, and 4.4.2, suggest that the slow rate of carbonation that had occurred over the 33 years had not significantly affected the cement integrity. The observations indicate that the levels of portlandite and calcite (from XRD) and content of CaO (from XRF) are comparable with laboratory and field samples reported by other authors, such as [181, 193, 199, 200].

No corrosion or chemical attacks were observed on the cement porous matrix in the interfaces between cement and casings when the fresh cuts were made. This may suggest that the risk of in situ ion attacks leading to corrosion is low.

4.6 Conclusions

The bibliographic review and comparison to relevant results performed in this research identified only a limited number of cement samples that have been exposed to downhole conditions and have been subsequently fully characterized. The published research on the analysis of core plugs recovered after in situ exposure to evaluate ageing is limited to the work performed by Duguid et al. [181] and Scherer et al. [199]. Most of the studies of field samples combine effects of ageing and CO_2 exposure, making it difficult to address the implications of CO_2 storage on long term well integrity alone, as the cement may have previously been altered by age effects [189–191, 200].

The elemental compositional analysis conducted by SEM, EDS, XRD and XRF has proved to be a powerful tool to understand the degree of contamination and degradation in the samples. Mechanical property measurements in combination with elemental analysis were able to explain the variations in the compressive strength.

The analyses performed on core plugs were limited to the material contained in the wider part of the annular space. The evaluation of the slim cross-section provided a better understanding of the azimuthal and radial variations in the cement properties and composition.

Despite the large dispersion in the mechanical properties of the samples, the cement recovered and studied in this work was demonstrated to have the mechanical and chemical structural integrity required to prevent fluid flux through the bulk cement matrix after 33 years of downhole exposure. Nevertheless, the record of SCP in the well prior to abandonment is an indication that factors such as the existence of preferential fluid migration paths can affect the well barrier integrity even when the bulk cement properties appear to have low degradation. The performed analyses showed that the overall decrease in cement matrix integrity was low, suggesting that the main migration paths, responsible for zonal isolation loss and seepage, might occur in the cement-casing interface, as discussed by Skadsem et al. [3, 175]. Those results are in agreement with previous research from Bourgoyne et al. [146] and Jung et al. [238].

The complementary studies of logging and flooding testing for Fish # 11 and Transition Joint, presented in the previuos chapter on section 3.6, suggests that the main migration paths on the sections might occur in the cement-casing interface. Those results seem to be in agreement with the finding that the overall decrease of cement matrix integrity is low, but they are also consistent with studies by other authors where the failure of the cement interfaces appears to be more relevant than barrier bulk properties in well barrier failures [146, 238].

Chapter 5

Large-Scale testing infrastructure to support the qualification of cement evaluation logging tools

The testing infrastructure presented in this chapter was designed by a group of engineers from Equinor, Schlumberger and NORCE. The author of this thesis has contributed to the research by selecting the materials, executing the job of building and running the well completion and planning the cementing operation. The content of this chapter was recently published in a conference paper in the IADC conference[239].

The goal of the construction of this new facility for testing logging tools was to mimic the most common subsurface well structures on the Norwegian continental shelf with a focus on current industrial needs for single and dual-casing diagnostic technology evaluation. The design is based on drilling practice and disregards the diagnostic physics used for evaluations. Additionally, specific elements are engineered so that claimed sensitivity to azimuthal and vertical extended "defect" for any given diagnostic technology could be tested. The testing infrastructure is built to support both operators and vendors to harmonize the specifications of technologies. Technologies with needs for development and improvement of specifications for the assessment of annular well barriers can be tested in this facility, so that they can fulfill the established requirements indicated by the regulator[19].

5.1 Existing facilities for logging tools testing

Large-scale facilities have been constructed previously for the purpose of investigating logging tool response under known conditions. For open-hole logging tool calibration, the Houston API pits were built in the 1950s but closed in 2013; like-

wise, the EUROPA/Callisto calibration facility built in the 1990s closed down in 2018 [240]. The Total Exploration & Production Alternative Subsurface Data, also known as TEP ASD, the facility was constructed by Total in Artigueloutan, France, for the purpose of well logging tool calibration. The facility offered 23 porous rock standards in addition to four fluid standards and a full set of metallic standards to investigate the effect of borehole size and fluids. In addition to open-hole logging, a casing could be installed to investigate the response of the formation evaluation tool in a cased-hole environment. The U.S. Environmental Protection Agency (EPA) operates the Robert S. Kerr Environmental Research Laboratory in Ada, Oklahoma. Three wells were constructed at this site in the 1980s in order to test available methods for measuring the mechanical integrity of injection wells [241]. Two of the wells have different-sized channels installed in the cement behind the casing, created by attaching PVC tubes full of water to the outside of the casing using fibreglass. Logging well 1 has four channel sizes ranging from 6° to 90° coverage, each being installed on four different casing sizes from 5 1/2-in. to 9 5/8-in., respectively. This well has been utilised to test the performance of cement evaluation logging tools [242]. The objective of the large-scale infrastructure is to establish conditions equivalent to those downhole, for testing annular barrier verification technologies. During the initial work phase, concepts were reviewed based on test cells previously built for cement evaluation logging experiments [2, 171]. These cells were built by introducing defects inside annular cement contained between two sections of casing. Such a design can be readily constructed and has proven to be useful for ultrasonic logging tool evaluation. However, for sonic logging tool evaluation, the depth of investigation of the measurement is much deeper, and this configuration is not acoustically representative of a casing cemented inside a borehole drilled in the rock. After considering alternatives for constructing representative cells on the surface, it was concluded that drilling a well would best meet the objective of mimicking the required conditions. A well has the advantage of enabling the logging of many casing/cement/defect configurations in one run. Different wellbore fluids can easily be introduced and also additional tubing strings hung-off for through-tubing logging. Rigging up logging tools would be the same as in a real well and the tools run to the bottom thanks to gravity alone. However, a challenge in a real well is the introduction of the required defects in the cement sheath. Ideal defects should be fluid-filled cavities; however, the approach employed by Thornhill was not considered sufficiently representative due to the multiple interfaces created between the casing/PVC tubing/fibreglass and cement that could disturb the tool signals[241]. It was concluded that defects with a known geometry could best be implemented by utilising a material to mimic a fluid-filled channel in the cement.

5.2 Material Selection

Before the installation of the well completion, a study was performed to select a suitable material to mimic defects in the well cement sheath. A variety of materials were initially considered based on tissue-mimicking phantoms used for medical ultrasound imaging such as gels, foams, and rubbers [243]. The material properties required included an acoustic response similar to water, suitability for installation on the outer surface of the casing, enough robustness to survive a trip downhole, and the ability to withstand the cement placement and curing process. Some of the materials considered were discarded due to the difficulty of bonding them to the casing surface whereas others were found unlikely to survive a trip downhole in a well environment. Synthetic rubbers were eventually selected as the primary solution given their overall physical robustness, relative ease of bonding them to steel, ready availability of expertise, and industrial facilities able to perform the installation on large steel objects. Four rubbers with different compositions—one nitrile butadiene rubber 35 shore A (NBR 35), two ethylene-propylene-diene monomer rubbers (EPDM 47, EPDM 73), and one Styrene butadiene rubber 59 (SLITEL 59)—were selected. All materials were available from a local industrial supplier of specialist rubber products and were used for further testing aiming to address the perceived project challenges and risks. First, small samples of each material with a thickness of 2 to 3 cm were tested using a JSR ultrasonic pulsar driving two Olympus transducers (1 MHz) and a Picoscope to digitise the signals. Rubber provides a good density contrast to cement density, which is expected to be 1.9 to 2 (gr/cm^2). Further, the rubber provides a good acoustic impedance contrast compared to class G cement with a typical AI in the order of 2.70 MRayl to 3.85 $MRayl$ for low-impedance cement 3.85 $MRayl$ to 5.00 $MRayl$ for medium-impedance cement and above 5.00 MRayl for high-impedance cement [89]. The physical properties of each rubber material are summarised in Table 5.1.

Table 5.1: Physical properties of rubber materials

Material	Density (gr/cm^3)	Speed of sound (m/s)	Acoustic Impedance ($Mrayl$)
NBR 35	1.1	1580	1.8
EPDM 47	1.1	1543	1.7
EPDM 73	1.1	1521	1.7
SLITEL 59	1.1	1597	1.8

To evaluate the response of compressional and shear waves in more detail, an ultrasonic logging tool was used. A short section of 9 5/8-in. casing with 25-mm-thick strips and the four different materials mounted on the external surface of the casing was constructed. The installation was a two-step process requiring the preparation

of the casing surface by sandblasting to remove any grease or contaminants and, thereafter, cold vulcanisation to create permanent adherence between rubber and steel. Each rubber material was installed with 100-mm of azimuthal coverage. A sketch showing the dimensions and a photograph of assembly 1 are shown in Fig. 5.1 A smaller gap of 70 mm was left between two of the strips (Slitel 59 and NBR35) to provide a reference position if required.

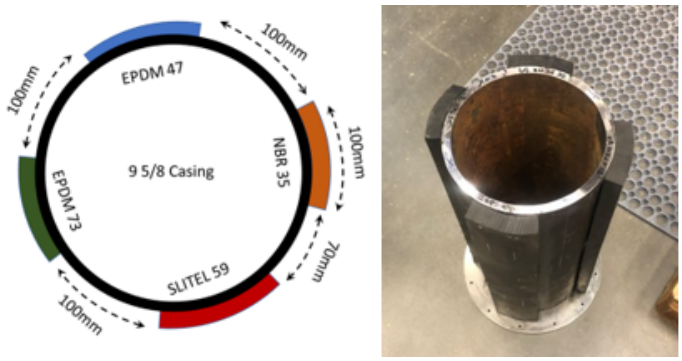

Figure 5.1: Assembly 1 for logging casing with attached strips of four different rubber materials.

Assembly 1 was thereafter mounted inside a water-filled and pressurised test chamber and subsequently logged to record the pulse echo and flexural response in the chamber. Fig. 5.2 shows a photographic snapshot of the pressurised test vessel for deploying the ultrasonic cement tool described to evaluate short casing sections; additional details of this vessel are in the public domain [126]. The vessel is equipped with brackets to secure the casing along with a cement sleeve if appropriate and allow the ultrasonic tool with a rotating sub to azimuthally scan the casing, as shown, and take pulse echo and pitch catch casing flexural measurements.

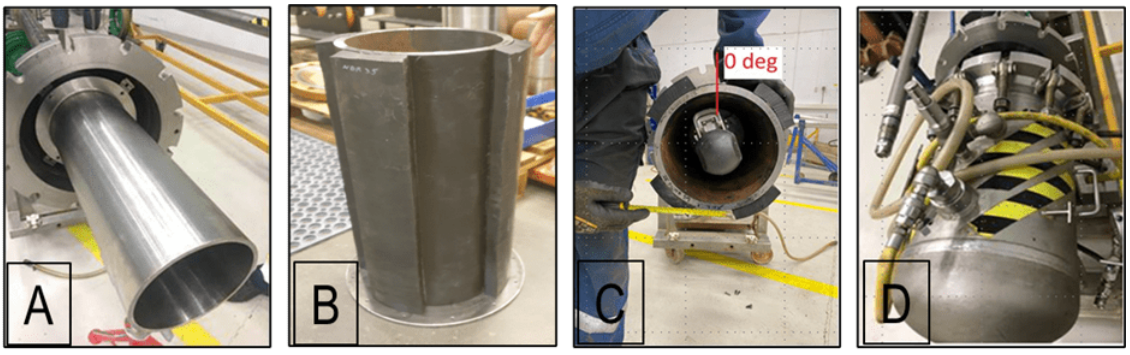

Figure 5.2: Assembly 1 for logging casing with attached strips of four different rubber materials.

Pulse-echo and flexural measurement transducers are mounted on a rotating sub and are routinely checked for accuracy. The rotating sub is inserted in a specially designed pressure vessel (Fig. 5.2D) where the measurements are carried out against

a known fluid type and casing tube of certain dimensions (Fig. 5.2A). After the function test was performed, the inner casing tube was replaced by assembly 1, with four stripes of different rubber materials mounted on the external surface (Fig. 5.2B and Fig. 5.2C). After the assembly was installed in a pressure vessel filled with water, pulse-echo and flexural measurement data were acquired to determine the sensor response against the rubber elements and water in pressurized conditions (Fig. 5.2D).

The position of four different rubber materials is shown in (Fig. 5.3C). The tool orientation sensor was aligned (Fig.5.3B) to the inner tube to measure the response from the four different rubber material strips. The log was recorded against time and is shown in Fig. 5.3A. The acoustic impedance from pulse-echo as well as from flexural measurements indicates a minor contrast between rubber elements and water. A combined solid-liquid-gas image indicates strips of different rubber elements are invisible to the measurement.

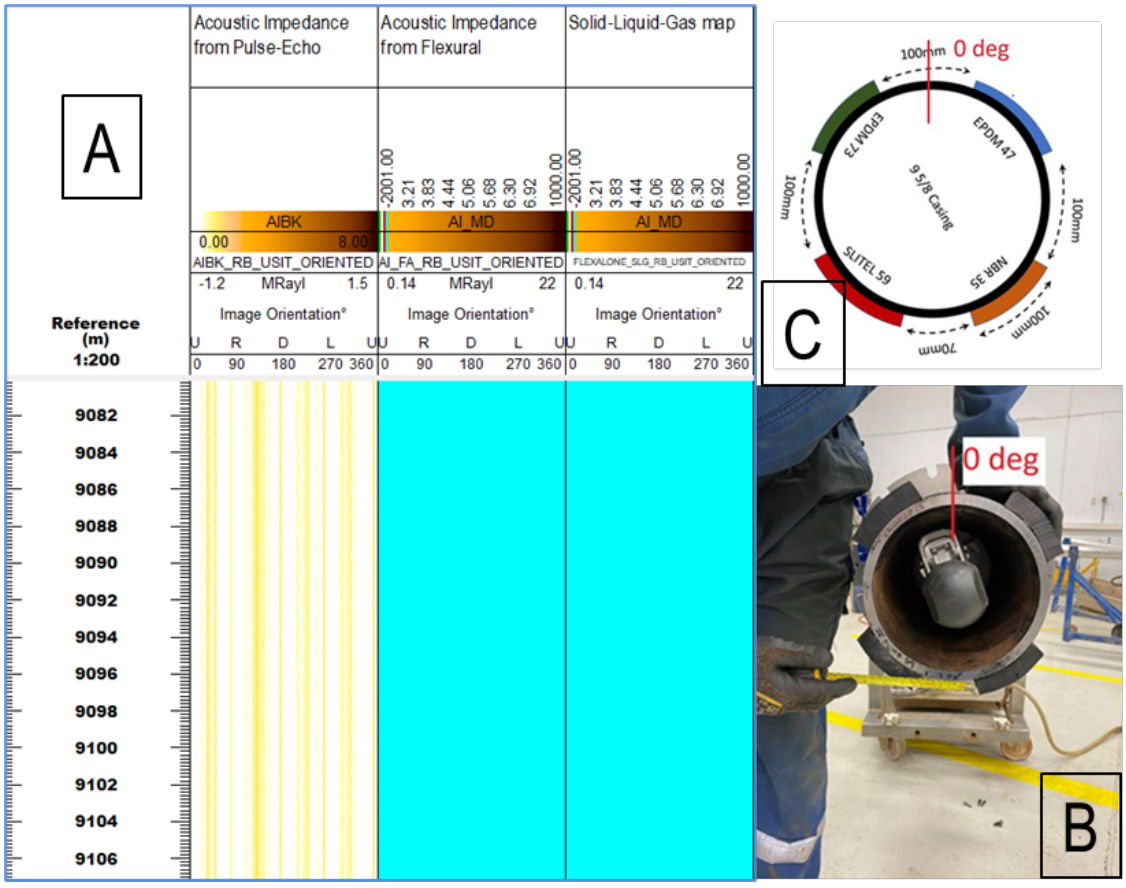

Figure 5.3: Ultrasonic evaluation logs showing acoustic impedance and solid-liquid-gas maps based on pulse echo and flexural measurements (A) using the azimuthal reference shown in (B) and (C).

Having established that all four rubber strips closely match the impedance of water, we examined the response in more detail to assess if there could be other

acoustic effects from the rubber that could affect the behaviour of the engineered channel and produce a distinct response from a water channel, particularly with respect to shear coupling to the casing and attenuation of propagating energy. To this end, we computed the casing flexural mode attenuation dispersion as a function of frequency for each of the scanned azimuths using techniques described in Zeroug and Bose[244] and plotted them as an image indexed by azimuth and frequency in Fig.5.4 (top left). We also plotted the attenuation dispersion curves at five selected azimuths corresponding to the centre of the rubber strips and water behind the casing. We see that the response is indeed distinct from the water behind the casing but the NBR35 strip generates the largest contrast. The phase velocity dispersions of the casing flexural mode are also computed and displayed in Fig.5.4 but do not show many differences as this is primarily determined by the steel casing.

We also observed a significant excitation of the casing extensional mode evidenced by ringing in the wave forms. Since the wave motion of the extensional mode is tangential to the casing surface, it is also of interest to examine this response. Accordingly, we estimated a crude measure of the extensional energy at the two ultrasonic receivers using appropriate time windowing and computed the extensional attenuation as a function of azimuth. This is displayed in Fig. 5.5, and again we observe that the NBR35 rubber shows the largest excursion from the behaviour of water behind the casing.

After the logging of the casing section was completed, a crude test was conducted to measure the strength of the adhesive bond between the rubber material and the casing surface. The test attempted to look at the shear strength of the bond in a manner equivalent to the end of a rubber strip hanging up on a ledge in the wellbore. A pulling load was applied in a controlled manner to the end of the rubber strip; see the purple band in Fig. 5.6. The test demonstrated that the NBR rubber bond strength to the casing was very low so that it was easily torn away from the casing. The EPDM 73 showed a much higher resistance and held 600 kg of load before it started to detach from the casing.

The second logging experiment investigated the logging tool response to variations in the azimuthal coverage and the contrast in tool response to cement versus rubber. Assembly 2 was constructed with three different rubber strip widths to provide variations in the defect size equivalent to 15°, 30°, and 45° degrees of azimuthal coverage (Fig. 5.7). An external casing of 11 $\frac{3}{4}$-in. was mounted around the 9 5/8-in. casing (with defects) and the annular space filled with Class G cement with 1.90 SG, as depicted in Fig. 5.7. Assembly 2 was logged using the procedure described for assembly 1, to record the pulse echo and flexural response.

After placing the casing section with the three rubber strips (Fig. 5.8C) and aligning the tool orientation (Fig. 5.8B) in the pressure vessel, a log was recorded

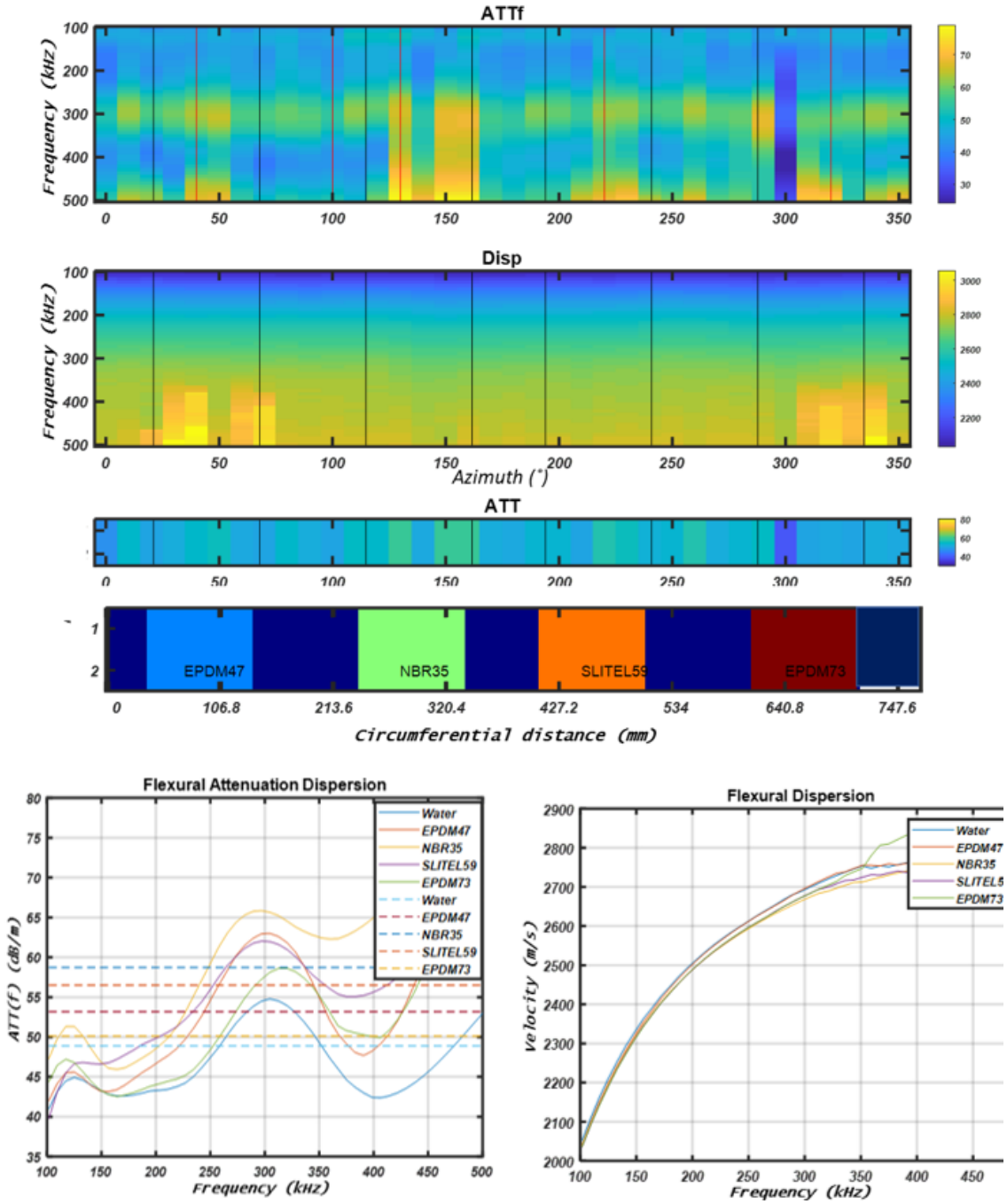

Figure 5.4: The estimated attenuation and phase velocity dispersion's as a function of frequency computed from the ultrasonic flexural data shown as maps for all scanned azimuths (upper figure) and as curves for selected azimuths (on bottom). The selected azimuths are indicated by the vertical red lines on the upper figure and correspond to the four rubber strips and water.

against time (Fig. 5.8A). Acoustic impedance from pulse-echo clearly shows the contrast between the cemented section and rubber materials. All the three varying width rubber materials were detected by the measurement. Note that the NBR35 strip was removed in this assembly due to the poor performance observed in the logging results. Acoustic impedance from the flexural measurement has passed beyond

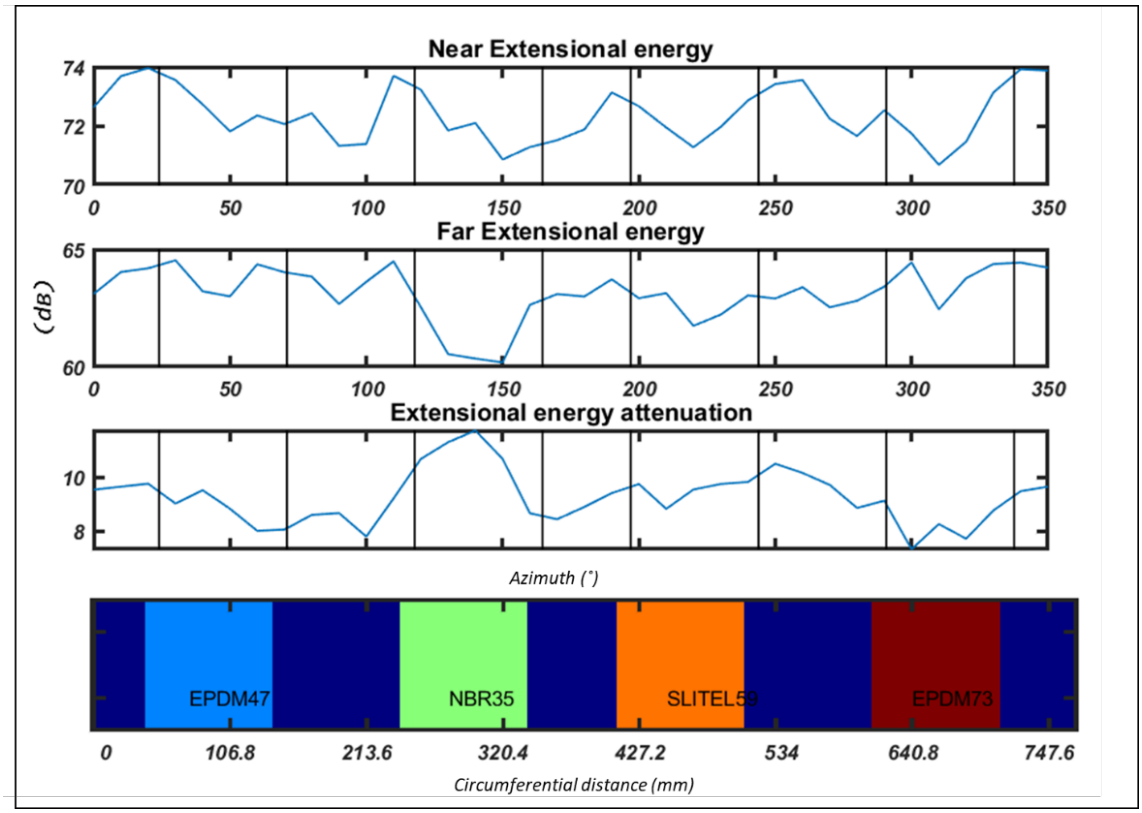

Figure 5.5: The estimated attenuation of the casing extensional energy as a function of azimuth. This serves as a measure of the tangential shear coupling to the rubber and indicates that the NBR35 rubber causes the greatest attenuation of the propagating extensional energy.

Figure 5.6: Crude test to evaluate the adhesive bond between the rubber materials and casing surface.

the critical impedance and is unable to distinguish between liquid and cement [2]. A combined solid-liquid-gas image indicates stripes of different width rubber elements are clearly detected.

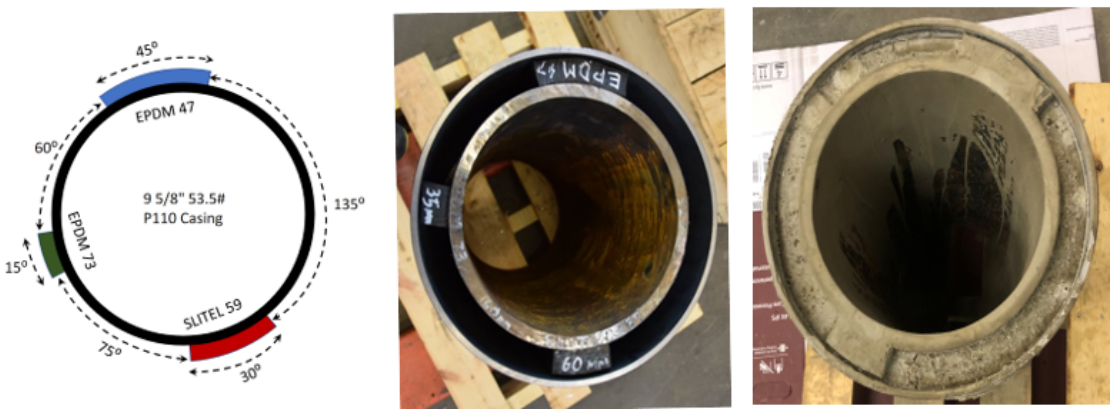

Figure 5.7: Assembly 2 for logging, instrumented with three rubber materials of different widths and cemented with cement Class G.

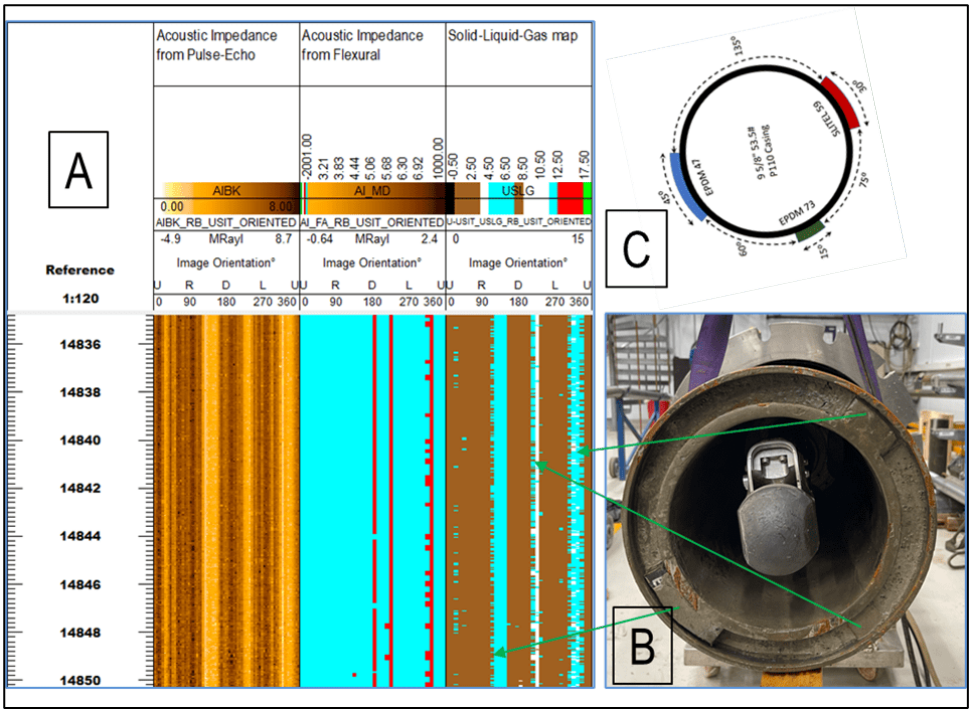

Figure 5.8: Ultrasonic evaluation logs showing acoustic impedance and solid-liquid-gas maps based on pulse echo and flexural measurements (A) using the azimuthal reference shown in (B) and (C) with positive values measured clockwise.

The overall conclusion from these experiments was that of the four rubbers tested, EPDM 47 was the optimal choice for the full-scale well experiment due to its ultrasonic response, the high shear strength when bonding to steel and its capacity to survive the cement curing process.

5.3 Well Selection

The well U7, located at the Ullrigg facilities in Stavanger, was selected as a suitable candidate for the full-scale test. The initial well status was a 13 3/8-in. surface casing with a shoe landed at 46 m and, below this, an open-hole section in the Phyllite formation reaching a total depth (TD) of 213 mRKB drilled with a 12 $\frac{1}{4}$-in. bit and a rat hole of 6 in. between 214 and 349 mRKB. The well deviation survey showed a deviation of 7.15° at 150 mRKB depth, and the extrapolated deviation at TD is estimated to be 10°. To accurately describe the initial well condition, a wireline logging operation was executed. Fig. 5.9 shows the results of the acquisition of gamma-ray and multiple-axis caliper logs. It was observed that the well was in overall good condition with an average open-hole diameter of 12 $\frac{1}{2}$-in. Washouts were found over two intervals: a first one below the casing shoe between 40 and 55 m, and a second one between 140 and 150 m, as indicated by yellow circles in Fig. 5.9. Note that the second washout was identified by only one set of caliper arms, indicating that the well has an ovalised shape over this depth interval.

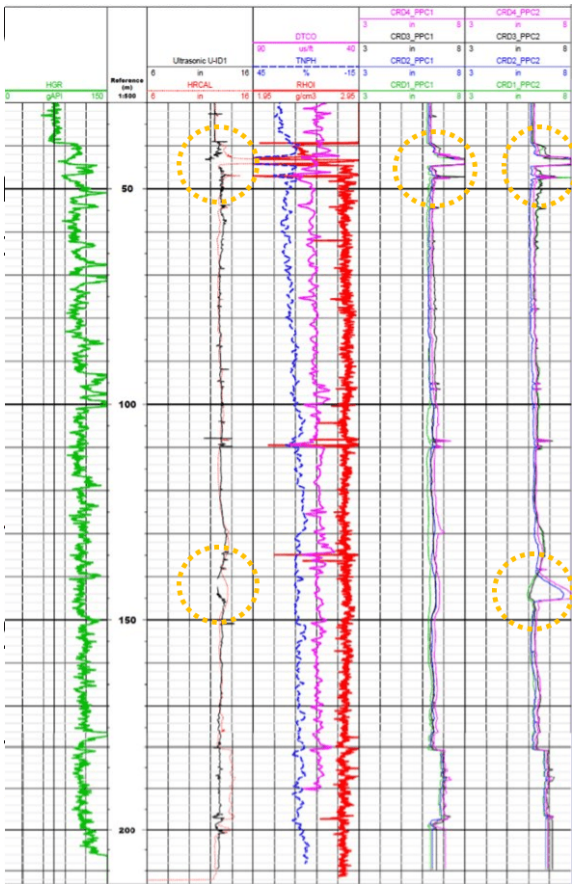

Figure 5.9: Logging response of well U7 presenting gamma ray and multiple-axis caliper

5.4 Dummy Run: Survival of Defects in the Well Environment

Considering the hole gauge, the radial clearance between the casing and borehole in the tightest spots was estimated to be 36.5-mm. The strips of rubber representing defects are 25 mm in thickness, and after they are mounted on the casing, the clearance to the borehole is reduced. In the worst-case scenario, with two strips of rubber installed, the clearance is only 11.5 mm, as illustrated in Fig. 5.10a and Fig. 5.10b. To address the risk of damage to the rubber strips during a run in the hole, a dummy run was planned and executed. The goal was to evaluate the risk of wear and tear of the defects on the casing joints when passing through the tight spots and washouts. Two casing joints with defects installed were fabricated and mounted with centralizers on the pin end (bottom). The rubber defects were installed using the sandblasting and vulcanization process as per the short casing assemblies. The ends of the rubber strips were cut at an angle of 45° to reduce the chance of hanging up on any sharp edges.

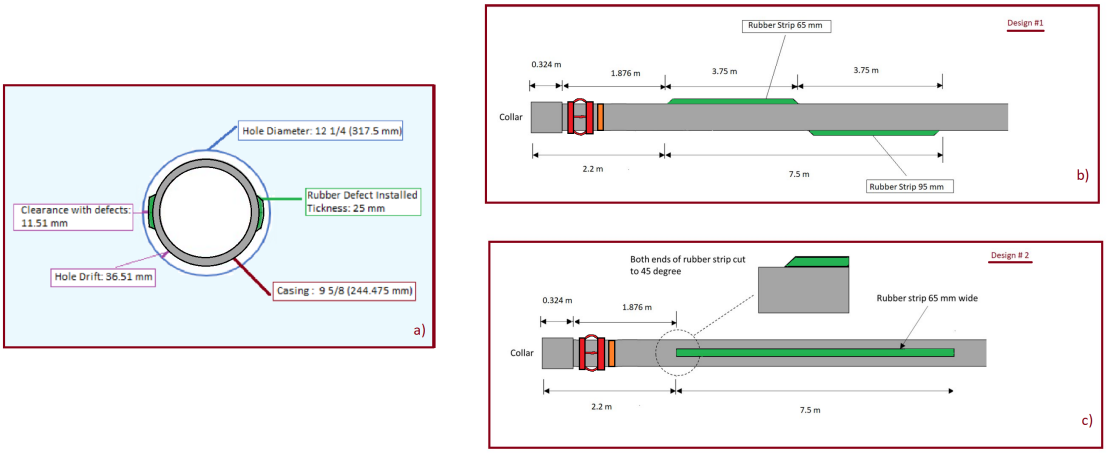

Figure 5.10: Schematics of casing joints: a) dimensions and clearance between the casing and borehole when defects are installed, b) casing joint with design 1, worst clearance scenario (when two strips are installed on the casing), c) Casing joint with design 2 with the typical design to be used (when a unique strip of rubber is installed).

A bottomhole assembly (BHA) comprising four joints of 9 5/8-in. casing (two blank joints on either end of the two joints with defects), a crossover, and a drillpipe were run to the well bottom and then recovered to the surface for inspection. As expected, the arms of the centralizer showed signs of wear, and there was also some evidence of contact between the rubber and borehole wall over a few sections of the strips. Although some contact with the borehole had occurred, the defects were recovered undamaged and were completely attached to the casing wall. The dummy

run proved the rubber to be a suitably robust material able to survive the trip downhole, and the risk of losing the defects during the full installation was deemed to be negligable.

5.5 Well Completion Design

For the completion operation, it was decided to run the 9 5/8-in. casing fully centralized to minimize the risk of damage to the rubber defects. The completion design consists of a shoe track, 16 casing joints, and a short pup joint. The details of the casing tally are presented in Table 5.2. All the casing joints were run with centralizers on the pin end of type Centrek 9 5/8 X 13 $\frac{1}{2}$ UROS. Ten of sixteen casing joints were run into the well with defects installed on the outer surface of the casing. For the joints with 10°, 20°, 30°, and 45° defects, the rubber strips were 7.5-m long and placed in the middle of the casing joint, as per the design in Fig. 5.10c. Two of each of these joints were installed over the lower and upper completion interval to have redundancy in the event of the actual cement placement varying from the design. In the case of the joint with combined defects of 30° × 45°, each strip is 3.75 m long, and the design corresponds to the schematic presented in 5.10b.

Table 5.2: Casing tally. Casing joints in open hole are listed in random order.

	Well Depth (m)	Number of Joints	Description	Defect Width (mm)
Joints into cased hole (13 3/8-in.)	8.75 – 35.95	4	Blank joint	
Open hole	35.95 -195.97	2	10°	20
		2	20°	45
		2	45°	95
		2	30°	65
		1	Surprise joint	
		1	30° x 45°	65 X 95
		2	Blank joint	
shoe Track	195.97	1	Black Joint	
	208.45	1	float Collar	
	209.11	1	shoe	

During the casing running, no evidence of significant drag or torque was observed. The casing was landed at 209 m depth and hung off at the rig floor in the slips to allow the installation of a casing cementing head.

5.6 Cementing Operation

The total volume of slurry mixed and pumped was based on the integrated volume estimated from the caliper log. The target top of cement (TOC) was at 50 mRKB, 10 m below the 13 3/8-in. casing shoe at 40 mRKB. The open-hole volume between

50 and 210 mRKB was estimated to be 14.18 m3, and the casing volume over the same interval was estimated to be 7.51 m3. Thus, the annular volume to be filled with cement was 6.67 m3 (openhole volume minus casing volume).

The total calculated cement volume required for the tail slurry includes the following:

Table 5.3: Cement volume estimation

Item	Volume (m^3)
Hole section (50 m to 210 m); annular volume from log	6.67 m3
Hole section (210 m to 214 m); inside diameter from log = 13 $\frac{1}{2}$-in	0.36 m3
Cement volume in shoe track	0.1 m3
Total slurry volume required:	7.1 m3

The cementing operation was designed to leave a few meters of free pipe in the interval just below the previous casing shoe for log response calibration. To avoid contamination of slurry by well fluid, top and bottom plugs were used. The risk of cement free falling effects was considered to be low, and no spacer fluid was required. It was planned to underdisplace the slurry so that the top plug did not reach the float collar and that 0.1 m3 of slurry would be left inside the casing above it. The pump schedule was performed as shown in Table 3.

Table 5.4: Pump Schedule

Event	Volume (m^3)	Flow Rate (L/m)	Time (min)	Pumping time (min) (min)
Water	15	600	25	25
Bottom Plug				
Cement Slurry	7.1	600	11.8	36.9
Top Plug				
Water	10.65	600	17.75	54.56

A total of 7,43 m3 of cement slurry was mixed on site. The slurry recipe comprised 4343 L of fresh water, 9.8 L of NF-6, 9774 kg of Class G cement, and 35 kg of a commercial lost circulation material. The slurry density measured on site before pumping was 1.92 SG. A cement sample was collected for an ultrasonic cement analyzer (UCA) at this stage to track the development of strength, while wireline logs were collected during the hardening process. During the pumping operation, the displacement was monitored by paying attention to the volume pumped downhole and the pressure observed. No unexpected events were observed. To confirm the correct displacement of the slurry, a string with tubing was run into the hole. The top of cement (TOC) was found higher than expected inside the casing, and the cement was dressed down to a depth of 205 mRKB. The cement operation was completed at a challenging and unusual low temperature of 3°C, where there existed a risk of water freezing in the pumping lines. This was identified as the root cause

for the under displacement observed that might create a possible miscounting of volumes pumped during the pumping. Despite this, the well was completed successfully. After the first wireline run, it was confirmed that all the defects attached to the casing wall survived. A schematic of the final and current status of the well is presented in Fig. 5.11.

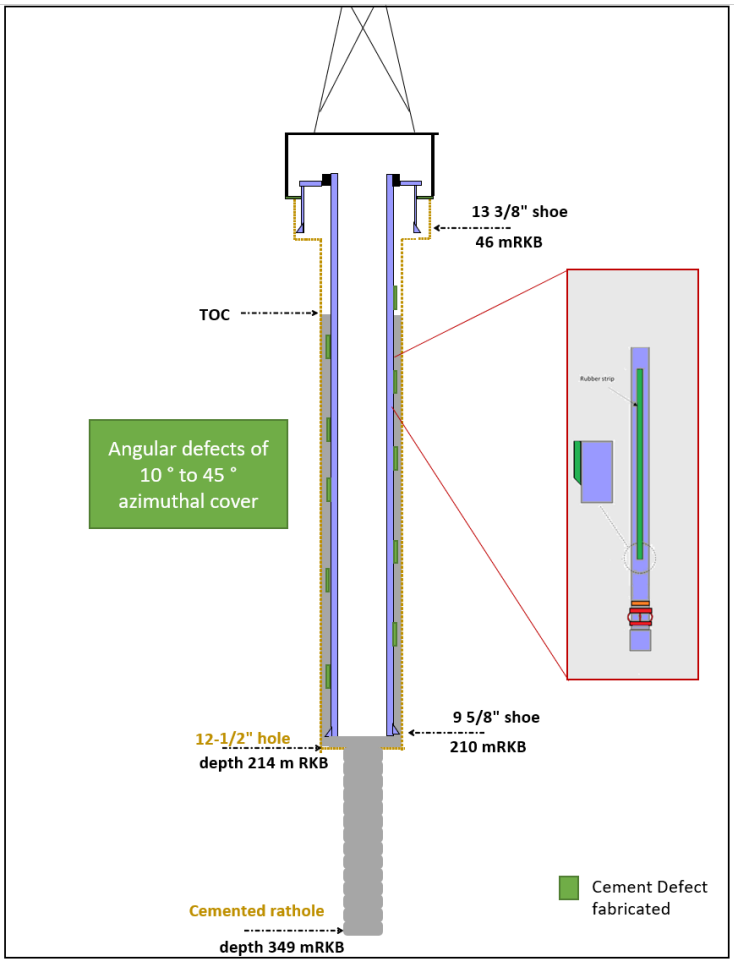

Figure 5.11: Schematic of the final completion of well U7.

5.7 Conclusion

A novel well facility was constructed with the aim of establishing a reference for the qualification of logging tools that can allow a direct comparison between log response and annular seal quality. This well provides the industry with the opportunity to compare different logging technologies to detect and evaluate cement defects and their performance to describe defects with specific lengths and sizes. At the time of writing, several logging surveys have been executed in this cement evaluation reference well facility.

Chapter 6

Final Conclusions and Recommendations

The annular cement placed between the casings and the formation becomes a critical barrier element for ensuring zonal isolation at the final phase of P&A. Regulations in Norway, UK and Brazil have clear requirements for their qualification, and all of them coincide that the minimum requirement of length is to have 30 m of continuous annular barrier verified by logs. More disagreement on the requirements was observed for internal plugs. Migration of fluids into the annular cement matrix and exposure to changes in pressure and temperature during the production phase can compromise the cement integrity and result in the creation of defects. Typical defects are channels, fractures and microannuli. The hydraulic properties and connectivity of such defects are relevant to evaluate the barrier integrity and estimate their isolation potential which ultimately defines their ability or not to be used as a permanent barrier element.

Six full-size test sections were constructed and tested to investigate the relation between cement quality and flow potential. The cells were instrumented with strain and pressure gauges while the cells were leak tested. Infrared thermography was used to visualize the leakage paths; it was observed that migration paths correlate well with the logging interpretation and fit well with the variations of hydraulic properties measured on the cells. During the experiments internal tubing pressure and annulus pressure were varied whilst casing radial deformation was measured. Leakage rates were correlated to the microannulus aperture using an analytical model to couple the microannulus pressure with the radial deformation. With the experiments presented it was possible to prove that the leakage paths and microannulus are normally not uniform and its behaviour under loading may be influenced by geometrical conditions such as tubing eccentricity. It was observed that it is more likely to have a higher permeability on the narrow side of the cemented annulus sheath. This might indicate that eccentricity should be considered when interpreting results of positive tests

performed in annular cement barriers in the field. Additionally, from the experiments presented in this thesis it was not possible to evaluate the effect of barrier length on the sealing ability of annular cement. As this topic is highly connected with ongoing discussions of minimal barrier length and stacked barriers more studies are recommended in this area in the future.

The revision of technologies currently available for evaluation of annular cement barriers shows that the correlation between barrier quality and hydraulic isolation is still unresolved and more research is required on this topic. Progress on technologies in wellbore diagnostics, milling, and cutting appears to be relevant for the evolution of regulation for qualification and acceptance of annular barriers. The road maps for P&A indicate that such technologies could significantly influence how the qualification will be executed and eventually impact removal decisions. The facility presented in Chapter 5 allows the evaluation of leakage paths simulating a water channel and can support the qualification of new tools for wellbore diagnosis and other activities, such as qualification of cement well barriers using thru tubing logging (TTL). Still, this facility is limited to evaluating migration of fluids behind the casing and other common defects such as microannuli.

The road map for cement durability and the results of the durability test from the cement material recovered from Vallhall well and presented in this thesis illustrate the difficulty of understanding the degradation and durability of cement, in particular under downhole conditions. However, the study presented in this thesis can provide a baseline for future comparisons of results to assess old-age cement from oil and gas wells. The future study of more cement samples that have been exposed to downhole conditions will contribute to a better understanding of the ageing effects and alteration/degradation of cement in well environments. This type of study might be particularly relevant in cases where detailed documentation of well integrity issues exist. The differences found between water permeability and gas permeability in the cement core plugs suggest that the interactions between pore structure and fluid migration is an area for further investigation.

Bibliography

[1] "Roadmap for New PA technologies, 2017-2020", https://offshorenorge.no/contentassets/f60cf93f2c9c4c129b0a73303ff8081c/00---welcome.pdf, Accessed: 2022-07-09.

[2] GOVIL, A., GARDNER, D., OBANDO, G., et al., "Validating Ultrasonic Log Response Against Reference Barrier Cells Simulating Downhole Well Conditions Encountered During Well Construction and Abandonment Operations". In: *IADC/SPE International Drilling Conference and Exhibition*, SP, 2020.

[3] SKADSEM, H. J., GARDNER, D., BELTRÁN-JIMÉNEZ, K., et al., "Study of Ultrasonic Logs and Seepage Potential on Sandwich Sections Retrieved from a North Sea Production Well", *SPE Drilling and completion1-15*, 2021.

[4] OBANDO PALACIO, G., GARDNER, D., DELABROY, L., et al., "An Evaluation of the Cement Sheath Quality of Casing Sections Recovered During a Well Abandonment Operation". In: *IADC/SPE International Drilling Conference and Exhibition, 3-5 March, Galveston, Texas, USA*, pp. 1–20, 2020, IADC/SPE 199609.

[5] TEODORIU, C., ASAMBA, P., "Experimental study of salt content effect on class G cement properties with application to well integrity", *Journal of Natural Gas Science and Engineering*, v. 24, pp. 324–329, may 2015.

[6] ARUP, *Oil and Gas Decommissioning From the UK ' s North Sea to the Brazilian Atlantic Implementation of the Regulatory Regime*, Tech. Rep. 249949, 2017.

[7] "Are we entering a decade of offshore decommissioning?" https://ihsmarkit.com/research-analysis/decade-of-offshore-decommissioning.html, note = Accessed: 2022-09-15.

[8] NORWEGIAN PETROLEUM DIRECTORATE, P. B. G. O., AS, G. C. N., *Decommissioning on the Norwegian Continental Shelf – Cost Effective and Innovative Solutions*, Tech. rep., 2019, J75064A-A-RT-00001/D1.

[9] VRÅLSTAD, T., SAASEN, A., FJÆR, E., et al., "Plug & abandonment of offshore wells: Ensuring long-term well integrity and cost-efficiency", *Journal of Petroleum Science and Engineering*, v. 173, n. September 2018, pp. 478–491, 2019.

[10] KOKAL, S., AL-KAABI, A., "Enhanced oil recovery: challenges & opportunities", *World Petroleum Council: Official Publication*, v. 64, pp. 64–69, 2010.

[11] "118,500 Oil Gas Wells To Be Drilled Worldwide Through 2022", https://oilprice.com/Energy/Energy-General/118500-Oil-Gas-Wells-To-Be-Drilled-Worldwide-Through-2022.html, Accessed: 2022-09-15.

[12] "Number of oil and gas wells set to hit 20-yearlow, Rystad says", https://www.offshore-energy.biz/number-of-oil-and-gas-wells-set-to-hit-20-year-low-rystad-says/, Accessed: 2022-09-15.

[13] BIVEN, M. M., PALACIOS, V., *Eliminating Orphan Wells and Sites in Texas*, Tech. rep., 2022, Xommission.

[14] BÖTTNER, C., HAECKEL, M., SCHMIDT, M., et al., "Greenhouse gas emissions from marine decommissioned hydrocarbon wells: leakage detection, monitoring and mitigation strategies", *International Journal of Greenhouse Gas Control*, v. 100, pp. 103119, 2020.

[15] "Webinar in Decommissioning and PA Session - Brazil Norway howpublished = https://www.youtube.com/watch?v=d_tneUVyJ-w&t=1583s note = Accessed: 2022-06-15", .

[16] "Estimated P&A Norwegian Continental Shelf: 2021 — 2026 January 2021", https://offshorenorge.no/contentassets/a068553616694ca18fbb0acd5646d4e6/pa--ncs---2021-2026.pdf, note = Accessed: 2022-09-15.

[17] BELTRÁN-JIMÉNEZ, K., LOHNE, H. P., FORD, E. P., et al., "Comparative Analysis of Permanent P&A Requirements and Consequences in Terms of Leakage - A Case Study". v. Day 2 Wed, October 30, 2019, *Offshore Technology Conference Brasil*, 10 2019.

[18] CAMPBELL, K., ROD SMITH, "Permanent Well Abandonment", *The Well Ahead*, v. 9, n. 3, pp. 25–27, 2013.

[19] "STANDARDS NORWAY", "NORSOk D-010. Well integrity in drilling and well operations", January 2021.

[20] "Well Decommissioning Guidelines – Issue 6, howpublished = `https://oeuk.org.uk/product/well-decommissioning-guidelines-issue-6/` note = Accessed: 2022-04-15", .

[21] HART, W., SMITH, T., "improved cementing practices reduce cementing failures", *Journal of Canadian Petroleum Technology*, v. 29, n. 06, nov 1990.

[22] CHEN, Z., CHAUDHARY, S., SHINE, J., "Intermixing of Cementing Fluids: Understanding Mud Displacement and Cement Placement". In: *IADC/SPE Drilling Conference and Exhibition*, Society of Petroleum Engineers, 2014.

[23] SKADSEM, H. J., KRAGSET, S., LUND, B., et al., "Annular displacement in a highly inclined irregular wellbore: experimental and three-dimensional numerical simulations", *Journal of Petroleum Science and Engineering*, v. 172, pp. 998–1013, jan 2019.

[24] DO PETROLEO, I. B., *Diretrizes para monitoramento de poço*, Tech. rep., 2017, Caderno de boas praticas de EP.

[25] VAN DER KUIP, M. D., BENEDICTUS, T., WILDGUST, N., et al., "High-level integrity assessment of abandoned wells", *Energy Procedia*, v. 4, pp. 5320–5326, 2011.

[26] "INTERNATIONAL ASSOCIATION OF OIL AND GAS PRODUCERS", "Overview of International Offshore Decommissioning Regulations". In: *Volume 2. Wells Plugging Abandonment*, IOGP, 2017.

[27] FANAILOO, P., BUCHMILLER, D., OUYANG, S., et al., "Risk Based Approach to Well Plugging Abandoning - Reducing Costs While Verifying Risk", v. Day 3 Wed, May 03, 2017, May 2017, D031S037R001.

[28] "NORSOK Standard", `https://www.standard.no/en/sectors/energi-og-klima/petroleum/norsok-standards/#.Ym5zxehByUk`.

[29] OF ECONOMIC AFFAIRS, D. M., CLIMATE, *MINING ACT OF THE NETHERLANDS*, Tech. rep., 2003, amended up to 2019.

[30] OF FEDERAL REGULATIONS (CFR), C., *30 CFR § 250.1715 - How must I permanently plug a well?*, Tech. rep., 2011, 76 FR 64462, Oct. 18, 2011, as amended at 77 FR 50900, Aug. 22, 2012; 81 FR 26038, Apr. 29, 2016.

[31] C-NLOPB, CNSOPB, *Drilling and Production Guidelines*, Tech. rep., 2017.

[32] COMPANY, A. D. N. O., *Drilling Code of Practice*, Tech. rep., 2015, Volume 2: Well Design and Planning.Chapter 7 Well Barriers.

[33] ENERGY REGULATOR, A. O., *Well operations management plan – content and level of detail*, Tech. rep., 2020, Doc No: N-04600-GN1602 A461074F.

[34] PETRONAS, *Petronas Procedures and Guidelines for Upstream Activities. Drilling and Well Operations Volume 8*, Tech. rep., 2013, (PPGUA 3.0/042/2013).

[35] American Petroleum Institute, *Wellbore Plugging and Abandonment Practices*, 2018.

[36] "PETROLEUM SAFETY AUTHORITY OF NORWAY REGULATIONS", *The activities regulations, section 85 and 88*, Tech. rep., Jan. 2018.

[37] "The facilities regulations, section 48: well barriers", Jan. 2014.

[38] BELTRÁN-JIMÉNEZ, K., SKADSEM, H. J., GARDNER, D., et al., "Leakage Through Micro-Annulus Geometries Incorporating Pressure-Driven Elastic Deformation". In: *Paper presented at the Offshore Technology Conference Brazil, Rio de Janeiro, Brazil, October 2019.*, Society of Petroleum Engineers, 2019.

[39] THE DEPARTMENT OF BUSSINES, E., (BEIS), I. S., *Petroleum Act 1998*, Tech. rep., 1998.

[40] THE DEPARTMENT OF BUSSINES, E., (BEIS), I. S., *Energy Act 2008*, Tech. rep., 2008.

[41] THE DEPARTMENT OF BUSSINES, E., (BEIS), I. S., *Energy Act 2016*, Tech. rep., 2016.

[42] THE DEPARTMENT OF BUSSINES, E., (BEIS), I. S., *The Offshore Installations and Wells (Design and Construction, etc.) Regulations*, Tech. rep., 1996.

[43] O&GUK, *Guidelines on Qualification of Materials for the Abandonment of Wells*, Tech. rep., 2015, – Issue 2.

[44] O&GUK, *Guidelines on Well Abandonment Cost Estimation*, Tech. rep., 2015, – Issue 2.

[45] "IHS Markit - Petrodata offshore rig data trends", `https://ihsmarkit.com/products/oil-gas-drilling-rigs-offshore-day-rates.html`, Accessed: 2022-03-14.

[46] DELABROY, L., RODRIGUES, D., NORUM, E., et al., "Perforate, Wash and Cement PWC Verification Process and an Industry Standard for Barrier Acceptance Criteria". In: *SPE Bergen One Day Seminar held in Bergen, Norway, 5 April 2017.*, Society of Petroleum Engineers, 2017.

[47] DELABROY, L., STOKKELAND, T. A., ÅSTRAND, G., et al., "Perforate Wash and Cement for Large Casing Sizes". In: *Decommissioning and Abandonment, Kuala Lumpur, Malaysia, December 2018.*, Society of Petroleum Engineers, 2018.

[48] LEESON, T., LARSEN, A. G., "When can Perforating, Wash and Cement PWC Reduce Abandonment Costs?" In: *SPE Asia Pacific Oil Gas Conference and Exhibition, 17 - 19 November 2020 - virtual event.*, Society of Petroleum Engineers, 2020.

[49] HOVDA, L., PHADKEA, A., MUELLER, D., et al., "Best Practice for Cementing and Zonal Isolation Using the Jet-Type Perforate, Wash and Cement Technique". In: *Asia Pacific Oil Gas Conference and Exhibition, Virtual, November.*, Society of Petroleum Enineers, 2020.

[50] ALLAPITCHAI, M. S. M., JOHAN, A. L., HEBOUL, E. K. M. M. B., et al., "Annulus Perforate, Wash and Cement : Establishing Barrier Verification Process for Deepwater Subsea Wells Abandonment and Its Lessons Learnt". In: *Decommissioning and Abandonment, Virtual, November 2021.*, Society of Petroleum Engineers, 2020.

[51] PETROLEUMSTILSYNET, *Qualification process for PA Perforate, Wash, Cement PWC*, Tech. rep., 2021, Final Report.

[52] AAS, B., SØRBØ, J., STOKKA, S., et al., "cement placement with tubing left in hole during plug and abandonment operations". In: *IADC/SPE Drilling Conference and Exhibition*, Society of Petroleum Engineers, 2016.

[53] FULKS, J., CARRAGHER, P., PRAPOO, H., "Bismuth Abandonment Plugs: The Possibilities are Endless". v. Day 2 Wed, December 04, 2019, *SPE Symposium: Decommissioning and Abandonment*, 12 2019, D021S006R001.

[54] FULKS, J. M., CARRAGHER, P., "A New Solution for Well Abandonment: Bismuth and Thermite". v. Day 4 Thu, November 05, 2020, *Offshore Technology Conference Asia*, 11 2020, D041S042R001.

[55] ZHANG, H., RAMAKRISHNAN, T. S., ELIAS, Q. K., et al., "Evaluation of Bismuth-Tin Alloy for Well Plug and Abandonment", *SPE Production Operations*, v. 35, n. 01, pp. 111–124, 02 2020.

[56] ZHANG, H., RAMAKRISHNAN, T. S., ELKADY, Y. M., et al., "Comparative Evaluation of Bismuth-Silver and Bismuth-Tin Alloys for Plug and Abandonment", *SPE Drilling Completion*, v. 36, n. 02, pp. 368–382, 06 2021.

[57] DOS SANTOS MAGALHÃES, E., DE LEMOS, M. J., "A thermal study of a new oil well plugging abandonment operation", *International Journal of Thermal Sciences*, v. 155, pp. 106421, 2020.

[58] SUN, RUITAO, ZHANG, JIE, LI, ZHILIN, et al., "Research on temperature propagation law based on thermite plugging and abandonment technology", *E3S Web Conf.*, v. 352, pp. 01066, 2022.

[59] PENA, F. J., DE LEMOS, M. J., "Unsteady heat conduction with phase change applied to a novel thermal plug and abandonment process", *International Journal of Thermal Sciences*, v. 170, pp. 107155, 2021.

[60] DE SOUZA, K. M., DE LEMOS, M. J., KAWACHI, E. Y., "Thermodynamics of thermite reactions for a new thermal plug and abandonment process", *CContinuum Mechanics and Thermodynamics - Springer*, v. 34, pp. 259–271, 2022.

[61] THORSTENSEN, E., VADSET, K., STRAUME, M. K., et al., "Bismuth Plugs Used to Cap All Wells During the Final Phase of the Valhall DP Abandonment Campaign, Offshore Norway". v. Day 1 Mon, May 02, 2022, *OTC Offshore Technology Conference*, 05 2022, D011S006R002.

[62] BAUER, A., STENEBRÅTEN, J., LI, L., et al., "Can heating-induced creep result in shale barriers for P&A applications", *Arma*, 2017.

[63] THOMBARE, A., ALDIN, M., VAN OORT, E., "Experimental Technique to Investigate Shale Creep for Annular Barrier Formation in Oil and Gas Wells". v. All Days, *U.S. Rock Mechanics/Geomechanics Symposium*, 06 2020, ARMA-2020-2073.

[64] LOZOVYI, M., FJÆR, E., GAWEL, K. M., et al., "Impact of Acid Treatment on Shale Creep and Formation of Natural Barrier". v. All Days, *U.S. Rock Mechanics/Geomechanics Symposium*, 06 2021, ARMA-2021-1931.

[65] VAN OORT, E., THOMBARE, A., ALDIN, M., et al., "Annular Creep Barrier Evaluation and Qualification Using Ultrasonic Measurements". v. Day 3 Thu, March 10, 2022, *SPE/IADC Drilling Conference and Exhibition*, 03 2022, D031S019R002.

[66] KRISTIANSEN, T. G., DYNGELAND, T., KINN, S., et al., "Activating Shale to Form Well Barriers: Theory and Field Examples". v. Day 1 Mon, September 24, 2018, *SPE Annual Technical Conference and Exhibition*, 09 2018, D011S001R004.

[67] BAUER, A., LOIZZO, M., DELABROY, L., et al., "Activated Shale Creep and Potential Micro-Annulus Investigated in the Field". v. Day 5 Fri, March 12, 2021, *SPE/IADC Drilling Conference and Exhibition*, 03 2021, D051S028R002.

[68] KRISTIANSEN, T. G., DELABROY, L., OBANDO PALACIO, G. A., et al., "Implementing a Strategy for Shale as Well Barrier in New Wells". v. Day 5 Fri, March 12, 2021, *SPE/IADC Drilling Conference and Exhibition*, 03 2021, D051S028R001.

[69] "Roadmap for New PA technologies, 2021-2025+", `https://offshorenorge.no/contentassets/a068553616694ca18fbb0acd5646d4e6/pa-roadmap-paf----final-100221.ppt.pdf`, Accessed: 2022-07-09.

[70] PLUGGING, ABANDONMENT COLLABORATICE ENVIRONMENT, "Three years into PACE", 2019.

[71] REDDY, B. R., SANTRA, A., MCMECHAN, D., et al., "Cement Mechanical-Property Measurements Under Wellbore Conditions." *SPE Drilling and Completion*, v. 22, pp. 33–38, 2007.

[72] LESLIE, I., BRADLEY, T., BALAMAGA, J., et al., "The Effect of Time on Apparent Cement Integrity – Time Lapse Logging of Cement Bond Logs". In: *Paper presented at the SPWLA 56th Annual Logging Symposium, Long Beach, California, USA*, SPE, 2015.

[73] BENGE, G., "Cement Evaluation—A Risky Business", *SPE Drilling and Completion*, v. 30, pp. 322–326, doi = 10.2118/170712–PA,, 2015.

[74] LECAMPION, B., BUNGER, A., KEAR, J., et al., "Interface debonding driven by fluid injection in a cased and cemented wellbore: Modeling and experiments", *International Journal of Greenhouse Gas Control*, v. 18, pp. 208–223, 2013.

[75] TALEGHANI, A., KLIMENKO, D., "An analytical solution for microannulus cracks developed around a wellbore", *Journal of Energy Resources Technology, Transactions of the ASME*, v. 137, n. 6, Nov. 2015, Publisher Copyright: Copyright © 2015 by ASME.

[76] DE ANDRADE, J., SANGESLAND, S., "Cement Sheath Failure Mechanisms: Numerical Estimates to Design for Long-Term Well Integrity", *Journal of Petroleum Science and Engineering*, v. 147, n. 1992, pp. 682–698, 2016.

[77] SKORPA, R., WERNER, B., VRÅLSTAD, T., "Effect of Mud on Cement Sheath Integrity". v. Day 1 Tue, May 14, 2019, *SPE Norway Subsurface Conference*, 05 2019, D011S007R003.

[78] WISE, J., NYGAARD, R., HARELAND, G., "Numerical Analysis of Wellbore Integrity and Cement Sheath Debonding for Wells in the Eugene Island OPD, Gulf of Mexico". v. All Days, *U.S. Rock Mechanics/Geomechanics Symposium*, 06 2019, ARMA-2019-0439.

[79] PAEGLE, I., MARCOS-MESON, V., FISCHER, G., "Characterization of crack formation and development in the oilgas well casing cement sheath". v. 660, n. 1, IOP Publishing, 2019, 4th International Conference "Innovative Materials, Structures and Technologies", IMST 2019 ; Conference date: 25-09-2019 Through 27-09-2019.

[80] SKORPA, R., VRALSTAD, T., "leakages through radial cracks in cement sheaths: effect of geometry, viscosity, and aperture", *Journal of Energy Resources Technology*, v. 144, 2022.

[81] VRÅLSTAD, T., TODOROVIC, J., SAASEN, A., et al., "Long-Term Integrity of Well Cements at Downhole Conditions". In: *SPE Bergen One Day Seminar*, Society of Petroleum Engineers, 2016.

[82] FERREIRA, E. G., MARUMO, J. T., FRANCO, M. K., et al., "10000 years cement – can hydrated cement last as much as long-lived radionuclides?" *Cement and Concrete Composites*, v. 103, pp. 339–352, oct 2019.

[83] ESCALANTE-GARCIA, J., SHARP, J., "The microstructure and mechanical properties of blended cements hydrated at various temperatures", *Cement and Concrete Research*, v. 31, n. 5, pp. 695–702, 2001.

[84] ESCALANTE-GARCÍA, J., SHARP, J., "Effect of temperature on the hydration of the main clinker phases in portland cements: part i, neat cements", *Cement and Concrete Research*, v. 28, n. 9, pp. 1245–1257, 1998.

[85] OROSZ, K., HEDLUND, H., CWIRZEN, A., "Effects of variable curing temperatures on autogenous deformation of blended cement concretes", *Construction and Building Materials*, v. 149, pp. 474–480, 2017.

[86] BULLARD, J. W., JENNINGS, H. M., LIVINGSTON, R. A., et al., "Mechanisms of cement hydration", *Cement and Concrete Research*, v. 41, n. 12, pp. 1208–1223, 2011, Conferences Special: Cement Hydration Kinetics and Modeling, Quebec City, 2009 CONMOD10, Lausanne, 2010.

[87] EL-HACHEM, R., ROZIÈRE, E., GRONDIN, F., et al., "New procedure to investigate external sulphate attack on cementitious materials", *Cement and Concrete Composites*, v. 34, n. 3, pp. 357–364, 2012.

[88] COLLEPARDI, M., "A state-of-the-art review on delayed ettringite attack on concrete", *Cement and Concrete Composites*, v. 25, n. 4, pp. 401–407, 2003, Concrete Durability.

[89] NELSON, E. B., GUILLOT, D., (eds), *Well Cementing*. 2nd ed. Schlumberger: Sugar Land, Texas, US, 2006.

[90] BENNET, T., (ed), *Well Cement integrity and Cementing Practices*. 1st ed. The University of Adelaide, 2016.

[91] RAHMANI, R., BOURGOYNE, D., SMITH, J., "Full-scale Testing Shows Advantages of a Quantitative Approach to Interpreting Negative Pressure Tests". In: *Drilling Conference, Amsterdam, The Netherlands, March.*, SPE/IADC, 2013.

[92] RAHMANI, R., BOURGOYNE, D., SMITH, J., "Full-Scale Testing Shows Advantages of a Quantitative Approach to Interpreting Inflow Tests", *SPE Production Operations.*, v. 29 (02), pp. 78 – 87, 2014.

[93] STEIN, A., "A Novel Approach to Barrier Integrity Testing in Well". In: *Annual Technical Conference and Exhibition held in Dallas, Texas, 24-26 September.*, SPE, 2018.

[94] BRUCE, T. J., STEIN, A. F., "A New Approach to Barrier Verification". In: *2021 Symposium Compilation, Virtual, November 2021.*, SPE, 2021.

[95] "A NEW WELL INTEGRITY VERIFICATION METHOD FOR PERMANENT PLUG AND ABANDONMENT", https://www.exedra.no/l, Accessed: 2022-04-01.

[96] ENRIGHT, R. J., "Sleuth for Down-Hole Leaks", *Oil Gas Journal*, pp. 78–79, 1955.

[97] KOROTAEV, Y. P., BABALOV, M., "Acoustic Method of Delineating Operating Intervals in Gas Bearing Formations", *Gazoyaya Prom*, 1970.

[98] STEIN, N., KELLY, J., BALDWIN, W., et al., *Journal Of Petroleum Technology , title = Sand Production Determined from Noise Measurements, year = 1972, volume = July, pages = 803-806,.*

[99] MCKINLEY, R., BOWER, F., , et al., "The Structure and Interpretation of Noise From Behind Cemented Casing", *Journal Of Petroleum Technology*, v. March, pp. 329 – 338, 1973.

[100] KOERNER, H. B., CARROLL, J. C., "USE OF THE NOISE LOG AS A DOWNHOLE DIAGNOSTIC TOOL". SPE, 1979.

[101] BAKERI, F. A. M., ASHQA, A., SHAH, J. M., et al., "First Successful Downhole Sand Detection in Malaysia". In: *Abu Dhabi International Petroleum Exhibition Conference, Abu Dhabi, UAE, November. Paper Number: SPE-197492-MS*, SPE, 2019.

[102] ZAKIR, M. M., HUSSAIN, S., QAZI, S. E., et al., "Application of Spectral Noise Logging and High Precision Temperature (SNL-HPT) To Identify Hydrocarbon and Water Bearing Zones in Naturally Fractured Reservoirs (NFR) – A Case Study of Potwar Region". In: *PAPG/SPE Pakistan Section Annual Technical Conference and Exhibition, Islamabad, Pakistan, November*, SPE, 2016.

[103] CICIONE, S., GALLI, G., PIRRONE, M., et al., "Quantitative Spectral Analysis of Noise Log Measurements for Enhanced Dynamic Characterization of Complex Reservoirs". In: *offshore Mediterranean Conference and Exhibition, Ravenna, Italy, March. Paper Number: OMC-2017-615*, SPE, 2017.

[104] MOLENAAR, M. M., COWAN, B. M., FIDAN, E., et al., "A Case Study: Profiling Gas Production in the Tubing/Casing Annulus, Using Noise/Temperature Logging Techniques". In: *nternational Oil and Gas Conference and Exhibition in China, Beijing, China, June*, SPE, 2010.

[105] NADEEM, A., STAIRS, M., USMAN, T. A. S. S. H. U. A. M., "High Precision Temperature – Spectral Noise Logging (HPT-SNL) at Well 'X' to Identify Zonal Contribution Behind Casing Communication – A Case Study". In: *SPE/PAPG Pakistan section Annual Technical Conference, Islamabad, Pakistan, November 2015. Paper Number: SPE-181118-MS*, SPE, 2015.

[106] SHAKER, A., ELAZIM, E. A., IBRAHIM, W., et al., "PRECISE BARRIER DIAGNOSTICS FOR WELL INTEGRITY PROBLEMS IDENTIFICATION USING SPECTRAL NOISE LOGGING. CASE STUDY: T4-10 OFFSHORE GAS WELL". In: *OMC Med Energy Conference and Exhibition in Ravenna, Italy, September 28-30*, SPE, 2021.

[107] "Chorus Specification - TGT", `https://tgtdiagnostics.com/wp-content/uploads/2019/10/Chorus-Platform.pdf`, Accessed: 2022-05-01.

[108] "VIVID®Acoustic Listening Platform", `https://www.archerwell.com/wp-content/uploads/2018/11/VIVID_2Page_Cat.pdf`, Accessed: 2022-05-01.

[109] RAAB, T., REINSCH, T., CIFUENTES, S. R. A., et al., "Real-Time Well-Integrity Monitoring Using Fiber-Optic Distributed Acoustic Sensing", *SPE Journal*, v. 24 (05), pp. 1997–2009, 2019.

[110] HABERER, S., PFRANG, D., MEINECKE, F. S. M., et al., "Permanent Fiber-Optic Installation in the Reservoir Section of a Deep Geothermal Well". In: *Conference Proceedings, First EAGE Workshop on Fibre Optic Sensing, Mar p.1 - 5*, European Association of Geoscientists Engineers, 2020.

[111] SCHÖLDERLE, F., LIPUS, M., PFRANG, D., et al., "Monitoring cold water injections for reservoir characterization using a permanent fiber optic installation in a geothermal production well in the Southern German Molasse Basin", *Geothermal Energy*, v. 8. Article number: 21, 2021.

[112] SUN, Y., XUE, Z., HASHIMOTO, T., "Fiber optic distributed sensing technology for real-time monitoring water jet tests: Implications for wellbore integrity diagnostics", *Journal of Natural Gas Science and Engineering*, v. 58, pp. 241–250, 2018.

[113] LIPUS, M., RAAB, T., REINSCH, T., et al., "Applications of Distributed Fiber Optic Strain Sensing for Real-Time Wellbore Integrity Monitoring". In: *Proceedings World Geothermal Congress 20201, Reyk-*

javik, Iceland, April - October 2021, year = 2021, https://gfzpublic.gfz-potsdam.de/pubman/item/item$_5$*007112,* .

[114] SCHUBERTH, M. G., BAKKA, H. S., BIRNIE, C. E., et al., "A Real-Time Fiber Optical System for Wellbore Monitoring: A Johan Sverdrup Case Study". In: SPE Offshore Europe Conference Exhibition*, SPE, 2021.*

[115] ANWAR, I., CAREY, B., JOHNSON, P., et al., Evaluating Two-Phase Flow Through Wellbore Cement Fractures Using Fiber-Optic Distributed Acoustic Sensing*, Tech. rep., 2022, AGU Advancing earth and space science.*

[116] GROSMANGIN, M., KOKESH, P., MAJANI, P., "A Sonic Method for Analyzing the Quality of Cementation of Borehole Casings", Journal of Petroleum Technology*, v. 13 (02), pp. 165–171, 1961.*

[117] GAI, H., LOCKYEAR, C. F., "Cement Bond Logging - A New Analysis to Improve Reliability". In: Advanced Technology Series 2 (01): 34–42.*, SPE-23729-PA, 1994.*

[118] KO KO KYI, GIH, A., "Issues with Cement Bond and Cement Evaluation Logs - Case Studies from Offshore Malaysia". In: International Petroleum Technology Conference held in Doha, Qatar, 6 –9 December 2015.*, SPE, 2015.*

[119] "Cement Bond Logging Tools", `https://www.slb.com/drilling/drilling-fluids-and-well-cementing/well-cementing/cement-evaluation/cement-bond-logging-tools`*, Accessed: 2022-05-02.*

[120] "Cement Bond Log (CBL) logging services", `https://hlsasia.com/wp-content/uploads/2017/10/cement.pdf`*, Accessed: 2022-05-02.*

[121] "Acoustic Cement Bond Log (CBL) service", `https://www.bakerhughes.com/evaluation/wireline-well-integrity-evaluation/cement-evaluation/acoustic-cement-bond-log-cbl-service`*, Accessed: 2022-05-02.*

[122] SHEIVES, T., TELLO, L., V.E. MAKI, J., et al., "A Comparison of New Ultrasonic Cement and Casing Evaluation Logs With Standard Cement Bond Logs". In: SPE Annual Technical Conference and Exhibition, New Orleans, Louisiana, October*, SPE, 1986.*

[123] HARRIS, K., "Chapter Eleven - Cement job evaluation", In: LIU, G. (ed), Applied Well Cementing Engineering*, pp. 523–567, Gulf Professional Publishing, 2021.*

[124] HAYDEN, R., RUSSELL, C., VEREIDE, A., et al., "Case Studies In Evaluation of Cement With Wireline Logs In a Deep Water Environment". v. All Days, SPWLA Annual Logging Symposium*, 05 2011, SPWLA-2011-XX.*

[125] FROELICH, B., "Multimode evaluation of cement behind steel pipe", The Journal of the Acoustical Society of America*, v. 123, 2008.*

[126] VAN KUIJK, R., ZEROUG, S., FROELICH, B., et al., "a novel ultrasonic cased-hole imager for enhanced cement evaluation". In: International Petroleum Technology Conference*, International Petroleum Technology Conference, 2005.*

[127] WANG, H., TOKSÖZA, M. N., FEHLER, M. C., Borehole Acoustic Logging – Theory and Methods. *Springer, 2020.*

[128] "Ultrasonic tool USI developed by Schulumberger", https://www.slb.com/-/media/files/wireline-production-services/brochure/isolation-scanner-br.ashx, Accessed: 2022-05-02.

[129] "Ultrasonic tool USI developed by Halliburton", https://www.halliburton.com/en/resources/cast-xr-tool-pushes-limits, Accessed: 2022-05-02.

[130] "Ultrasonic tool USI developed by Halliburton", https://www.bakerhughes.com/evaluation/wireline-well-integrity-evaluation/simultaneous-cement-and-casing-evaluation, Accessed: 2022-05-02.

[131] ALBAWI, A., ANDRADE, J. D., TORSÆTER, M., et al., "Experimental Set-Up for Testing Cement Sheath Integrity in Arctic Wells". In: OTC Arctic Technology Conference, Houston, Texas, February 2014. Paper Number: OTC-24587-MS*, SPE, 2014.*

[132] TAGHIPOUR, A., OPEDAL, N., SKORPA, R., et al., "Improved laboratory set-up for pressurized and confined cement sheath integrity tests". In: 36th International Conference on Ocean, Offshore and Arctic Engineering*, ASME, 2017.*

[133] SKORPA, R., VRÅLSTAD, T., "Visualization of fluid flow through cracks and microannuli in cement sheaths", SPE Journal*, v. 23, 2018.*

[134] SKORPA, R., OIA, T., TAGHIPOUR, A., et al., "Laboratory Set Up for Determination of Cement Sheath Integrity During Pressure Cycling". In: Proceedings of the ASME 2018 37th International Conference on Ocean, Offshore and Arctic Engineering*, ASME, 2018.*

[135] TAGHIPOUR, A., GHADERI, A., CERASI, P., et al., "Novel laboratory setup for realistic wellbore cement and formation integrity studies", Journal of Petroleum Science and Engineering*, v. 208 Part D, pp. 109664, 2022.*

[136] SPANNUTH, M., "Improving Intervention Efficiency with Downhole X-ray Diagnostics". In: SPE Norway — Well Performance*, SPE The first, 2017.*

[137] "The Downhole X-Ray Platform", https://www.visuray.com/products-services/downhole-x-ray-platform, Accessed: 2022-05-02.

[138] TEAGUE, P. N., "Imaging of Backscattered Ionizing Radiation - A Key Enabler for through Mud Borehole Imaging". In: Offshore Technology Conference, Houston, Texas, USA, May*, SPE, 2011.*

[139] SPANNUTH, M., ESMAEILI, M., GUNN, S., et al., "X-ray Backscatter Imaging in an Oil Well". In: SPE Annual Technical Conference and Exhibition, Amsterdam, The Netherlands, October*, SPE, 2014.*

[140] SPANNUTH, M., ACHIHAI, R., ANGEL, J., et al., "Innovative Wireline X-Ray Diagnostic Service Reduces Risk During Well Interventions: A Case Study". In: Abu Dhabi International Petroleum Exhibition Conference, Abu Dhabi, UAE, November*, SPE, 2016.*

[141] SPANNUTH, M., ACHIHAI, R., CAMPOS, J. A. G., et al., "Improving Intervention Efficiency with a Novel X-ray Diagnostic Service: A Case Study". In: SPE/ICoTA Coiled Tubing Well Intervention Conference Exhibition held in Houston, TX, USA, 21-22 March.*, SPE, 2017.*

[142] HAMID, S., ALMULHIM, A. A., ACHIHAI, R., et al., "Eliminating Guesswork in Downhole Diagnostics with Definitive Answers from Downhole X-ray Technology". In: SPE Annual Technical Conference and Exhibition, Calgary, Alberta, Canada, September*, SPE, 2019.*

[143] MILLIKAN, C., "Temperature Surveys in Oil Wells". In: Trans 142 (01) 15 - 23. Paper Number SPE - 941015G*, Society of petroleum engineers, 1940.*

[144] ALEXANDER, L., ANDRE, S. T., DAVID, J., et al., "Improving the Understanding, Application and Reliability of the Perforate, Wash and Cement Technique through the Use of Cement Bond Logs, Tool Enhancements and Barrier Verification via Annular Pressure Monitoring". In: SPE Annual Technical Conference and Exhibition*, Society of Petroleum Engineers, 2018.*

[145] VIGGEN, E. M., MERCIU, I. A., LOVSTAKKEN, L., et al., "Automatic interpretation of cement evaluation logs from cased boreholes using supervised deep neural networks", Journal of Petroleum Science and Engineering*, v. 195, pp. 107539, 2020.*

[146] BOURGOYNE, A., SCOTT, S., MANOWSKI, W., A review of sustained casing pressure occurring on the OCS*, Tech. rep., 2000, Final report submitted to the US Department of Interior Minerals Management Service.*

[147] OBODOZIE, I., TRAHAN, S., JOPPE, L., "Eliminating sustained casing pressure in well abandonment". In: Offshore Technology Conference Asia*, Offshore Technology Conference, 2016.*

[148] WOJTANOWICZ, A., NISHIKAWA, S., RONG, X., diagnosis and remediation of sustained casing pressure in wells*, Tech. rep., Louisiana State University, 2001.*

[149] K GOODWIN, R CROOK, "Cement sheath stress failure", , n. SPE–20453–PA, pp. 291–296, 1992.

[150] JACKSON, P., MURPHEY, C. E., "effect of casing pressure on gas flow through a sheath of set cement". In: SPE/IADC Drilling Conference, Amsterdam, Netherlands*, Society of Petroleum Engineers, 1993.*

[151] BOUKHELIFA, L., MORONI, N., JAMES, S. G., et al., "Evaluation of Cement Systems for Oil and Gas-Well Zonal Isolation in a Full-Scale Annular Geometry", SPE Drill Compl*, v. 20, 2005.*

[152] NAGELHOUT, C., BOSMA, G., MUL, J., et al., "Laboratory and field validation of a sealant system for critical plug and Abandon situations", SPE Drill Compl*, v. 25, 2010.*

[153] VAN EIJDEN, J., CORNELISSEN, E., RUCKERT, F., et al., "Development of experimental equipment and procedures to evaluate zonal isolation and

well abandonment materials". In: SPE/IADC Drilling Conference and Exhibition*, Society of Petroleum Engineers, 2017.*

[154] FORCHHEIMER, P., "Wasserbewegung Durch Boden: Zeitschrift des Vereines Deutscher Ingenieure, v. 45", 1901.

[155] ANDRADE, J. D., SANGESLAND, S., SKORPA, R., et al., "experimental laboratory setup for visualization and quantification of cement-sheath integrity", SPE Drilling & Completion*, v. 31, n. 04, pp. 317–326, dec 2016.*

[156] CORINA, A. N., SKORPA, R., SANGESLAND, S., et al., "Simulation of fluid flow through real microannuli geometries", Journal of Petroleum Science and Engineering*, v. 196, pp. 107669, 2021.*

[157] STORMONT, J. C., FERNANDEZ, S. G., TAHA, M. R., et al., "Gas flow through cement-casing microannuli under varying stress conditions", Geomechanics for Energy and the Environment*, v. 13, pp. 1–13, mar 2018.*

[158] MOEINIKIA, F., FJELDE, K. K., SAASEN, A., et al., "A Probabilistic Methodology To Evaluate the Cost Efficiency of Rigless Technology for Subsea Multiwell Abandonment", SPE Production & Operations*, v. 30, n. 04, pp. 270–282, 2015.*

[159] WILLIS, B. M., STRUTT, J. E., EDEN, R. D., "Long Term Well Plug Integrity Assurance – A Probabilistic Approach". In: e Offshore Technology Conference held in Houston, Texas, USA, 6 to 9 May 2019*, Society of Petroleum Engineers, 2019.*

[160] JOHNSON, C., HAGHIGHAT SEFAT, M., DAVIES, D., "Developing a Well-Centric Flow Model - the First Step in a Risk-Based Approach to Oil and Gas Well Decommissioning", Journal of Petroleum Science and Engineering*, v. 204, Sept. 2021.*

[161] AL RAMADAN, M., SALEHI, S., TEODORIU, C., "Robust Leakage Modeling for Plug and Abandonment Applications". v. Volume 8: Polar and Arctic Sciences and Technology; Petroleum Technology, International Conference on Offshore Mechanics and Arctic Engineering*, 06 2019, V008T11A054.*

[162] SKADSEM, H. J., KRAGSET, S., SØRBØ, J., "Cementing an Irregular Annulus Geometry: Full-Scale Experiments and 3D Simulations". In: SPE/IADC International Drilling Conference and Exhibition, The Hague, The Netherlands, March 2019*, pp. 1–15, 2019, SPE/IADC 194091.*

[163] WEBSTER, W., EIKERTS, J., "Flow After Cementing : A Field And Laboratory Study". In: SPE Annual Technical Conference and Exhibition*, pp. 1–8, 09 1979, SPE-8259-MS.*

[164] SABINS, F. L., "Problems in Cementing Horizontal Wells", Journal of Petroleum Technology*, v. 42, pp. 398 – 400, 1990.*

[165] BELTRÁN-JIMÉNEZ, K., SKADSEM, H., SUNDE, J., et al., "Restoration of annular zonal isolation using localized casing expansion (LCE) technology: Treatment of near-horizontal test sections containing a free-water channel", Journal of Petroleum Science and Engineering*, v. 208, pp. 109792, 2022.*

[166] WHITE, F. M., Viscous fluid flow*. 2nd ed. McGraw-Hill, Inc., 1991.*

[167] MUNNS, J. W., "The valhall field: a geological overview", Marine and Petroleum Geology*, v. 2, n. 1, pp. 23–43, feb 1985.*

[168] BARKVED, O., HEAVEY, P., KJELSTADLI, R., et al., "valhall field - still on plateau after 20 years of production". In: Offshore Europe*, Society of Petroleum Engineers, 2003.*

[169] AKERBP, annual report 2018*, Tech. rep., Aker BP SA, 2018.*

[170] "STANDARDS NORWAY", ""NORSOk D-010. Well integrity in drilling and well operations"", June 2013.

[171] PALACIO, G. O., GARDNER, D., DELABROY, L., et al., "an evaluation of the cement sheath quality of casing sections recovered during a well abandonment operation". In: IADC/SPE International Drilling Conference and Exhibition*, Society of Petroleum Engineers, 2020.*

[172] GUILLOT, D. J., FROELICH, B. G., CACERES, E., et al., "Are Current Casing Centralization Calculations Really Conservative?" In: IADC/SPE Drilling Conference*, Society of Petroleum Engineers, 2008.*

[173] GUPTA, S., GOVIL, A., OBANDO, G., et al., "State of the art development in annulus evaluation". In: Abu Dhabi International Petroleum Exhibition & Conference*, Society of Petroleum Engineers, 2019.*

[174] JUTTEN, J., HAYMAN, A., "Microannulus Effect on Cementation Logs: Experiments and Case Histories". In: SPE Asia Pacific Oil and Gas Conference, Singapore, 8–10 February*, SPE, 1993.*

[175] SKADSEM, H. J., GARDNER, D., BELTRÁN-JIMÉNEZ, K., et al., "Fluid migration characterization of cemented sections retrieved from a north sea production well". In: IADC/SPE International Drilling Conference and Exhibition*, Society of Petroleum Engineers, 2020.*

[176] STORMONT, J. C., GARCIA FERNANDEZ, S., TAHA, M. R., et al., "Gas flow through cement-casing microannuli under varying stress conditions", Geomechanics for Energy and the Environment*, v. 13, pp. 1–13, 2018.*

[177] LAU, C., AHMAD TAJALIE, A., WA, W., et al., "Successful Implementation of Improved Cementing Workflow in Heavily Depleted Brown Field through Advanced Integrated Cement Evaluation". v. Day 1 Tue, October 17, 2017, SPE Asia Pacific Oil and Gas Conference and Exhibition*, 10 2017, D012S036R050.*

[178] GOVIL, A., KALYANRAMAN, R. S., CONSTABLE, K., "Accurate Determination of Annular Content Behind Casing and Prevention of Remedial Action During Well Construction". v. Day 2 Wed, March 04, 2020, SPE/IADC Drilling Conference and Exhibition*, 03 2020, D091S007R004.*

[179] KALYANRAMAN, R. S., CHEN, X., WU, P.-Y., et al., "Autonomous Interpretation Methods of Ultrasonic Data Through Machine Learning Facilitates Novel and Reliable Casing Annulus Characterization". v. Day 4 Thu, March 11, 2021, SPE/IADC Drilling Conference and Exhibition*, 03 2021, D041S016R001.*

[180] WISE, J., KARAMI, H., CORINA, A. N., et al., "Prediction of Methane Leakage Through Primary Cement Barrier in the High Island OPD, Gulf of Mexico", Journal of Natural Gas Science and Engineering*, v. 101, pp. 104511, 2022.*

[181] DUGUID, A., BUTSCH, R., CAREY, W. J., et al., "Pre-injection baseline data collection to establish existing wellbore leakage properties", Energy Procedia*, v. 37, pp. 5661–5672, 2013.*

[182] KHALIFEH, M., MURI BØ, E., SHAHMORADI, M. A., "Utilization of Settled Barite as Permanent Well Barrier Element - Feasibility Study". v. Day 1 Wed, April 27, 2022, SPE Norway Subsurface Conference*, 04 2022, D012S013R001.*

[183] CALÇADA, L. A., SCHEID, C. M., MELEIRO, L. A., et al., "Barite Sag and Its Impact On Annular Pressure Build Up Mitigation In Producing

Offshore Wells". v. Day 2 Tue, September 27, 2016, SPE Annual Technical Conference and Exhibition*, 09 2016, D021S023R008.*

[184] RAJA ISMAIL, R. M. H., ZAINAL ABIDIN, F., THUZAR, M., et al., "Concerted Approach for Annular Pressure Build-Up APB Mitigations to Safeguard Well Integrity of Subsea, High Temperature Carbonate Exploration Well". v. Day 2 Wed, March 23, 2022, Offshore Technology Conference Asia*, 03 2022, D021S008R005.*

[185] RAJ, K., CATALIN, T., YOUNAS, D., et al., "Identification and evaluation of well integrity and causes of failure of well integrity barriers (A review)", Journal of Natural Gas Science and Engineering*, v. 45, n. June, pp. 511–526, 2017.*

[186] BOURGOYNE, A., SCOTT, S., REGG, J. B., "Sustained Casing Pressure in Offshore Producing Wells". In: SPE Offshore Technology Conference, Houston, Texas*, 1999, OTC-11029-MS.*

[187] JUSTNES, H., SKALLE, P., SVEEN, J., et al., "Porosity of oil well cement slurries during setting", Advances in Cement Research*, v. 7, pp. 9–12, jan 1995.*

[188] AGBASIMALO, N., RADONJIC, M., "Experimental study of portland cement/rock interface in relation to wellbore stability for carbon capture and storage CCS", 46th U.S. Rock Mechanics/Geomechanics Symposium, 24-27 June, Chicago, Illinois*, 2012.*

[189] DUGUID, A., RADONJIC, M., BRUANT, R., et al., "The effect of CO2 sequestration on oll well cements", In: Greenhouse Gas Control Technologies 7*, pp. 1997–2001, Elsevier, 2005.*

[190] DUGUID, A., "An estimate of the time to degrade the cement sheath in a well exposed to carbonated brine", Energy Procedia*, v. 1, n. 1, pp. 3181–3188, feb 2009.*

[191] DUGUID, A., SCHERER, G. W., "Degradation of oilwell cement due to exposure to carbonated brine", International Journal of Greenhouse Gas Control*, v. 4, n. 3, pp. 546–560, may 2010.*

[192] RAOOF, A., NICK, H., WOLTERBEEK, T., et al., "Pore-scale modeling of reactive transport in wellbore cement under CO2 storage conditions", International Journal of Greenhouse Gas Control*, v. 11, pp. S67–S77, nov 2012.*

[193] *LÉCOLIER, E., RIVEREAU, A., SAOÛT, G., et al., "Durability of hardened portland cement paste used for oilwell cementing",* Oil & Gas Science and Technology - Rev IFP, *v. 62, n. 3, pp. 335–345, June 2007.*

[194] *WOLTERBEEK, T. K., HANGX, S. J., SPIERS, C. J., "Effect of CO 2 -induced reactions on the mechanical behaviour of fractured wellbore cement",* Geomechanics for Energy and the Environment, *v. 7, pp. 26–46, sep 2016.*

[195] *NOIK, C., RIVEREAU, A., "Oilwell Cement Durability". In:* SPE Annual Technical Conference and Exhibition, *Society of Petroleum Engineers, 1999.*

[196] *BUZZI, O., BOULON, M., HERVÉ, M., et al., "Leaching of rock-concrete interfaces",* Rock Mechanics and Rock Engineering, *v. 41, n. 3, pp. 445–466, nov 2007.*

[197] *XIE, S., SHAO, J., BURLION, N., "Experimental study of mechanical behaviour of cement paste under compressive stress and chemical degradation",* Cement and Concrete Research, *v. 38, n. 12, pp. 1416–1423, dec 2008.*

[198] *GARNIER, A., LAUDET, J. B., PATIL, S., et al., "Effect of Acid Gas on Cement Sheath Integrity: Experimental Findings". In:* SPE Saudi Arabia Section Technical Symposium and Exhibition, *Society of Petroleum Engineers, 2012.*

[199] *SCHERER, G. W., KUTCHKO, B., THAULOW, N., et al., "Characterization of cement from a well at Teapot Dome Oil Field: Implications for geological sequestration",* International Journal of Greenhouse Gas Control, *v. 5, n. 1, pp. 115–124, jan 2011.*

[200] *CAREY, J. W., WIGAND, M., CHIPERA, S. J., et al., "analysis and performance of oil well cement with 30 years of CO2 exposure from the SACROC Unit, West texas, USA",* International Journal of Greenhouse Gas Control, *v. 1, n. 1, pp. 75–85, apr 2007.*

[201] *CROW, W., CAREY, J. W., GASDA, S., et al., "Wellbore integrity analysis of a natural CO2 producer",* International Journal of Greenhouse Gas Control, *v. 4, n. 2, pp. 186–197, mar 2010.*

[202] *KLINKENBERG, L., "The permeability of porous media to liquids and gases",* API Drilling and Production Practice, *1941.*

[203] MOGHADAM, A. A., CHALATURNYK, R., *"Expansion of the Klinkenberg's slippage equation to low permeability porous media"*, International Journal of Coal Geology, *v. 123, pp. 2–9, mar 2014.*

[204] LI, J., SULTAN, A. S., *"Klinkenberg slippage effect in the permeability computations of shale gas by the pore-scale simulations"*, Journal of Natural Gas Science and Engineering, *v. 48, pp. 197–202, dec 2017.*

[205] KATENDE, A., LU, Y., BUNGER, A., et al., *"Experimental quantification of the effect of oil based drilling fluid contamination on properties of wellbore cement"*, Journal of Natural Gas Science and Engineering, *v. 79, pp. 103328, jul 2020.*

[206] TANIKAWA, W., SHIMAMOTO, T., *"Klinkenberg effect for gas permeability and its comparison to water permeabilityfor porous sedimentary rocks"*, Hydrology and Earth System Sciences Discussions, *2006.*

[207] TANIKAWA, W., SHIMAMOTO, T., *"Comparison of klinkenberg corrected gas permeability and water permeability in sedimentary rocks"*, International Journal of Rock Mechanics and Mining Sciences, *v. 46, n. 2, pp. 229–238, feb 2009.*

[208] REN, Y., GUO, X., XIE, C., et al., *"Experimental study on gas slippage of marine shale in southern china"*, Petroleum Journal, *v. 2, pp. 171–176, 2016.*

[209] LETHAM, E. A., BUSTIN, R. M., *"Klinkenberg gas slippage measurements as a means for shale pore structure characterization"*, Geofluids, *v. 16, n. 2, pp. 264–278, jul 2015.*

[210] SHAR, A. M., MAHESAR, A. A., CHANDIO, A. D., et al., *"Impact of confining stress on permeability of tight gas sands: an experimental study"*, Journal of Petroleum Exploration and Production Technology, *v. 7, n. 3, pp. 717–726, nov 2016.*

[211] WANG, G., REN, T., WANG, K., et al., *"Improved apparent permeability models of gas flow in coal with Klinkenberg effect"*, Fuel, *v. 128, pp. 53–61, 2014.*

[212] FIROUZI, M., ALNOAIMI, K., KOVSCEK, A., et al., *"Klinkenberg effect on predicting and measuring helium permeability in gas shales"*, International Journal of Coal Geology, *v. 123, pp. 62–68, 2014, Special issue: Adsorption and fluid transport phenomena in gas shales and their effects on production and storage.*

[213] KUMAVAT, H. R., CHANDAK, N. R., PATIL, I. T., *"Influence of wettability on flow characteristics of water through microtubes and cores"*, Case Studies in Construction Materials, *v. 14, pp. e00491, 2021.*

[214] AHRENHOLZ, B., TÖLKE, J., LEHMANN, P., et al., *"Prediction of capillary hysteresis in a porous material using lattice-Boltzmann methods and comparison to experimental data and a morphological pore network model"*, Advances in Water Resources, *v. 31, n. 9, pp. 1151–1173, 2008, Quantitative links between porous media structures and flow behavior across scales.*

[215] ZHOU, C., CHEN, W., WANG, W., *"Evolution of gas permeability for concrete materials under and after uni-axial loading". In:* Proceedings of the Second International Conference on Performance-based and Life-cycle Structural Engineering (PLSE 2015), *School of Civil Engineering, The University of Queensland, jan 2015.*

[216] LOOSVELDT, H., LAFHAJ, Z., SKOCZYLAS, F., *"Experimental study of gas and liquid permeability of a mortar"*, Cement and Concrete Research, *v. 32, n. 9, pp. 1357–1363, 2002.*

[217] UEDA, T., OKI, T., KOYANAKA, S., *"Experimental analysis of mineral liberation and stereological bias based on X-ray computed tomography and artificial binary particles"*, Advanced Powder Technology, *v. 29, n. 3, pp. 462–470, mar 2018.*

[218] BOSSA, N., CHAURAND, P., VICENTE, J., et al., *"Micro- and nano-X-ray computed-tomography: A step forward in the characterization of the pore network of a leached cement paste"*, Cement and Concrete Research, *v. 67, pp. 138–147, jan 2015.*

[219] BRISARD, S., DAVY, C. A., MICHOT, L., et al., *"Mesoscale pore structure of a high-performance concrete by coupling focused ion beam/scanning electron microscopy and small angle X-ray scattering"*, Journal of the American Ceramic Society, *oct 2018.*

[220] YANG, X., KURU, E., GINGRAS, M., et al., *"CT-CFD integrated investigation into porosity and permeability of neat early-age well cement at downhole condition"*, Construction and Building Materials, *v. 205, pp. 73–86, apr 2019.*

[221] CAI, M., Rock mechanics: achievements and ambitions. *Taylor & Francis Ltd., 2011, Page 246.*

[222] M.W.I.BRAHIM, "geothermal gradient anomalies of hydrocarbon entrapment, ukcs quadrants 35 to 54", 15- 17 March,, *1994.*

[223] CORNELIUS, C., "geothermal aspects of hydrocarbon exploration in the north sea area", 1975.

[224] ROY-DELAGE, S. L., BAUMGARTE, C., THIERCELIN, M., et al., "new cement systems for durable zonal isolation". In: IADC/SPE Drilling Conference*, Society of Petroleum Engineers, 2000.*

[225] MORRIS, W., CRIADO, M. A., ROBLES, J., et al., "Design of High Toughness Cement for Effective Long Lasting Well Isolations". In: SPE Latin American and Caribbean Petroleum Engineering Conference*, Society of Petroleum Engineers, 2003.*

[226] TEODORIU, C., YUAN, Z., SCHUBERT, J., et al., "Experimental measurements of mechanical parameters of class G cement". In: SPE/EAGE European Unconventional Resources Conference and Exhibition*, Society of Petroleum Engineers, 2012.*

[227] LESTI, M., TIEMEYER, C., PLANK, J., "CO2 stability of Portland cement based well cementing systems for use on carbon capture & storage (CCS) wells", Cement and Concrete Research*, v. 45, pp. 45–54, mar 2013.*

[228] LI, Z., LIU, H., GUO, X., et al., "Contamination of cement slurries with oil based mud and its components in cementing operations", Journal of Natural Gas Science and Engineering*, v. 29, pp. 160–168, 2016.*

[229] EID, E., TRANGGONO, H., KHALIFEH, M., et al., "Impact of Drilling Fluid Contamination on Performance of Rock-Based Geopolymers". In: SPE Journal*, Society of Petroleum Engineers, 2021.*

[230] KOSMATKA, S., PANARESE, W., design and control of concrete mixtures*. Portland Cement Association, 1988.*

[231] DUERAMAE, S., TANGCHIRAPAT, W., SUKONTASUKKUL, P., et al., "Investigation of compressive strength and microstructures of activated cement free binder from fly ash - calcium carbide residue mixture", Journal of Materials Research and Technology*, v. 8, n. 5, pp. 4757–4765, sep 2019.*

[232] BAHAFID, S., GHABEZLOO, S., DUC, M., et al., "Effect of the hydration temperature on the microstructure of Class G cement: C-S-H composition and density", Cement and Concrete Research*, v. 95, pp. 270–281, 2017.*

[233] "ASTM INTERNATIONAL, WEST CONSHOHOCKEN, PA ", "ASTM 805/C805M-18: Standard Test Method for Rebound Number of Hardened Concrete", 2018.

[234] SZILÁGYI, K., BOROSNYÓI, A., ZSIGOVICS, I., "Extensive statistical analysis of the variability of concrete rebound hardness based on a large database of 60years experience", Construction and Building Materials*, v. 53, pp. 333–347, 2014.*

[235] KUMAVAT, H. R., CHANDAK, N. R., PATIL, I. T., "Factors influencing the performance of rebound hammer used for non-destructive testing of concrete members: A review", Case Studies in Construction Materials*, v. 14, pp. e00491, 2021.*

[236] "Principal component analysis", Chemometrics and Intelligent Laboratory Systems*, v. 2, n. 1, pp. 37–52, 1987, Proceedings of the Multivariate Statistical Workshop for Geologists and Geochemists.*

[237] SHENOLD, C., TEODORIU, C., "Development of a structured workflow for enhanced well cement integrity Lessons learned and the way ahead", Journal of Natural Gas Science and Engineering*, v. 36, pp. 824–836, 2016.*

[238] JUNG, H. B., JANSIK, D., UM, W., "Imaging wellbore cement degradation by carbon dioxide under geologic sequestration conditions using X-ray computed microtomography", Environmental Science and Technology*, v. 47, pp. 283–289, 2013.*

[239] BELTRÁN-JIMÉNEZ, K., MERCIU, I. A., GARDNER, D., et al., "Construction of a Reference Well to Support the Qualification of Cement Evaluation Logging Tools and Data Processing". v. Day 3 Thu, March 10, 2022, SPE/IADC Drilling Conference and Exhibition*, 03 2022, D031S019R004.*

[240] CHUILON, P., PUYOU, G., CAROLI, E., et al., "From Houston API Calibration Pits to Artigueloutan Logging Metrological Facility". In: SPWLA 60th Annual Logging Symposium*, Society of Petroleum Engineers, 2019, OTC-31302-MS.*

[241] J THORNHILL, "mechanical integrity testing and training facility ada, oklahoma", v. 1, pp. 37–43, n. 1, 1993.

[242] BIGELOW, E. L., DOMANGUE, E. J., LESTER, R. A., "A New and Innovative Technology for Cement Evaluation". In: SPE Annual Technical Conference and Exhibition*, 1990, SPE-20585-MS.*

[243] CULJAT, M., GOLDENBERG, D., TEWARI, P., et al., "a review of tissue substitutes for ultrasound imaging", Ultrasound in Medicine Biology*, v. 36, n. 6, pp. 861–873, 2010.*

[244] ZEROUG, S., BOSE, S., "Ultrasonic Cement Evaluation with the Flexural Wave Imager: A New Workflow to Estimate Cement Wavespeeds". v. Day 2 Tue, September 25, 2018, SPE Annual Technical Conference and Exhibition*, 09 2018, D021S017R001.*

4036 Stavanger
Tel: +47 51 83 10 00
E-mail: post@uis.no
www.uis.no

ISBN: 978-82-8439-135-9
ISSN: 1890-1387